MEASUREMENT AND IMAGING OF TISSUE PERFUSION USING COMPUTED TOMOGRAPHY

Thesis submitted for the degree of
Doctor of Medicine
at the University of Leicester

by

Kenneth Alan Miles

July 1993

ProQuest LLC
789 East Eisenhower Parkway
P.O. Box 1346
Ann Arbor, MI 48106-1346

CONTENTS.

1. INTRODUCTION:

1.1 Background

1.2 Development of Computed Tomography

1.3 Dynamic Computed Tomography (CT)

1.4 Aims of the Study

1.1 Background

Ever since the discovery of x-rays by Roentgen in 1895, the main emphasis of radiology has been in the demonstration of anatomy. The diagnosis and assessment of disease states by imaging changes in physiological processes, including blood flow, have been largely within the remit of nuclear medicine. However, newer radiological techniques such as Computed Tomography (CT), Doppler ultrasound, Digital Subtraction Angiography and Magnetic Resonance Imaging have been increasingly applied to evaluation of organ function. But when might the use of imaging to demonstrate abnormalities of function be of advantage?

There are a number of circumstances where changes in physiology may become apparent before structural changes are detectable. For example, the changes in cerebral blood flow associated with acute stroke are frequently demonstrable (e.g. by radio-isotope cerebral perfusion imaging) before any morphological change becomes apparent on a CT examination, which may only become abnormal ten days later. Alternatively, the functional effects of a disease state may be more significant in determining management of the patient than the morphological changes. An example of this is the presence of a dilated renal tract visualised on ultrasound examination. The dilatation is only significant if there is outflow obstruction. This requires an evaluation of urine flow which is readily performed with renal scintigraphy. There will also

be a reduction in blood flow to the renal cortex of an acutely obstructed kidney whereas no morphological change in the renal parenchyma will be visible. Assessment of tissue perfusion and organ blood flow are also of importance in research. Knowledge of the changes in organ function caused by various diseases can direct the application of drugs for treatment and the effects of drugs themselves can be usefully assessed non-invasively by functional imaging (e.g. the effects of Cyclosporin-A on renal blood flow.)

Radionuclide imaging is well suited to evaluation of organ function partly due to the wide range of radiopharmaceuticals available, enabling assessment of multiple physiological processes. But also the great sensitivity of the detector system and the ability to quantify data are of great importance. The main limitation is the lack of spatial resolution. X-ray computed tomography (CT) equipment is also very sensitive to changes in x-ray attenuation and these changes are readily and accurately quantifiable. In addition, the technique benefits from high spatial resolution. Thus, if CT could be used for functional imaging, a technique benefiting from combining physiological information and good spatial resolution would be obtained.

1.2 Development of Computed Tomography:

Computed tomography was introduced in 1973 and the concept of imaging by direct interaction between an X-ray machine and a computer was completely new. The computer in CT scanning both guides the X-ray apparatus in acquisition of data but also reconstructs the data to form a cross sectional image displayed on a television screen. The mathematical method of back projection used in reconstructing the images was pioneered by Hounsfield [1] who was awarded a Nobel prize for his work. The same method is used for magnetic resonance imaging (MRI) and emission computed tomography techniques in isotope imaging.

Computed tomography was first applied to the brain where the greater contrast resolution of CT, compared with plain radiography, demonstrated anatomy and pathology of the brain far better than was previously possible. The contrast resolution was further improved by the administration of intravenous contrast agents previously used for urography. Lesions within the brain, such as tumours, damage the blood-brain barrier locally and allow contrast medium to pass from the vascular compartment into the extracellular fluid thereby causing the lesion to "enhance".

As computed tomography began to be applied to the rest of the body, it was an early hope that the good contrast resolution would allow tissue differentiation, and thus a pathological

diagnosis, by measuring the X-ray attenuation of the tissue. These hopes were only partially born out, in that the technique was merely able to distinguish fatty lesions and cysts accurately whereas, for solid tissues, there was marked overlap in the range of attenuation values of normal and pathological tissues [2] making tissue characterisation by CT number impossible.

The same hopes were then held for images enhanced by contrast media. In the brain, these hopes were born out in that the enhanced appearances, combined with the anatomical position of the lesion, often allowed accurate pathological diagnosis. However, this was not so for the abdomen where a blood-tissue barrier is lacking and the tissue differentiation after contrast medium was limited to estimating the vascularity of a lesion.

Early CT systems took several minutes to obtain a single axial image at each slice location but as the technology improved, the data acquisition time has been reduced to less than one second. This has allowed easier application of CT to other areas of the body such as the abdomen where respiratory movement prevents adequate imaging with long exposure times. The shorter data acquisition times also allowed rapid repeated evaluation following the injection of a bolus of intravenous contrast medium and this technique became known as "dynamic scanning".

1.3 Dynamic Computed Tomography:

Dynamic Computed Tomography describes the acquisition of a rapid sequence of images usually after the administration of an intravenous contrast agent. By considering contrast medium as a physiological indicator, it has been possible for dynamic CT to provide qualitative and quantitative information about function in addition to good anatomical resolution. However, the application of many of these techniques has not been widespread. There are essentially two types of dynamic CT protocol; those with table movement (known as "incremental" sequences) and those without table movement ("single location" sequences).

Incremental Sequences:

These sequences comprise a series of images performed at several locations through an organ, allowing it to be visualised during the period of maximal contrast enhancement. It may be performed after a bolus injection or during an infusion of intravenous contrast medium. With data acquisition times on modern systems having become shorter, infusions are used less often as the series of images can be completed during the time course of a bolus injection which provides much greater enhancement. Depending on the minimum data acquisition time of the system and the number of slices to be performed, the sequence can be performed either with or without breath holding. If breath holding is used, held expiration is preferable as the degree of inspiration on

successive breaths can vary considerably and part of the organ to be imaged may be missed. However, most structures can be adequately examined in quiet respiration.

On images obtained during the first minute after a bolus injection, the contrast agent will be largely intravascular and hence the vascularity or otherwise of organs can be assessed. This has been shown to be of advantage in the staging of strongly enhancing tumours such as renal carcinoma [3,4] and bladder carcinoma [5]. Avascular lesions can also be demonstrated; the absence of perfusion will be seen as non-enhancement. An example of this is the detection of pancreatic necrosis which is an important indicator of poor prognosis in acute pancreatitis and is considered an indication for operative intervention in some centres [6,7,8]. Necrotic pancreas may be indistinguishable from normal pancreas on unenhanced images but is seen as an area of non-enhancement during an incremental dynamic sequence after a rapid bolus of intravenous contrast medium. The same technique also enables the demonstration of small pancreatic adenocarcinomas which appear as an area of non-enhancement. Furthermore, the detection of islet cell tumours is greatly improved as these should enhance strongly during the arterial phase (and later become isodense with normal pancreas).

Single Location Sequences:

These allow the observation of the change in enhancement in structures in one slice location with time following the administration of an intravenous bolus of contrast agent. An example of this is the technique used for the diagnosis and staging of thoracic aortic dissection [9]. A single location sequence with six images within one minute are performed at three different levels in the aortic arch. The accuracy of diagnosis is improved by demonstrating different enhancement within the true and false lumina due to the different flow rates within them. An intimal flap may not always be visible and a dissection could be missed if a single slice were performed when the two lumina are isodense. A similar technique can be used to evaluate vascular lung lesions [10], the phase and intensity of enhancement determining whether the mass arises from the pulmonary artery, pulmonary vein or soft tissue.

Such evaluation of function can be further improved by using the ability of CT to quantify x-ray attenuation. If this is done within a region of interest (ROI) during a single location sequence, the change in attenuation of a structure with time can be measured and displayed as a time-density curve (TDC). Most CT systems have the necessary computer software available and the construction of curves is not time consuming. In effect, it is the concentration of contrast medium within the ROI that is measured.

By studying time-density curves, different tissues can be characterised to a greater or lesser extent. The early portion of the curve (0 to 30 seconds) will largely reflect the perfusion of the tissue whilst the later portions will be determined by the blood volume of the organ, the capillary surface area and the permeability of the capillary basement membrane [11]. Dynamic CT has been used in this way to help tissue characterisation of tumours, such as cavernous haemangiomata of the liver [12] and cystadenoma of the pancreas [13] and in diffuse lesions such as hepatic cirrhosis [14].

Studying time-density curves from ROIs over the renal cortex and medulla allows information about renal function to be obtained, including assessment of glomerular filtration [15]. This has been used in the diagnosis of renal artery stenosis [16,17], in predicting the onset of the polyuric phase of acute tubular necrosis [18] and in assessing the function of renal transplants [19]. The time at which the aortic and renal cortical curves cross is said to reflect renal perfusion and the time when cortical and medullary curves cross correlates with glomerular filtration rate. Normal values for these times have been derived and, as a general rule, renal impairment is present if the cortex and medulla have not become isodense by 70 seconds, provided the patient is not dehydrated. An increased cortico-medullary

time does not predict the nature of the renal impairment which may be due to pre-renal (i.e. dehydration), renal and post-renal causes. Time-density data from the renal veins and inferior vena cava can be used to evaluate flow within these vessels. I have previously reported the application of this technique in the diagnosis of venous involvement by renal carcinoma [20].

Time-density data have been used to provide quantitative and semi-quantitative measurements of physiological processes by applying data processing techniques similar to those used in nuclear medicine. Axel et al [21] have described determination of cardiac output from analysis of aortic enhancement during the first pass of a bolus of contrast medium, based on the Stewart-Hamilton equation [22,23]. The application of deconvolutional mathematics to time-density data has allowed determination of mean transit times [24] which can be used to distinguish hepatic cirrhosis from fatty infiltration [25].

A number of methods for evaluating tissue perfusion by dynamic CT have been proposed, but all have their limitations and no fully quantitative method applicable to all tissues has been developed. The use of stable Xenon as a contrast agent for CT has allowed measurement of cerebral perfusion with reasonable accuracy [26]. However, such techniques require special equipment and the use of xenon is complicated

by significant side effects and flow activation. A number of methods for evaluating tissue perfusion using conventional iodinated contrast media with dynamic CT have been proposed (and are discussed in detail in Section 3.2). A semi-quantitative measure of tissue perfusion derived from comparing the maximum rates of enhancement of the tissue and aorta, similar to the perfusion index routinely used for radionuclide assessment of renal transplants, has been described by Jansen et al [27]. When applied to renal transplants, the technique was able to distinguish between rejection and Cyclosporin toxicity. Quantitative measures of perfusion have been described for the human brain [28] and for the canine kidney [29,30] and heart [31,32]. These techniques have a number of limitations and, in particular, cannot be applied to all tissues. Until recent publication by myself of an image of renal perfusion [33] based on work presented in this thesis, parametric images of physiological parameters (including relative but not absolute perfusion) derived using iodinated contrast media and dynamic CT had only been described for the brain [34-38]. Furthermore, the analysis used for such brain studies required complex curve fitting procedures for individual pixel time-density curves and was rather time consuming.

1.4 Aims of this study:

Assessment of the value and use of dynamic CT in functional imaging is as yet far from complete. This thesis describes the development and evaluation of a new method of measuring tissue perfusion using iodinated contrast agents and dynamic CT. The concept arose out of my fortunate position of working in both radiology and nuclear medicine. I was thus able to envisage how nuclear medicine data processing techniques might be applied to dynamic CT data. The technique so derived is relatively simple, provides absolute quantification, is applicable to multiple organs and suitable for the generation of functional images with high spatial resolution.

The technique has been applied to patients and the results inseveral organs, both normal and diseased, are presented and evaluated. Patients were recruited from three sources: 1) The perfusion examination was performed as part of a research protocol approved by the local ethics committee. 2) A single location dynamic CT sequence had been performed for clinical reasons (e.g. evaluation of renal veins for thrombosis [4], possible cavernous haemangioma of the liver [12]) providing an opportunity for perfusion measruements to be made from the same data. 3) Later, as experience was gained, some patients were referred for perfusion studies on clinical grounds. Data for individual organs were derived either from the organ under clinical scrutiny or when an organ was coincidentally included on the anatomical slice under study.

The advantages and drawbacks of the technique, its relation to other non-invasive methods for evaluating blood flow and its potential applications are discussed.

2. EQUIPMENT:

2.1 Construction and operation of computed tomography systems.

2.2 Data processing equipment.

2.3 Potential errors in time-density curve construction.

2.4 Assessment of photon noise of a computed tomography system.

2.1 Construction and operation of computed tomography systems:

Computed Tomography (CT) systems use x-rays to produce images of the body in cross section, thereby allowing organs to be visualised without being obscured by overlying tissue. The basic principle is that the internal structure of an object can be reconstructed from multiple projections of that object. X-ray projections of the object are derived by passing a beam of x-rays through a thin cross section of the patient whilst measuring the transmitted radiation with a sensitive radiation detector placed opposite the x-ray source. The numerical data acquired is processed by a computer to reconstruct the image.

The equipment comprises the x-ray tube and an array of detectors mounted in an opposing fashion on a circular gantry. Commonly, the detector is an ionisation chamber filled with compressed Xenon gas. The gantry is rotated around the patient who lies on a movable table near the centre of rotation of the gantry. During the rotation, a thinly collimated beam of x-rays is produced and the intensity of beam emerging from the patient is recorded by the detectors. The thickness of the beam determines the slice width and is controlled by collimators positioned close to the x-ray tube and also adjacent to the detectors. The computer is not only used for data processing but also controls the data acquisition parameters including movement

of the gantry and table, slice thickness and the x-ray exposure factors. For each projection, the amount by which the intervening soft tissue attenuates the beam (linear attenuation coefficient) is calculated from:

$$N_t = N_0 \, e^{-\mu x}$$

where N_t is the number of transmitted photons, N_0 the number of initial photons, x the thickness of tissue and μ the linear attenuation coefficient. This attenuation coefficient is usually converted to an attenuation value, measured in Hounsfield Units (HU), by comparison with the linear attenuation coefficient of water as follows:

$$\text{Attenuation Value (HU)} = \frac{\mu_{tissue} - \mu_{water}}{\mu_{water}} \times 1000$$

Thus water has an attenuation value of 0 HU and air (linear attenuation coefficient virtually zero) -1000 HU.

The final image is displayed as a matrix of tiny picture elements or pixels. For modern scanners the matrix used is usually 512 x 512 or 1024 x 1024. Each pixel will represent the attenuation value coefficient of a volume of tissue or voxel with a cross-sectional area determined by the pixel dimensions but a depth equal to the thickness of the slice examined. The value of attenuation for an individual pixel is represented as a shade of grey from a grey scale (ranging from black; low attenuation e.g. air, to white; high attenuation e.g. bone) The values represented by the grey

scale can be chosen by the operator using computer software; a process known as "windowing". The value represented by the mid point of the grey scale is determined by selecting the window level, whilst the window width prescribes the range of attenuation values represented by the scale. Thus a typical window level, of 40 HU with a width of 300 HU will display all values from -110 HU (black) to 190 HU (white).

The image is reconstructed from the series of projections obtained at different tube positions by the computer using a mathematical process known as filtered back projection. The image can be considered as a matrix of numbers i.e. attenuation values comprised of several rows or rays. The values of the attenuation measurements made from the first projection are projected back into the matrix along these rays. This is repeated for all of the projections obtained during the scanner rotation and as the rays from different projections overlap, the final attenuation values are determined. To prevent a star artefact which is particularly likely to occur with sudden changes in attenuation, the projections are filtered before back projection to reduce their high frequency components (i.e. sudden changes). The characteristics of the filter can be chosen by selecting different reconstruction algorithms. A high resolution algorithm will suppress only the very highest frequency components of the image to maintain resolution. However, noise within the image is typically of high frequency also,

so that images reconstructed with such a filter will contain more noise and appear "grainy". So called "soft tissue" reconstruction algorithms will suppress more of the higher frequencies thereby reducing noise but also reducing spatial resolution.

During the development of CT equipment, a number of technological advances have occurred to allow improvements in dynamic CT techniques. As design of the x-ray tubes has improved, data acquisition times have become shorter; now as short as 0.7 seconds for a complete tube rotation. In an early attempt to reduce data acquisition times, image (or data) segmentation was performed. This describes only using data from part of the rotation for image reconstruction. Although proposed to enable more accurate determination of peak aortic enhancement [39], generally the benefits of the technique were offset by an associated increase in image noise. Also, the heat dissipation of x-ray tubes has become better, enabling the delay between consecutive data acquisitions for tube cooling to be reduced (and even become unnecessary on some equipment).

Until recently, there has been a minimum time delay between data acquisitions to allow reversal of the direction of rotation of the gantry. This change in direction was required to prevent twisting of the cables supplying high voltage to the x-ray tube and passage of data from the detectors to the computer. This problem has now been eliminated by advances in

slip ring technology. Electrical connections to the gantry are made using these slip rings which allow continual rotation of the gantry in one direction.

An alternative approach to such rapid CT is provided by the ultrafast CT systems (e.g. Imatron). Rather than use a rotating gantry, such equipment comprises a special large x-ray tube with a curved target arranged in an arc around the patient and an array of detectors opposite. An electron beam is rapidly moved around the target under electrical control in a manner similar to the electron gun in a television set. (Figure 2.1) Thus, there are no moving parts and data acquisitions can be performed in as little as 50 milliseconds. However, image reconstruction relies on a less than 180^{o} data set and so, as for the image segmentation techniques described above, image noise is increased making individual pixel measurements of attenuation less accurate.

Compared with many other radiological procedures, CT examinations are often associated with a moderately high radiation dose to the patient. This becomes increasingly important with more modern CT systems as, for single location dynamic techniques, the number of data acquisitions is no longer limited by the capabilities of the machine. For instance, a system developed in the early 1980's (the IGE 8800) could only manage 7 data acquisitions during a 60 second study (which would include arterial and venous

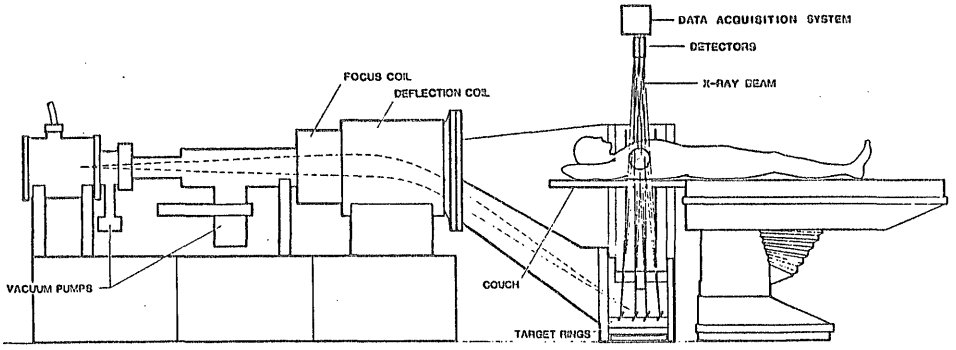

Imatron C-100 Cine-CT Scanner: Longitudinal View

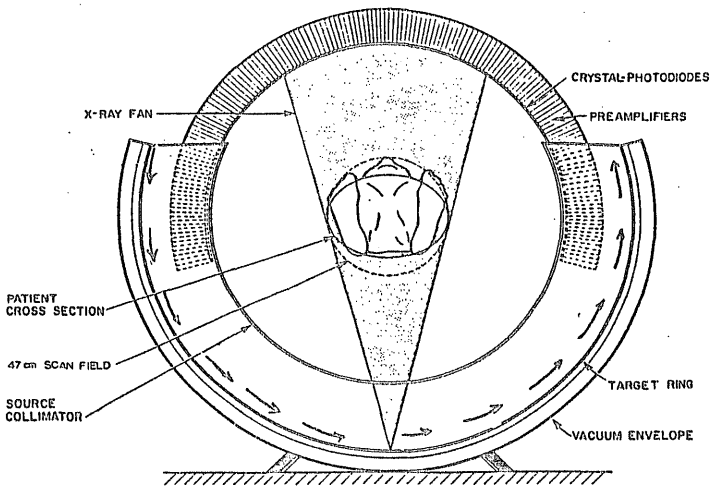

Imatron C-100 Cine-CT Scanner: Cross-Sectional View

Figure 2.1 The "Imatron" ultrafast CT system.

phases). By contrast, a more modern system (the Siemens Somatom Plus) with continual rotation capabilities can perform 24 data acquisitions within 24 seconds. However, a larger number of images acquired through the same volume of tissue significantly increases the radiation dose received by the patient. Whole body dose equivalents have been determined for CT systems using a phantom and thermoluminescent dosimeters [40]. For an examination of the upper abdomen comprising 13 slices of 10mm thickness, the mean dose (whole body equivalent) was 3.7 mSv with a range of 2.5 mSv to 7.4 mSv, depending on the CT system used. Thus, for most systems, a typical single location sequence comprising 10 data acquisitions will be associated with a radiation dose of less than 5 mSv; the annual limit for members of the public. For studies of cerebral perfusion, the radiation dose from dynamic CT is more favourable. Whilst clearly greater than for techniques without ionising radiation, such as magnetic resonance, the radiation dose from a cranial CT examination is generally less than that received from equivalent radionuclide investigations. A typical CT study comprising 10 single level contrast enhanced data acquisitions (iodinated or xenon) will typically be associated with an effective whole body dose of 0.5mSv (range 0.23 to 0.7mSv) [40], which compares to 8.9mSv for a ^{99m}Tc exametazine (HMPAO) cerebral perfusion single photon emission tomography study (using 550 MBq) or 1.7mSv for a $^{15}C\text{-}O_2$ positron emission tomography examination (4200 MBq).

The balance between frequency of data acquisitions and radiation burden will always be a compromise but radiation doses should be kept as low as reasonably achievable. With faster CT systems, this requirement can be met with little loss of information by varying the time between acquisitions over the duration of the study. Thus, early in the sequence data acquisitions are performed rapidly, say every 3 seconds, as this is the period during which contrast medium concentrations within structures are changing most rapidly. Later in the sequence, when such changes are less rapid, the interval between data acquisitions can be increased to 5 or even 7.5 seconds.

Two CT systems were used for the work presented in this thesis: a) an IGE 8800 system (General Electric), located at the Leicester Royal Infirmary and b) a Somatom Plus system (Siemens), located at Addenbrooke's Hospital, Cambridge. The latter machine is more modern. The single location dynamic scanning capabilities of the two systems are compared in Table 2.1.

TABLE 2.1: Comparison between IGE 8800 and Somatom Plus CT systems.

	IGE 8800	Somatom Plus
Minimum Data Acquisition Time:	6 sec	0.7 Sec
Minimum Interscan Delay:	2 sec	0 sec
Time-density curve software available:	Yes	Yes
Continual Rotation:	No	Yes

2.2 Data processing equipment.

Many CT systems have dynamic evaluation software installed in their computer systems to allow construction of regions of interest (ROI) and display of time-density data. Some systems perform simple numerical analyses (e.g. maximum change in attenuation value, time to peak enhancement) or curve fitting procedures (e.g. gamma variate). A few systems allow generation of some parametric images such as time to peak enhancement. As yet, no manufacturers offer commercial software packages to calculate tissue perfusion, but Siemens have produced prototype software, based on the technique developed in this thesis, which is currently under evaluation at Addenbrooke's Hospital.

With the intention to develop new data processing techniques, the standard commercially available time-density analysis programmes were considered too limited for the purposes of this thesis. Initially, the data acquisition times and corresponding attenuation values from regions of interest were manually entered into an IBM compatible personal computer. To produce the first perfusion images, transfer of data was somewhat laborious. The image data from the single location dynamic sequence were down-loaded onto floppy disc in compressed format. These were then decompressed using software on a radiotherapy planning work-station that was already in use in the radiotherapy department. The decompressed images were then transferred via a serial link

to an IBM personal computer for final processing to produce the perfusion image. Later, a direct serial link (supplied by Siemens UK) from the Siemens Somatom Plus CT system to a separate work station, an Acorn Archimedes (Acorn, Cambridge UK), was used. Appropriate software for all data analysis was written to run on this separate work station (by M.P.Hayball; see acknowledgements).

2.3 Potential errors in dynamic CT and time-density curve construction.

When quantifying physiological processes using time-density measurements, errors will be caused by any change in the measured attenuation within a region of interest or pixel that is not due to a change in the concentration of iodinated contrast medium.

These errors fall broadly into two areas; 1) errors arising from variations in the equipment and 2) errors arising from the subject studied. The accuracy of perfusion calculations may also be affected by the quality of the bolus of injected contrast medium.

1. Errors due to the equipment:

a) Photon Noise: When using an x-ray tube as a source of radiation, there is an inherent statistical variation in the production of the x-ray photons. This is a variation of both intensity and energy of the photons (although the maximum photon energy is limited by the voltage applied across the tube). With plain film radiography this can produce an effect known as "quantum mottle". Also with CT equipment, there will be similar variations in the detector measurements. These effects are known as photon noise and produce a variation in the measured attenuation value within any individual voxel. Thus for a phantom of uniform density, such as water, a range of attenuation values for each pixel of the image is

produced. These will be distributed around a mean value with a normal of Gaussian distribution pattern. If a region of interest of sufficient size is constructed, values for the mean attenuation and the standard deviation can be derived. Furthermore, if the phantom is examined repeatedly, the attenuation value for a given pixel will vary between data acquisitions, the values again being distributed normally about a mean.

The photon noise to signal ratio can be reduced by increasing the amount of radiation. This can be achieved by increasing the tube current (mA) or lengthening the time of each tube exposure; either by increasing the pulse width (in systems using pulsed x-ray beams, such as the IGE 8800) or prolonging the data acquisition time. Improving detector sensitivity or selecting a "soft tissue" reconstruction algorithm will also reduce photon noise.

When constructing time-density curves, the size of the area of interest will alter the effect of photon noise. A large region of interest will be relatively unaffected, as the effect of the noise will tend to be cancelled out across the region. For small regions of interest or individual pixels the sampling error will be increased. Thus a large as possible region of interest should be used whilst avoiding partial volume effects from regions close to the edge of an organ (see below) and not including tissue areas where there

are inherent variations in attenuation.

b) Detector Calibration Errors: on a third generation scanner such as the IGE 8800, a detector calibration error in one detector will produce ring artefacts of alternating increased and decreased density on the image. In systems with a complete ring of detectors the effect of one badly calibrated detector will be less perceptible. Furthermore, if the whole detector system is calibrated badly, the attenuation value returned for a region of interest or individual pixel will be incorrect.

To avoid these problems, a phantom of known attenuation is examined daily. With some systems, the air within the gantry can be used for detector calibration whilst in others a water or polythene phantom is used. Such phantom studies will both confirm that the correct attenuation value is being returned for a region of interest and that there are no ring artefacts from a single detector calibration error.

c) The effect of data acquisition time: If the attenuation within a region of interest, such as over the aorta, is changing rapidly during a single location sequence, then these changes will be averaged over the time span of the data acquisition. With a relatively long data acquisition, such as 6 seconds, which is the shortest available on the IGE 8800, the effect on time-density curves derived from the aorta is to flatten the peak seen after the injection. This error can

be reduced by segmentation of the images [39]. This may improve the accuracy of time-density constructed from the sequence as there can be up to three times as many points but there will be an associated increase in photon noise. With more modern equipment, segmentation of images is not necessary as data acquisition times of one second or less are available without segmentation.

2. Subject dependent errors;

a) Variation in tissue attenuation.

In any one organ, the attenuation of the parenchyma may vary depending on the location of the region of interest within the organ. For example, in the liver large portal veins usually have a lower attenuation than the liver parenchyma itself. If a region of interest contains several large portal veins, then the mean attenuation of that region will be affected. Furthermore, after intravenous contrast medium the pattern of enhancement with time within that region of interest will also be affected as the portal veins will enhance at a different time and to a different extent compared with liver parenchyma.

Tissue may also show artefactual variation in attenuation with time even without the administration of contrast medium due to other effects such as the effect of respiration or

posture. An example of this is seen on the effect of inspiration and expiration and posture on the CT appearances of the lung. The attenuation within a given region of interest will be higher on expiration and in dependent parts of the lung.

Errors of this nature can be minimised by careful choice of imaging protocol with reference to respiration and posture and by defining regions of interest that avoid potential sources of error (such as blood vessels within the organ).

b) Artefacts:

Several artefacts occur in CT studies which affect the attenuation value returned for a particular region of interest. These include i) the partial volume effect, ii) streak artefacts due to movement, iii) artefacts due to regions of very high density and iv) beam hardening.

i) Partial volume effect: The attenuation value determined for each picture element (pixel) of the CT image reflects the attenuation of a volume of tissue (voxel) whose dimensions are the pixel area by the slice thickness. The attenuation value calculated for the voxel is an average of all the materials within it. Thus if a voxel contains a small amount of bone, the attenuation value will be increased; if it contains some fat then it will be decreased. With time-density curve construction this can be a problem when

assessing small or thin structures such as blood vessels, for example the renal veins. Not only will fat around the vessel reduce the base line value for the curve, but any movement of the patient during the imaging sequence may alter the proportion of fat within the voxel providing a potential source of error. Movement of this kind is usually due to changing position of the structure under study with respiration. Imaging protocols with sequences performed in quiet respiration are usually satisfactory unless dyspnoea increases the excursion of the respiratory movements. Protocols with suspended respiration are also prone to errors of this kind as the position of suspended respiration may not be exactly reproduced with each breath-hold, causing alteration of the position of structures in relation to the scanning location. The position held in suspended expiration is less variable than that held in suspended inspiration. The flushing that may be experienced by the patient after a rapid bolus of iodinated contrast medium can exacerbate problems with movement but can be minimised by using low osmolar agents and careful instruction of the patient beforehand (see Chapter 3).

ii) Movement artefacts: Physiological movements during a data acquisition can produce artefacts which appear as streaks of alternating increased and decreased density across the image. They usually originate from regions of large density differences such as gas in bowel or the cardiac-lung interface. The mean attenuation within a region of interest

incorporating such an artefact will clearly be affected. These artefacts are best avoided by using short data acquisition times, although the effect of moving bowel can be reduced by administering drugs that suppress peristalsis (such as glucagon or hyoscine-N-butylbromide).

iii) Areas of very high density: Metallic structures or residual barium in bowel can cause serious artefacts on account of their high density. The artefact appears as a starburst pattern extending across the image. The artefact results from the object absorbing so much radiation that the detectors measure no transmitted radiation along that line. This makes the value for all points along that line meaningless. The centre of the high density zone may appear as black because the calculated density of the area is greater than the range which the machine can represent.

iv) Beam hardening: The x-ray beam emitted from the tube contains a spectrum of x-ray energies. The attenuation of the lower energy photons by an object is higher than for the higher energy photons. Thus as the beam passes through an object the average energy of the beam increases as the lower energies are preferentially absorbed. This means that the attenuation of areas towards the centre of an object of uniform density will appear lower. In practice, this is only a problem when the beam has passed through large expanses of bone (such as between the shoulders). Furthermore, there are

design features included in most CT systems to correct for this effect. Many machines will have a filter in the gantry and computer software able to perform a correction for beam hardening prior to reconstructing the images.

3) Bolus quality:

Bolus quality is an important consideration. A narrow bolus is required for accurate perfusion measurements so as to avoid errors due to loss of contrast medium from the tissues before the time of maximal enhancement (see Chapter 3). The 50ml bolus used in the studies in this thesis is relatively large. A smaller bolus, perhaps of 25 ml, will make a narrow bolus easier to achieve but this is at the expense of reduced tissue enhancement and hence greater susceptibility to noise. A mechanical pump injector was not used for injection of contrast medium. Adequate bolus quality can be achieved by hand injection where 50 ml of warm contrast medium can be injected in approximately 7 seconds. A narrower bolus shape within the aorta may not be obtained with a more rapid injection due to bolus spreading within the lung [41]. Many other factors can alter bolus shape in a manner not readily predictable including cardiac output and central blood volume. However, a wider bolus with lower peak aortic enhancement will be associated with a lower rate of tissue enhancement and thus, to some extent, the effects of slight variations in bolus shape should cancel each other out.

2.4 Assessing the photon noise of a computed tomography system.

Evaluation of the noise characteristics of a CT system is essential prior to quantification of physiological processes using time-density data. This will determine the smallest size of region of interest that can reasonably be used and indicate the magnitude of error in subsequent measurements. A series of sequential attenuation measurements of a phantom of known attenuation (e.g. water of polythene) will vary due to photon noise. This section describes such an evaluation on the IGE 8800.

Method:

A polythene phantom of attenuation -112 HU was used. A series of seven data acquisitions were performed without table movement using the same protocol as used in a clinical setting (i.e. pulse width 2.7 msec, data acquisition time 6 seconds). Regions of interest of sizes 1, 4, 9, 16, 25, 64, and 100 pixels were constructed within the resulting images of the phantom and a series of seven measurements derived for each. The mean attenuation value and standard deviation were calculated for each series of measurements.

The same data acquisitions were then processed using image segmentation software. This enabled production of a series of 21 images by using data from only part of each rotation to produce an image. Each image used data from 240^{o} of tube rotation and hence the segments overlapped. Using the same sized regions of interest, mean attenuation values and standard deviations were calculated for each series of 21 measurements.

Graphs plotting standard deviation against size of region of interest were plotted for both processing methods.

Results:

The standard deviation of the mean from the series of measurements are recorded in Table 2.2 and displayed in figure 2.2. Figure 2.3 shows the time-density curves with and without segmentation processing for regions of interest of 1, 9 and 100 pixels size. The photon noise can be seen to have a greater effect the smaller the region of interest, as shown by the increasing standard deviation of the mean measurement. Image segmentation had no significant effect on the standard deviation values.

TABLE 2.2: Mean and Standard Deviation (SD) of the series of attenuation from various sizes of ROI, with and without image segmentation. (Data from the IGE 8800 CT system)

	No segmentation		Segmentation	
Number of pixels	Mean(HU)	SD(HU)	Mean(HU)	SD(HU)
1	-124.14	16.17	-108.95	10.52
2	-116.71	10.33	-115.67	9.31
4	-110.14	6.87	-113.48	6.25
9	-114.00	2.88	-109.19	3.82
16	-110.71	2.86	-113.52	2.38
25	-112.00	1.41	-112.81	1.87
64	-111.43	1.29	-111.57	0.95
100	-112.57	0.49	-112.62	0.95

The effect of size of region of interest on photon noise.

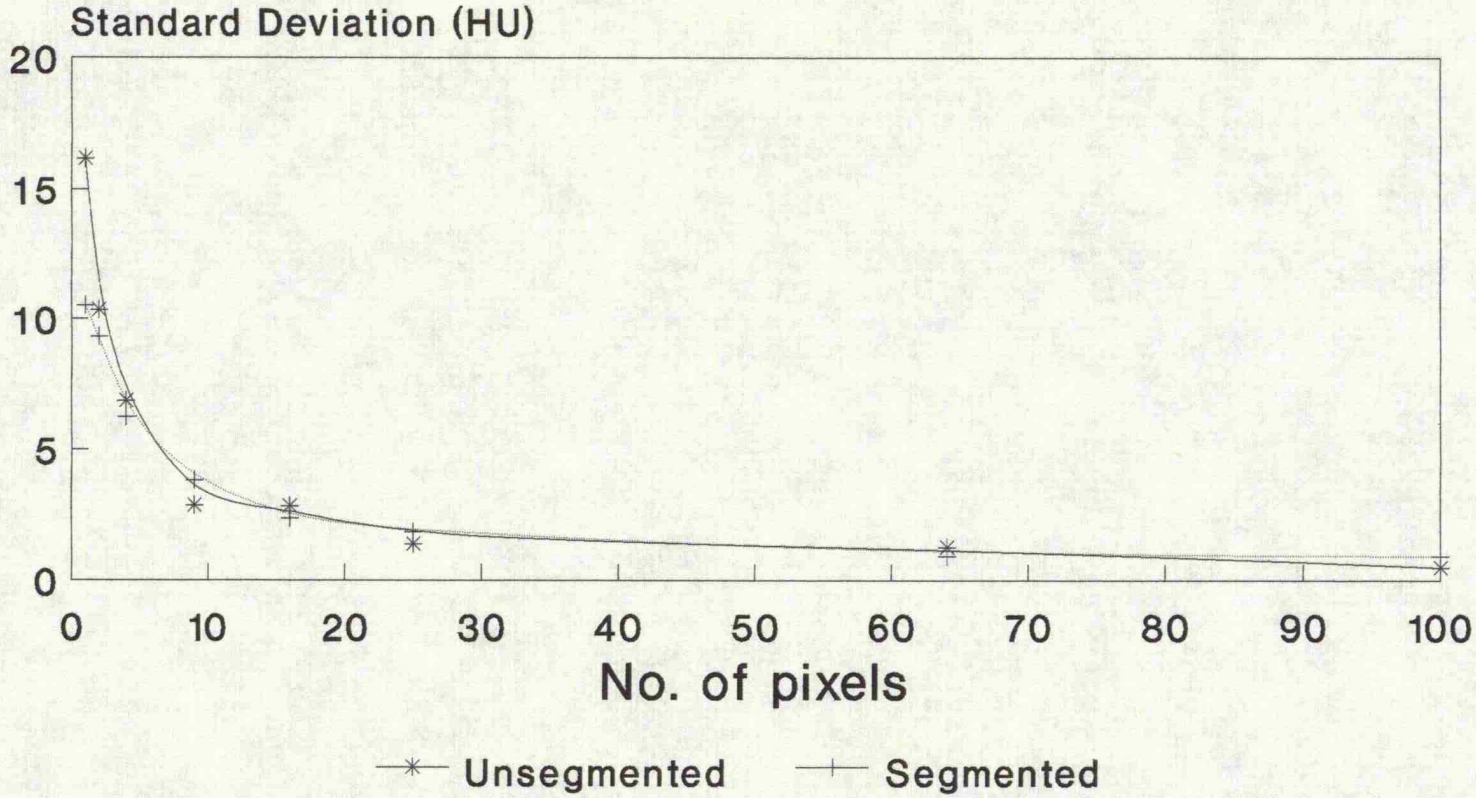

Figure 2.2

Time-density curves using different sizes of region of interest:
A: non-segmented images

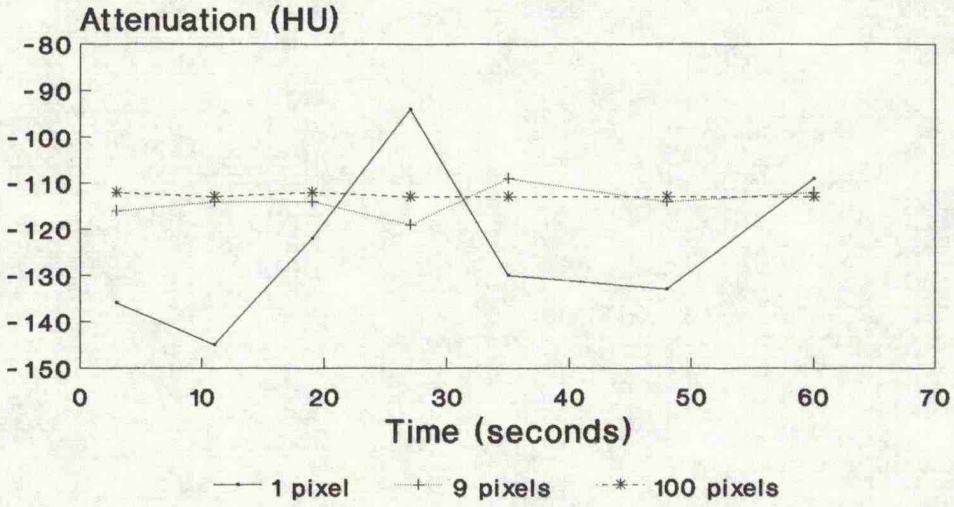

B: segmented images

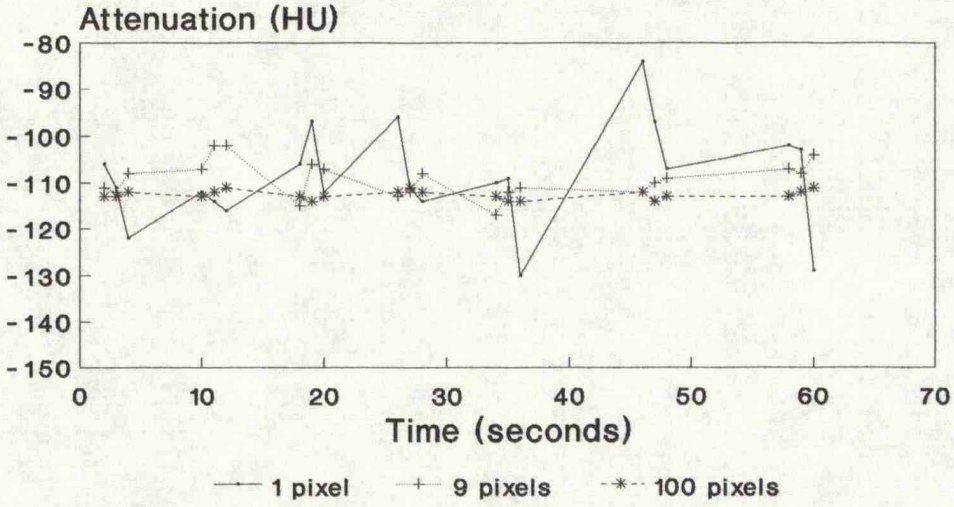

Figure 2.3

Discussion:

Performing such measurements enables the smallest size of region of interest that can be reasonably used for time-density measurements to be determined for any particular CT system. For the IGE 8800, a region containing no fewer than 16 pixels is likely to be acceptable as the error will be approximately +/- 5HU (2 standard deviations). Clearly, larger regions of interest should be used whenever possible. The noise characteristics of the more modern Siemens Somatom Plus system are much superior [42]. A region of interest of 4 pixels (equivalent in area to 1 pixel size on the IGE 880 due to the 1024 x 1024 display matrix used on the Somatom Plus as opposed to the standard 512 x 512 matrix) has a typical standard deviation of only 1 HU. This is likely to be due to superior performance of the detectors as the amount of radiation produced by the x-ray tube will be limited by dosimetry considerations. The low noise level of the Somatom Plus means that reasonable accuracy can be achieved with time-density curves derived from individual pixels. This makes derivation of functional images feasible whereas this would not be possible using the IGE 8800.

3.THEORETICAL BASIS OF DYNAMIC CT PERFUSION MEASUREMENTS:

3.1 Contrast media for computed tomography; Xenon and conventional iodinated agents.

3.2 Existing CT techniques for assessing perfusion.

3.3 Proposed method of perfusion measurement.

3.4 Proposed method for assessing perfusion of the liver.

3.5 Functional imaging.

3.6 Relation to existing CT techniques.

3.1 Contrast media for computed tomography; Xenon and conventional iodinated agents.

There are two types of contrast media available for CT; stable xenon and conventional iodinated agents. Both types of agent produce enhancement of images by increasing the x-ray attenuation of the tissues to which they are distributed on account of the high atomic number of the xenon or iodine. Xenon is administered as a gas by inhalation whereas conventional iodinated agents are usually given intravenously.

Xenon:

The utility of stable xenon as an indicator of cerebral perfusion was first proposed by Winkler et al [43]. It is highly lipid soluble and freely crosses the blood-brain barrier. Cerebral perfusion is determined by studying the rate of wash-in (and sometimes wash-out) of xenon in different regions of the brain.

The amount of brain enhancement, and hence the signal to noise ratio, is limited by the administered concentration of Xenon gas. At a concentration of 80%, xenon is a potent anaesthetic agent and even concentrations of 50 to 60% may cause sedation, bronchospasm or respiratory depression. 33% Xenon (with 67% oxygen) is tolerated by 90% of patients [26] and yet transient sensory disturbances or occasionally

respiratory depression may occur. Blood pressure, arterial oxygen saturation, end tidal CO_2 concentration and respiratory rate should also be monitored continuously during the study.

A further problem is the flow activation in the brain that may occur during Xenon inhalation, although such an error is likely to be small compared to the effects of photon noise [44]. Movement of the patient between data acquisitions will also cause artefacts due to mis-registration of images from the sequence. The tendency for movement is increased by the sensory disturbances caused by the Xenon inhalation which some patients find distressing. Movement can be minimised by adequate preparation of the patient, reassurance during the study and a suitable head holder.

Conventional Iodinated Contrast Media:

By the time CT scanning was developed, organic contrast media for intravascular administration were used primarily for imaging the renal tract and vascular system. Intrathecal agents were available for myelography. The degree to which a contrast agent is radio-opaque depends upon the concentration of iodine and this is usually stated on the preparation (e.g. 300 $mg.ml^{-1}$). Over the range of attenuation changes associated with typical blood or tissue concentrations of contrast media, there is a linear relationship between contrast medium concentration and attenuation value. An

iodine concentration of $1mg.ml^{-1}$ increases the x-ray attenuation as measured by CT by 25 HU [45]. Thus time-density data acquired from a dynamic CT study directly correspond with temporal changes in contrast concentration.

Iodine in the form of the iodide ion is too toxic for use as a contrast agent, and thus iodine is incorporated into organic molecules. Initially, these molecules were in ionic form, being salts of meglumine or sodium. However, at concentrations sufficient to produce adequate contrast, these compounds have an osmolarity markedly greater than plasma and this causes some of the adverse effects of such agents. By increasing the number of iodine atoms per molecule and creating non-ionic compounds (thereby loosing the osmolar effect of the anion) modern low osmolar contrast agents were produced.

Adverse Reactions:

These may be due to either a) the hyperosmolarity of the agent or b) idiosyncratic or allergic responses.

Perhaps the most immediate effect of the increased osmolarity of contrast media is vasodilatation [46] occurring in most tissues apart from the kidney which demonstrates a transient vasodilatation followed by vasoconstriction [47]. After systemic administration, this causes a feeling of warmth which can be intense and uncomfortable for the patient. This

in turn can cause the patient to be restless and artefacts may result if such movement occurs during a single location dynamic sequence (see section 2.4). If vasodilatation is marked, this can lead to systemic hypotension with diminished venous return to the heart. However, this rarely occurs with the lower osmolar agents. The hyperosmolarity can produce an increase in circulating blood volume (as much as 10% with ionic agents) due to osmotic attraction of extracellular fluid [48]. High intravascular concentrations can also cause loss of intra-erythrocytic water leading to rigidity of red blood cells and a reduction in the deformability required to pass through capillaries [49].

All these haemodynamic effects must be considered when using contrast media as physiological indicators. Because of these effects, contrast agents cannot strictly be considered tracers as tracer theory specifies that the administration of the agent should not alter the system under study. When using radiographic contrast media to study blood flow, this clearly may not be the case. However, the vasodilation and hypervolaemia are unlikely to occur within the time course of a first pass study and, with intravenous administration, concentrations will not be sufficiently high to produce significant red cell changes.

Many mechanisms have been postulated for the allergic and idiosyncratic reactions, including the release of vasoactive

substances such as histamine [50]. These mechanisms will not be considered in detail, but any potential haemodynamic effects are unlikely to be significant within the first pass, unless a severe reaction occurs causing circulatory collapse. However, such adverse reactions will create a morbidity and mortality associated with CT studies to evaluate blood flow. Intermediate reactions include urticaria, bronchospasm and moderate hypotension and occur in less than 2% of administrations. Severe reactions occur in less than 0.2% and the risk of death is about 1 in 20 000 to 40 000.

Pharmacokinetics of Iodinated Contrast Media:

After injection into the vascular system, contrast agents rapidly distribute through the tissues with a volume of distribution similar to that of the extracellular space. Thus, for the first 40 to 60 seconds, contrast agents will be largely intravascular. The rate of subsequent passage into the extracellular space of a particular organ will depend on the blood flow, capillary surface area, capillary permeability and the amount of protein binding of contrast agents within the blood [51]. Excretion is by glomerular filtration and hence contrast agents have similar kinetics to the tracer DimethylTriethylPentacetic Acid (DTPA) used extensively in nuclear medicine.

Despite the differences in physicochemical properties, the kinetics of all contrast agents are broadly similar [52]. The choice of contrast medium is largely determined by its osmolarity and viscosity. A low osmolar agent is advisable to minimise the chance of movement of the patient due to flushing or nausea, and low viscosity allows a more rapid bolus injection (unless an injection pump is used). Although ionic contrast media do have a lower viscosity than the low osmolar agent, the benefit is not sufficient to outway the disadvantages of the associated increase in side effects.

3.2 Existing CT methods of assessing perfusion

Although the use of CT has been predominantly as an anatomical imaging modality, techniques for both qualitative and quantitative assessments of tissue perfusion have been described. These techniques use one of the two available contrast agents as a physiological indicator; either stable Xenon or iodinated contrast media.

Xenon enhanced CT:

The xenon technique for determination of cerebral perfusion is as follows: After two baseline images (subsequently averaged) at two or three different slice locations, xenon is administered to the patient by inhalation over 4 to 5 minutes during which three to six enhanced images are acquired at each anatomical level. The concentration of xenon within brain tissue at any time will depend upon the arterial concentration, tissue perfusion and the blood/brain partition coefficient (see appendix 3.2.1 for mathematical derivation). The arterial concentration is determined indirectly by assuming instantaneous equilibrium with end-tidal pulmonary xenon concentration which can be measured using a thermoconductivity analyser. The value for perfusion, expressed in $ml.min^{-1}100g^{-1}$ tissue, is calculated for each pixel thereby creating a quantitative perfusion map. Values for perfusion can also be determined from analysis of data derived from regions of interest. This has the benefit of

reducing inaccuracies due to noise that is inherent in the system but such regions are likely to include both grey and white matter. The typical error from a 1 cm^2 region is about 12% [26].

More recently, wash in/wash out protocols have been developed [53,54] which benefit from a shorter inhalation, with a lower probability of flow activation or movement of the patient, and improved noise characteristics.

Xenon CT techniques have been validated in baboons by comparisons with radiolabelled microspheres, showing a high degree of correlation over a wide range of flows [55]. The clinical situations in which it has been used include acute stroke, occlusive vascular disease, carotid occlusion testing, vasospasm, arterio-venous malformations and head trauma [26]. However, it has not been applied to organs other than the brain.

Conventional Contrast Enhanced Dynamic CT:

Quantitative or semi-quantitative methods of assessing tissue perfusion with iodinated contrast media have been applied only to three organs; the brain, the kidney and the heart. All techniques have required single location dynamic scanning and some have been described only for ultra-fast CT systems. Much of the research has been limited to animals.

The use of dynamic CT following intravenous bolus administration of iodinated contrast agents for determination of tissue perfusion was first proposed by Axel in 1980 [28]. He described a technique for measuring cerebral perfusion using rapid sequences on existing CT equipment but also proposed application of the Stewart-Hamilton equation to arterial time-density data to determine the cardiac output and central blood volume [21]. He considered iodinated contrast media to be a non-diffusible tracer (unlike xenon) as within the intact brain it is unable to cross the blood-brain barrier and therefore will remain entirely intravascular. However, even when the blood-brain barrier is damaged (or at sites elsewhere in the body), the amount of contrast medium passing from the vascular compartment into the extracellular space within the first 40 to 60 seconds is minimal and so, during the first pass following bolus injection, contrast agents will be largely intravascular.

The method requires determination of the mean transit time from the temporal changes in contrast medium concentration in brain substance and blood. The theory is outlined in appendix 3.2.2. Axel suggested that, in practice, due to technical difficulties in acquiring an arterial time-density curve within the brain, the reciprocal of transit time could more readily be used as a measure of relative perfusion.

The following year, Axel with coworkers from the same institution had applied the technique pixel by pixel, producing a functional image of relative cerebral perfusion, illustrated by a case of carotid occlusion with cerebral infarction [34]. In 1983, Axel also described an alternative method for determination of transit time by using constrained deconvolution [24]. However, using this technique with an assumed brain fractional blood volume of 5%, cerebral blood flow tended to be over estimated (e.g. grey matter perfusion was measured as 115 $ml.min^{-1}$100 ml $tissue^{-1}$.)

Other workers have applied similar techniques to measure cerebral perfusion to series of patients. Cases of acute stroke have been studied both with region of interest analysis [56] and functional imaging [38], demonstrating a correlation between severity of haemodynamic change and clinical outcome. Dynamic CT with functional imaging has also been used to study the haemodynamics of arterio-venous malformations [35], following extracranial-intracranial by-

pass surgery [36] and cerebral tumours [37]. No workers have directly validated their work against a gold standard such as microspheres, but comparison with radionuclide cerebral perfusion imaging has been performed [38].

Renal time-density data from rapid CT sequences were first studied in detail by Ishikawa et al in 1981 [15] who observed that the initial part of the cortical curve is influenced by perfusion. Later, these workers proposed that the time taken for the aortic and cortical time-density curves to cross could be used as a measure of perfusion [18]. They recorded an increase in this parameter in the oliguric and polyuric phases of acute renal failure with a return to normal values occurring in the recovery phase. Fuld et al [19] used the same method of analysis to study renal transplants and observed an increase in the cortico-aortic time in transplant rejection. Although this methodology has never been directly validated, Fuld et al [19] describe a "complete correlation between the dynamic CT and radionuclide studies" but give few details.

Another semi-quantitative method of assessing renal cortical and medullary perfusion using dynamic CT was reported by Jansen et al in 1987 [27]. The ratio of the slopes of renal cortical or medullary time-density curves and the slope of the aortic time-density curve was used as an index of perfusion in a way analogous to that used in dynamic renal

studies with radionuclides. This technique was able to distinguish between renal transplant rejection and cyclosporin toxicity, there being a greater reduction in cortical perfusion in the later condition. They also measured the aorto-cortical junction time, as described by Ishikawa but changes in this parameter did not mirror the results obtained using the slopes ratio method. This finding raises doubt as to whether the aorto-cortical junction time truly reflects only perfusion.

Absolute measurements of renal cortical and medullary perfusion have been performed using ultra-fast CT equipment as described by Jaschke et al [29,30], but studies to date have been limited to the experimental dog. The theory is based on the Mullani-Gould application of the Fick principle [57] and requires time-density curves from the aorta, renal vein and renal cortex or medulla. (see appendix 3.2.3 for theory.) The requirement for renal vein data limits the technique to only studying the slice location at the level of the renal hilum. Also, as all the renal cortex contributes to the renal vein output, intrarenal variations in cortical perfusion cannot be measured. Indeed, uniform cortical perfusion must be assumed, which may not be the case in practice.

The technique described by Jaschke et al [29,30] has been validated against radiolabelled microspheres for a wide range of perfusion values. Normal canine cortical perfusion was

measured 5.3 $ml.min^{-1}ml^{-1}$ and inner medullary perfusion at 0.45 $ml.min^{-1}ml^{-1}$. It was also shown that measurements of mean transit time correlated with microsphere measurements of perfusion.

CT measurements of myocardial perfusion have also been limited to studies in the experimental dog using ultra-fast CT equipment [31,32]. The theory used is broadly similar to that developed by Jaschke et al for the kidney but no venous time-density data is used (See Appendix 3.2.3). Perfusion is given by the maximal height of the myocardial TDC divided by the area under the arterial curve up to the time of maximal myocardial enhancement. Both Wolfkiel et al [31] and Gould et al [32] correlated CT perfusion measurements with radiolabelled microspheres and found a good correlation up to values of approximately 2 $ml.min^{-1}ml^{-1}$. Above this value, the CT method significantly underestimated perfusion. This is almost certainly due to the fact that, at lower perfusion rates, the transit time is sufficiently long so that little or no contrast medium has left the myocardium and passed into the venous system by the time of maximal myocardial enhancement. Above 2 $ml.min^{-1}ml^{-1}$, the transit time is sufficiently short for some washout of contrast medium to have occurred, thus underestimating the perfusion. In an attempt to correct for this, Wolfkiel et al [31] used a washout correction but found this did not improve the results. Gould et al [32] used an empirical correction

factor. Whereas functional images of perfusion have been produced for the brain, this had not been the case for either the kidney nor the heart, until images of renal perfusion were published by myself, obtained using the techniques described in this thesis [33].

3.3 Proposed CT method for perfusion measurements.

This section describes the derivation of the new method of using dynamic CT data to measure tissue perfusion which was developed for this thesis. It originates from the application of nuclear medicine data processing techniques to dynamic CT methodology.

The nuclear medicine data processing technique used was developed by Peters et al [57] to allow measurement of blood flow from first pass studies using radio-isotopes not completely extracted by the organ studied. The method was subsequently validated in animals [58] and is based on the determination of blood flow as a proportion of cardiac output using radiolabelled microspheres. A time-activity curve over an organ after a bolus injection of microspheres into the left ventricle will rise and reach a maximum height H (cts/sec).

$$\frac{OBF}{CO} = \frac{H \times \alpha}{\text{Dose injected}} \qquad (1)$$

where OBF is organ blood flow and CO is cardiac output. The dose injected will be measured in MBq and "α" is a correction factor relating cts/sec to Mbq determined by detector efficiency and photon attenuation. If one considers the integrated arterial time-activity curve, corrected for recirculation using a gamma-variate function fit (see appendix 3.2.2), its shape will be the same as that obtained from the organ using microspheres but reaching the plateau at

a value A (cts) and with a maximal slope $g_{arterial}$ (cts.sec^{-1}) (figure 3.1). (A is also the area under the arterial curve before integration and $g_{arterial}$ will be its maximum height.) The integrated arterial curve and the organ curve will be related as follows:

$$\frac{g_{organ}\ (cts.sec^{-2})}{g_{arterial}\ (cts.sec^{-1})} = \frac{H\ (cts.sec^{-1})}{A\ (cts)} \qquad (2)$$

where g_{organ} is the maximal slope of the organ time-activity curve (cts.sec^{-2}). However, a tracer that is not completely extracted by the organ on its first pass, such as Tc^{99m} DTPA, will produce a time-activity curve which will not reach this plateau value. But its maximal slope, g_{organ}, will be the same as that which would have been obtained using microspheres, as long as the transit time through the organ is sufficiently long that the time of maximal slope has occurred before any tracer has left the organ. In practice, Peters et al found this to be true even for organs with high blood flow, such as the kidney. Thus by using equation (2) to substitute for H in equation (1),

$$\frac{OBF}{CO} = \frac{A}{\text{Dose injected}} \times \frac{g_{organ}}{g_{arterial}} \times \alpha \qquad (3)$$

As discussed in section 3.1, intravascular contrast medium has pharmacokinetics very similar to those of DTPA. Thus the calculations outlined above can be applied to dynamic CT by determining the temporal changes in contrast medium concentration within the aorta and tissue to be studied from

their respective time-density curves (TDCs). The correction factor "α" is not required with CT as A is measured in HU.sec and the dose injected can be expressed in HU.ml. (As an iodine concentration of $1mg.ml^{-1}$ is equivalent to 25HU, 1mg of iodine is equivalent to 25 HU.ml [43].) Because concentration (i.e. the amount of iodine per ml of tissue) is measured rather than total organ iodine, it is blood flow per ml of tissue, or perfusion, that is determined. Thus for CT:

$$\frac{\text{Organ blood flow/ml tissue}}{\text{cardiac output}} = \frac{A(HUs)}{Dose(HU.ml)} \times \frac{g_{organ}\ (HU.sec^{-1})}{g_{arterial}\ (HU)} \quad (4)$$

Furthermore, as the cardiac output can be determined by dynamic CT from the injected dose of iodine and the area under the arterial TDC after correction for recirculation (A) [21] by:

$$CO = \frac{\text{Dose Injected (HU.ml)}}{A\ (HU.sec)} \quad (5)$$

the tissue perfusion is thus given by:

$$\text{Tissue perfusion}(ml.sec^{-1}ml^{-1}\ \text{tissue}) = \frac{g_{organ}\ (HU.sec^{-1})}{g_{arterial}\ (HU)} \quad (6)$$

g_{organ} is derived from the maximum gradient of tissue TDC and $g_{arterial}$ is given by the peak height of the arterial TDC (before integration and after subtraction of the pre-contrast attenuation value). A multiplication factor of 60 converts $ml.sec^{-1}ml^{-1}$ to $ml.min^{-1}ml^{-1}$. The advantages of applying this method to CT are its simplicity and the avoidance of the correction factors required when using

radio-isotopes. In particular, the dose injected is cancelled from the equation, and thus the exact volume of contrast medium injected is not critical.

Figure 3.1. Stylised time-activity curves.

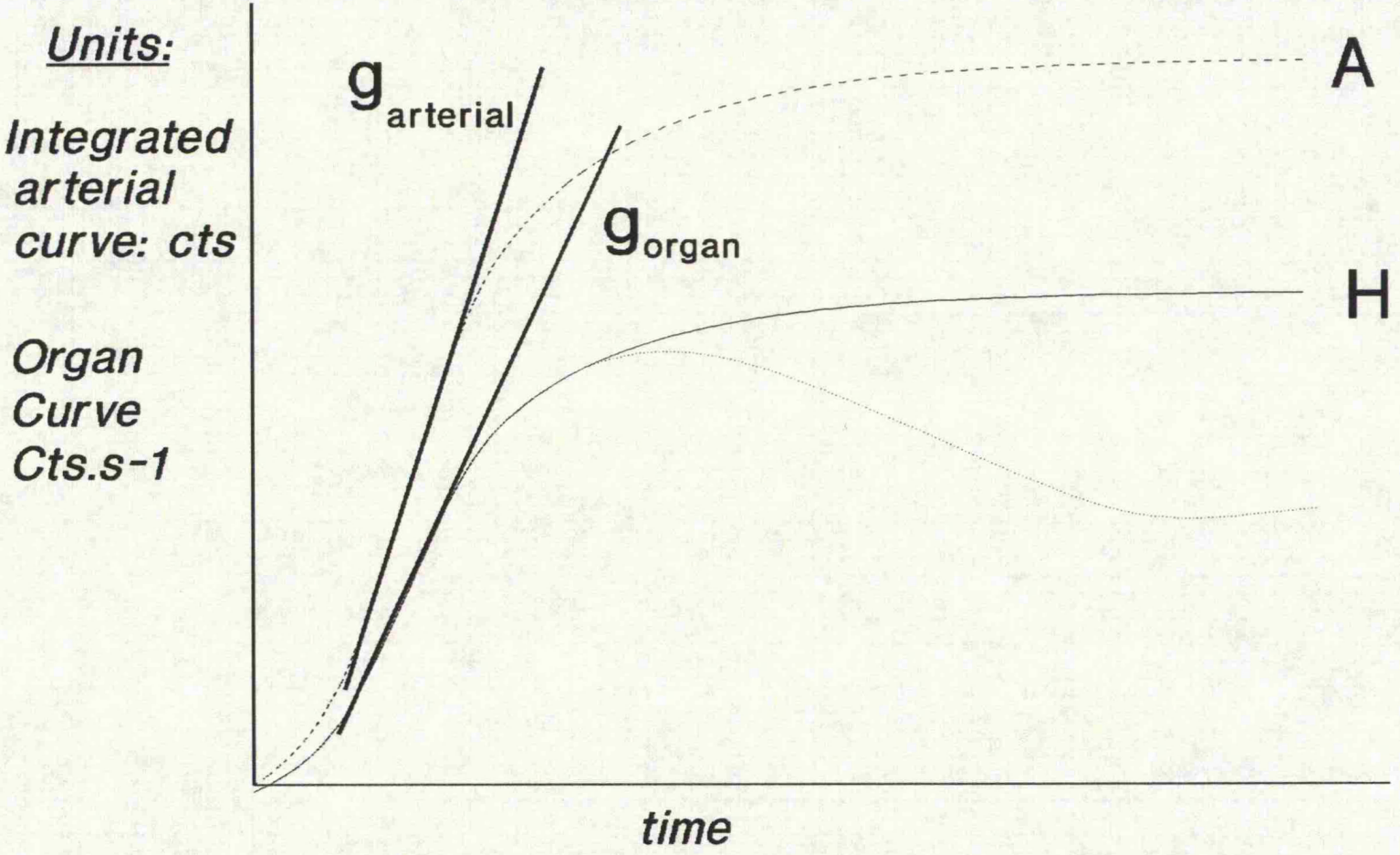

Dashed line: Integrated arterial curve.
Solid Line: Organ curve using microspheres
Dotted Line: Organ curve using incompletely extracted tracer

3.4 Proposed CT method for assessing hepatic perfusion:

This section describes a new CT technique for quantifying hepatic perfusion which was developed for this thesis. There are no previous reports of the use of dynamic CT to determine hepatic perfusion. It is based on the perfusion technique described above in Section 3.3, but its application to the liver is complicated by the biphasic pattern of enhancement resulting from contrast medium first arriving with the hepatic arterial blood and slightly later via the hepatic portal system (figure 3.2).

Various radionuclide techniques have attempted to evaluate these two components separately, using the time of peak splenic activity to divide arterial and portal phases [60,61,62]. The techniques have been of value in studying patients with liver metastases [62], hepatic cirrhosis [60,63,64] and following liver transplantation [65]. The time of peak splenic enhancement during dynamic CT can also be used to separate the arterial and portal phases of the liver TDC. By applying equation (6) (Section 3.3) to the liver TDC before the splenic peak, hepatic arterial perfusion will be determined by:

$$\text{Hepatic Arterial Perfusion } (ml.min^{-1}ml^{-1}) = \frac{\text{maximal slope of liver TDC before the splenic peak } (HU.min^{-1})}{\text{peak aortic enhancement (HU)}} \qquad (7)$$

Portal perfusion (this value will not be true portal perfusion due to loss of contrast medium into the extracellular space of the spleen and gut during its first pass through these organs prior to passage to the liver in the portal blood) can likewise be determined from:

Portal Perfusion ($ml.min^{-1}ml^{-1}$) =

$$\frac{\text{maximal slope of liver TDC after the splenic peak } (HU.min^{-1})}{\text{peak aortic enhancement (HU)}} \qquad (8)$$

These two parameters can be combined to give total hepatic perfusion and the hepatic perfusion index (HPI, expressing the proportion of hepatic perfusion that is arterial) as follows:

Total perfusion ($ml.min^{-1}ml^{-1}$) =

$$\text{arterial perfusion} + \text{portal perfusion} \qquad (9)$$

and

$$HPI = \frac{\text{Arterial Perfusion}}{\text{Total Perfusion}} \times 100\% \qquad (10)$$

One of the advantages of the CT technique is that, unlike nuclear medicine techniques, it is applicable to the left lobe of liver as the transaxial format of the images allows separation from the large vessels.

(g_a = max. arterial slope g_p = max. portal slope)

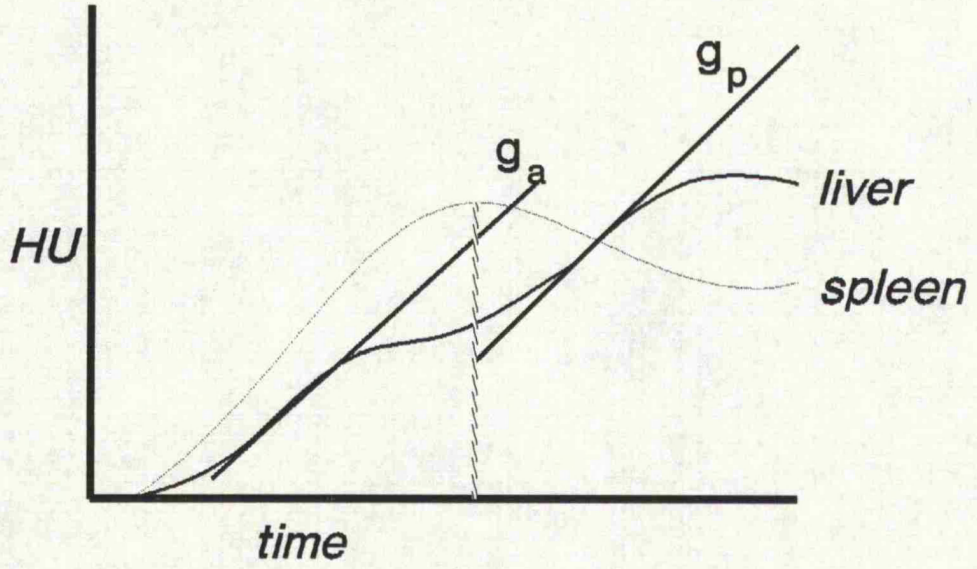

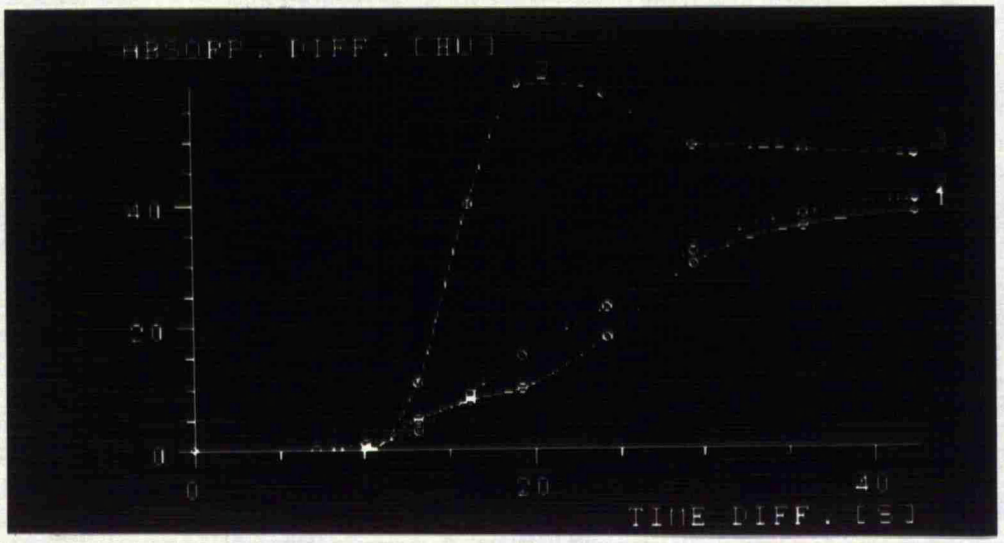

Figure 3.2: Above: Stylised time-density curves (TDC) from liver and spleen. Below: Actual TDCs from a study performed using the Siemens Somatom Plus (1,2: Liver, 3: Spleen).

3.5 Functional Images:

If TDCs for the analysis in section 3.3 were derived from smaller and smaller regions of interest, eventually the ROI would be the size of one pixel. That pixel could then be assigned a value for perfusion rather than x-ray attenuation and the resulting functional image would be a perfusion map. CT images are of high spatial resolution, displayed using a matrix of size 512 x 512 or even 1024 x 1024, and thus the corresponding images would be of similarly high resolution. However, as seen in section 2.3, the smaller the ROI the greater the effect of photon noise and such functional images will only be accurate if CT equipment with very low noise characteristics are used. Using a slightly coarser matrix of 256 x 256 would further reduce noise and yet provide functional images with greater spatial resolution than that afforded by radionuclide techniques, including positron emission tomography. The analyses in Section 3.4 could similarly be applied to the liver pixel by pixel and thus CT can be used to create the following functional images:

1) Tissue Perfusion
2) Hepatic Arterial Perfusion
3) Hepatic Portal Perfusion
4) Total Hepatic Perfusion
5) Hepatic Perfusion Index

Other functional images, such as time to peak enhancement and peak enhancement values, are also feasible.

Software was written (M.P. Hayball, see Acknowledgements) to perform a pixel by pixel analysis with creation of functional images using the workstation (Acorn, Archimedes) that had been linked to the Siemens Somatom Plus CT system at Addenbrooke's Hospital.

To avoid artefacts that would be created by slight movement of structures with very high or very low density due to varying partial volume effect (section 2.3) a thresholding process was performed before the analysis. This eliminated pixels with attenuation values above or below the chosen thresholds from the perfusion analysis and such pixels were assigned a perfusion value of zero. The threshold values chosen were 0 HU (lower threshold) and 400 HU (upper threshold) as this eliminated pixels with significant amounts of air, fat and bone.

Rather than use time consuming gamma-variate curve fitting procedures, smoothing was achieved as follows. An initial 9 point spatial smooth was performed and individual pixel TDCs created. These pixel TDCs were further smoothed using a cubic spline function fitted to 4 points; 2 either side of the time of maximal slope.

The final functional images were displayed using a colour scale. It was possible to window these images and thus alter the perfusion values assigned to the lowest and highest

colours (black and red respectively). Images were NOT automatically scaled to the maximum perfusion value.

3.6 Relationship to other CT methods:

Of the existing CT methods for assessing perfusion (Section 3.2), the most useful of the semi-quantitative methods is probably the slopes ratio technique of Jansen et al [27]. Experience of this approach within nuclear medicine has demonstrated that the method provides a good index of perfusion. The technique is simple, could easily be applied to other organs and could potentially be used to create functional images. Its main drawback is that the measurements are not presented in units of flow or perfusion (e.g. $ml.min^{-1}ml^{-1}$). Absolute quantification is beneficial as it allows the results to be compared with or validated against other techniques. Also, there may be particular pathological significance associated with a certain perfusion rate measured in absolute terms. For instance, for cerebral cortex, infarction is liable to occur below a threshold of 0.15 $ml.min^{-1}ml^{-1}$ tissue [26]. Such significance could not be appreciable using semi-quantitative measurements or techniques merely assessing relative cerebral perfusion.

The transit time methods of Axel et al [24,28] are potentially applicable to multiple organs, although reports are limited to its application to the brain. However, as stated by Axel himself, measurement of the fractional blood volume within the tissue and correction for the transit time of the bolus make absolute quantification extremely difficult.

The technique proposed by Jaschke et al [29,30] works well for the kidney and provides absolute quantification but is limited by the need for venous time-density data and its inability to evaluate regional differences in perfusion within renal cortex or medulla. The former limitation renders the technique applicable to very few organs as there must be a single draining vein of sufficient size for construction of a region of interest and visible on the slice studied. The spleen is probably the only other organ amenable to such analysis. The inability to assess regional variations in perfusion makes functional imaging impossible.

The analysis of myocardial perfusion used by Wolfkiel [31] and Gould [32] is closely related to the technique developed and evaluated in this thesis in that the equation I have proposed for perfusion (equation 6) is the integral of that used for the myocardium (appendix 3.2.3, equation 33).

$$\text{Perfusion} = \frac{\text{Maximal slope of tissue TDC}}{\text{Peak aortic enhancement}} \qquad (11)$$

$$= \frac{dC_t}{dt}\ \max \ \times \ 1/C_a\ \max \qquad (12)$$

integrated can become:

$$= C_t\ \max \ \times \ 1/\int_0^t C_a\ dt \qquad (13)$$

where C_t and C_a are tissue and arterial concentrations of contrast medium respectively. However, the major difference between the methods of analysis is the time at which the data is evaluated. The time of peak tissue enhancement occurs later than the time of maximal slope of the tissue time-density curve. This is important as both methods rely on the tissue transit being sufficiently long so that no contrast medium has left the tissue at the time of data evaluation. This is clearly less likely to be true using the method of Wolfkiel or Gould and, as discussed above, is the reason why the technique underestimates perfusion values above 2 $ml.min^{-1}ml^{-1}$. On the other hand, experience within nuclear medicine of the technique developed by Peters et al [58,59] (upon which the method presented in this thesis is based) has shown that the transit time of high flow organs such as the kidney is sufficiently long for this assumption to be met. The use of empirical washout correction factors, as suggested by Gould et al [32] for the myocardium, is not ideal as a new correction will be required for each organ to which the technique is applied. Furthermore, the correction factor will have been determined from normal tissue and cannot be assumed to be appropriate for pathological tissue, such as tumour, where the washout characteristics may be quite different.

Of the methods providing absolute quantification, only Axel's technique has been applied to humans. The techniques of Jaschke et al [29,30] for the kidney and Wolfkiel et al [31] and Gould et al [32] for the myocardium have merely been

performed in dogs and have used special ultra-fast CT equipment. There are no previous reports of CT evaluation of liver perfusion.

The use of curve fitting techniques, such as the gamma variate benefit from reducing the effects of photon noise as resulting curves are smoothed. However, for functional imaging, it is necessary to apply such curve fitting techniques to time-density curves from individual pixels. This becomes cumbersome and time consuming even when using powerful computers; the shortest time reported for generating such a functional image is 4 minutes. Using spatial smoothing and the modified curve fitting procedure described above (section 3.5), adequate suppression of photon noise is achievable and yet perfusion images are created within a few seconds. Functional imaging using dynamic CT data has only been previously described for the brain and there are no reports of perfusion imaging of other organs.

There are many advantages of the method developed in this thesis over existing CT techniques. It is simple, requiring only time-density data from the tissue and an artery. It can be applied to nearly all tissues (the lung and blood vessels themselves have a transit time so short as to render the measurements meaningless.) The results are absolutely quantifiable and expressed in true units of perfusion i.e. $ml.min^{-1}ml^{-1}$. Unlike xenon CT which requires special

equipment such as a gas analyser, no additional apparatus is necessary, apart from a personal computer such as is readily available at low cost. Ultimately, the necessary software could be incorporated into existing CT systems, making the additional computer unnecessary. The technique is applicable to existing standard CT equipment and an ultra-fast scanner is not essential. The use of iodinated contrast medium is an advantage over xenon as there are fewer side effects and flow activation is avoided by using a first pass technique. Furthermore, the use of iodinated contrast medium is often an integral part of a patient's CT examination. Thus, the perfusion data can be gathered using an additional bolus during a routine study by merely including a few additional exposures.

APPENDIX 3.2.1:

Derivation of equation of CT measurement of tissue perfusion using stable xenon.

The techniques uses the Kety application of the Fick principle of indicator dilution [66] which relates the tissue concentration of a freely diffusible tracer to its arterial concentration and the tissue perfusion as follows:

$$CXe_{Br}(t) = \lambda k \int_0^t CXe_{art}(u)\, e^{-k(t-u)}\, du \qquad (14)$$

where $CXe_{Br}(t)$ = the concentration of xenon in brain tissue at time, t, λ = brain:blood partition coefficient, k = the brain uptake rate constant and CXe_{art} (u) = the arterial concentration of xenon at time, t.

Cerebral blood flow per unit mass or perfusion, P, is given by:

$$P = \lambda k \qquad (15)$$

The build up of xenon in the blood with time is described by:

$$CXe_{art}(u) = CXe_{max}\ (1-e^{-bu}) \qquad (16)$$

where CXe_{max} = maximum arterial xenon concentration, u = time and b = arterial uptake rate constant. Rather than determine the arterial xenon concentration directly, instantaneous equilibrium with end-tidal pulmonary xenon concentration is assumed. This is valid in the absence of severe pulmonary

disease or right to left intracardiac or intrapulmonary shunts. Maximum arterial concentration of xenon ($mg.ml^{-1}$) is related to maximum percentage arterial uptake by:

$$CXe_{max} = C(\%)_{max} \ (5.15) \ (S_{Xe}) \ (0.01) \qquad (17)$$

where $C(\%)_{max}$ = maximum percent xenon uptake, 5.15 = density of xenon ($mg.ml^{-1}$) at a temperature of $37^{o}C$ and pressure of 1 atmosphere, and S_{Xe} = solubility of Xenon in blood, related to the haematocrit (Hct) by:

$$S_{Xe} = 0.1 + 0.0011 \ (\%Hct) \qquad (18)$$

The brain xenon concentration is related to the amount of enhancement (E), measured in Hounsfield Units (HU) by:

$$E = CXe_{Br}/(\mu^{W}/\mu^{Xe}) \qquad (19)$$

where μ^{W} and μ^{Xe} are the mass attenuation coefficients of water and Xenon respectively.

Using the above relationships, the brain uptake data is fitted to equation 1 using an iterative least squares fit with simultaneous determination of k and λ and hence perfusion P. As λ and k vary inversely, any mild errors in determining k are compensated for by λ, and vice versa. Thus, the solution for P is mathematically stable. These values can be determined either for regions of interest or for individual pixels with production of functional images.

APPENDIX 3.2.2

A gamma variate curve fitting procedure is performed on the time-density data to correct for recirculation [67] (figure 3.3). The gamma variate function is described by:

$$H(t) = s(t-T_0)^a \, e^{-(t-T0)/b} \qquad (20)$$

where H(t) is the increase in attenuation due to contrast medium at time,t, s is a scaling factor, T_0 the bolus arrival time and a and b are the curve fit parameters. The transit time is given by the time to the centre of gravity of the fitted curve and is described by:

$$\text{mean transit time, } \bar{t} = \frac{\int_0^\infty tH(t)\,dt}{\int_0^\infty H(t)\,dt} \qquad (21)$$

Transit time is related to flow,F, by:

$$\bar{t} = \frac{V}{F} \qquad (22)$$

where V is the vascular volume of brain tissue. This can be determined from the gamma variate fitted time-density curves from an artery and from brain tissue as follows:

$$C_b = fC_v \qquad (23)$$

where C_b = measured concentration in brain tissue, C_v the vascular concentration within brain tissue and f the fractional blood volume.

The amount of contrast medium entering this portion of brain

after a bolus injection is given by:

$$\int_0^\infty FC_a(t)\,dt \tag{24}$$

where $C_a(t)$ is the arterial concentration at any time, t. Similarly, the amount leaving the brain substance is given by:

$$\int_0^\infty FC_v(t)\,dt = (1/f) \int_0^\infty FC_b(t)\,dt \tag{25}$$

$$\text{Thus} \quad \int_0^\infty FC_a(t)\,dt = (1/f) \int_0^\infty FC_b(t)\,dt \tag{26}$$

or

$$f = \frac{\int_0^\infty FC_b(t)\,dt}{\int_0^\infty FC_a(t)\,dt} \tag{27}$$

Also, the observed transit time must be corrected for the transit time of the bolus from:

$$\bar{t}_{obs} = \bar{t}_{inj} + \bar{t} \tag{28}$$

where $\bar{t}_{obs}$ and $\bar{t}_{inj}$ are the observed and injection transit times respectively.

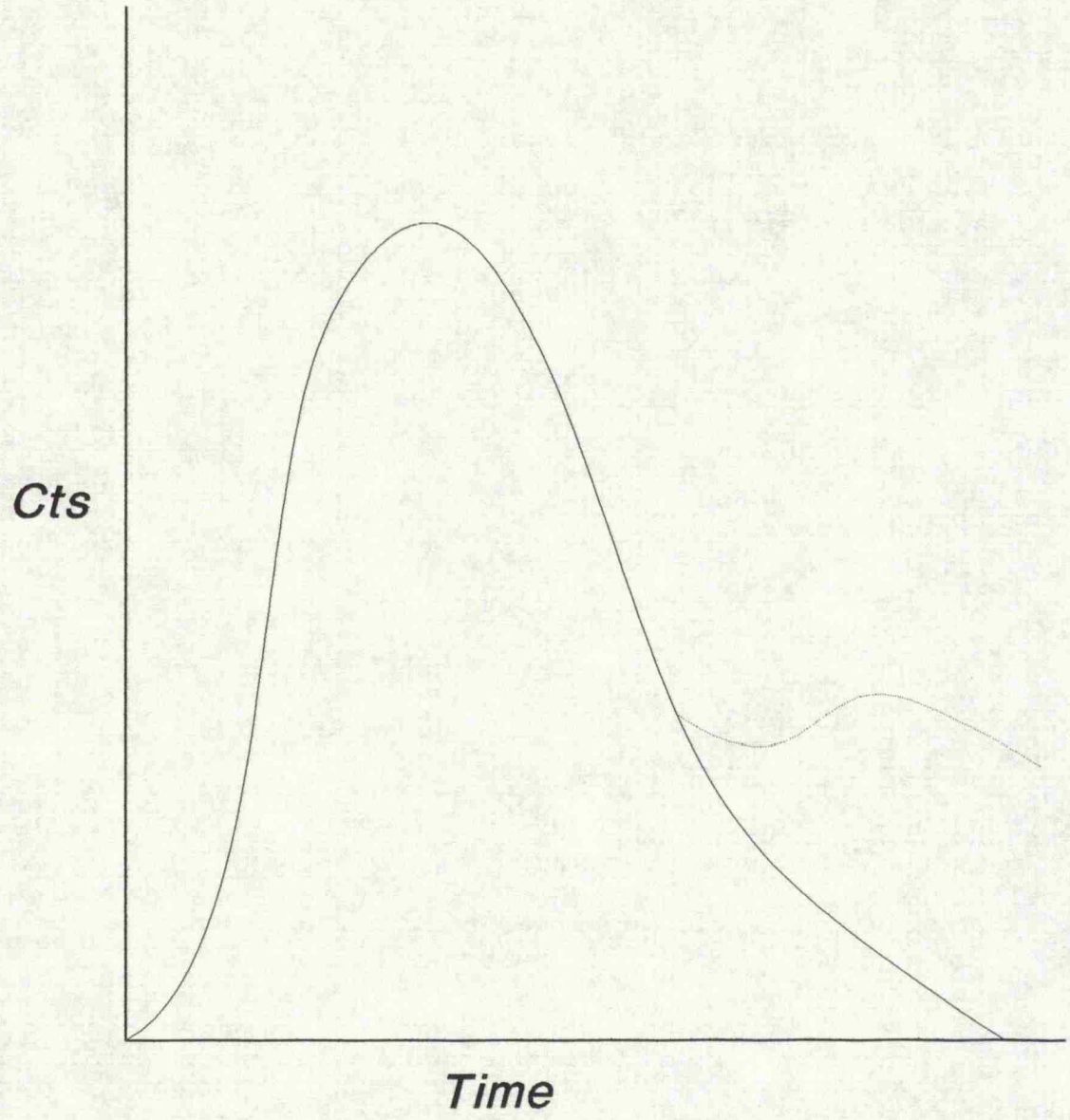

Figure 3.3: Time activity curve with recirculation (dotted line) and gamma variate fit (solid line).

APPENDIX 3.2.3

A gamma variate function (see appendix 3.2) is fitted to each time-density curve. Based on the Mullani-Gould application of the Fick equation [57], the amount of contrast medium kidney at any time t, $Q_k(t)$, is given by:

$$Q_k(t) = F \left(\int_0^t C_a(t)\, dt - \int_0^t C_v(t)\, dt \right) \quad (29)$$

where $C_a(t)$ and $C_v(t)$ are the arterial and venous concentration at time, t, and F is the flow within the renal artery and vein (assumed to be equal). Alternatively,

$$F = Q_k(t) / \int_0^t C_a(t)\, dt - \int_0^t C_v(t)\, dt \quad (30)$$

As

$$Q_k(t) = C_k(t)\, V_k \quad (31)$$

where $C_k(t)$ is the concentration of contrast at time, t, within a set volume of kidney, V_k, flow per unit volume, or perfusion, is given by:

$$F/V_k = C_k(t) / \int_0^t C_a(t)\, dt - \int_0^t C_v(t)\, dt \quad (32)$$

The value of t used is the time to maximal renal cortical enhancement as the error in measuring C_k will be lowest at this time. Thus $C_k(t)$ is given by the maximal height of the renal cortical TDC and $\int_0^t C_a(t)\, dt$ and $\int_0^t C_v(t)\, dt$ are given by the areas under the arterial and venous TDCs up to time t. Due to the presumed relatively long transit time through the

medulla, it is assumed that only blood flowing through the renal cortex contributes to the renal venous output during the time course used in the analysis. Thus, medullary perfusion is given more simply by:

$$F/V_k = C_k(t) / \int_0^t C_a(t)\ dt \qquad (33)$$

These values are determined from the tissue and arterial curves only. Equation 33 is also the calculation used by Gould et al [32] and Wolfkiel et al [31] for determination of myocardial perfusion using ultra-fast CT.

4. KIDNEY

4.1 Cortical and medullary perfusion: Region of interest analysis

4.2 Perfusion imaging of the normal kidney

4.3 Perfusion imaging of the diseased kidney: case studies.

4.1 Renal cortical and medullary perfusion: Region of interest analysis.

Introduction:

The aim of this study was to determine whether quantitative information about renal cortical and medullary perfusion, evaluated separately, could be obtained using the data processing technique derived in section 3.3 in normal and diseased kidneys.

Patients and methods:

The patients examined were undergoing dynamic CT for staging of renal carcinoma, diagnosis of renal vein thrombosis in the nephrotic syndrome or diagnosis of renal artery stenosis. The kidneys studied were contralateral kidneys in patients with renal tumours (18 kidneys), apparently normal portions of kidneys containing renal tumours (9 kidneys), patients with known renal failure (4 kidneys) and hypertensive patients with (6 kidneys) and without (2 kidneys) captopril treatment.

The CT machine used for this part of the thesis was the IGE 8800 situated at the Leicester Royal Infirmary. A series of unenhanced images were obtained at the level of the second lumbar vertebra and the image best demonstrating the renal veins was chosen. A single location dynamic sequence was then performed at the same anatomical level as the chosen image with data acquisitions obtained as rapidly as possible, i.e. six second data acquisitions every eight seconds, during quiet breathing. 50 ml of iopamidol 370 $mg.ml^{-1}$ was injected intravenously by hand as rapidly as possible and time-density curves (TDCs) were derived from regions of interest (ROIs) constructed over the abdominal aorta, renal cortex and medulla. ROIs were made as large as possible to reduce the effects of photon noise whilst avoiding partial volume effects. Perfusion values were calculated using the formula derived in Chapter 3.3.

Results:

Examples of time-density curves are given in figure 4.1 and mean values and standard deviations for the renal cortex and medulla in the groups of kidneys studied are displayed in figure 4.2. There was no significant difference in cortical or medullary perfusion in the kidneys containing tumour when compared to normals and perfusion appeared normal (even in one case where the renal vein was occluded by tumour thrombus). Renal failure produced a significant decrease in medullary perfusion ($p<0.01$, Wilcoxon Rank-Sum test) with cortical perfusion reduced also but not reaching statistical significance ($p=0.07$). The renal cortical perfusion was significantly reduced in hypertension without captopril treatment when compared to normals ($p<0.05$, Wilcoxon Rank-Sum test), whereas in hypertensive patients treated with captopril cortical perfusion was not significantly reduced. Neither hypertension nor captopril therapy had any significant effect on medullary perfusion.

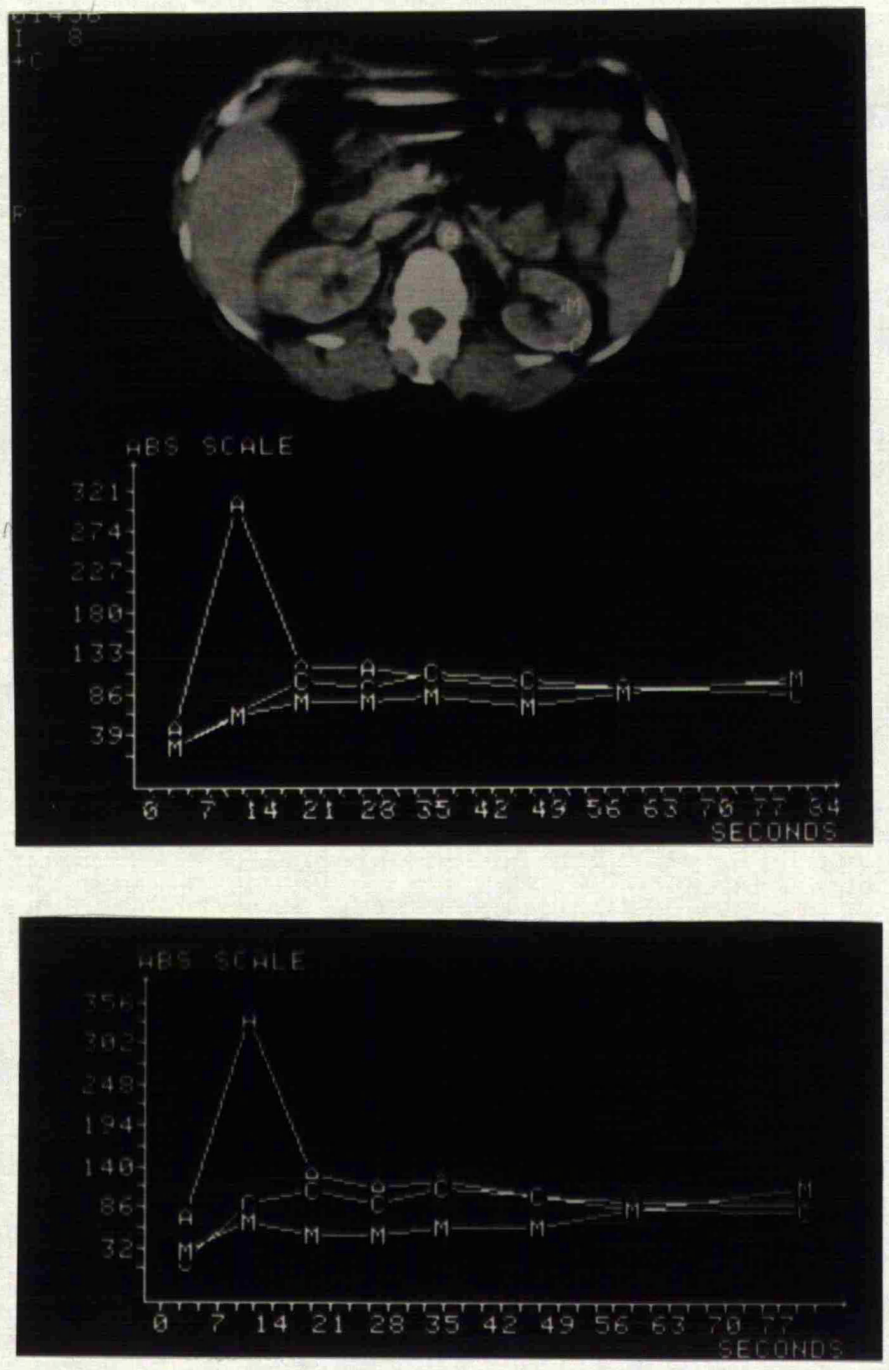

Figure 4.1 Aortic (A), cortical (C) and medullary (M) time-density curves from a hypertensive patient before (above) and after (below) captopril therapy. Note the increased slope of the cortical TDC after captopril.

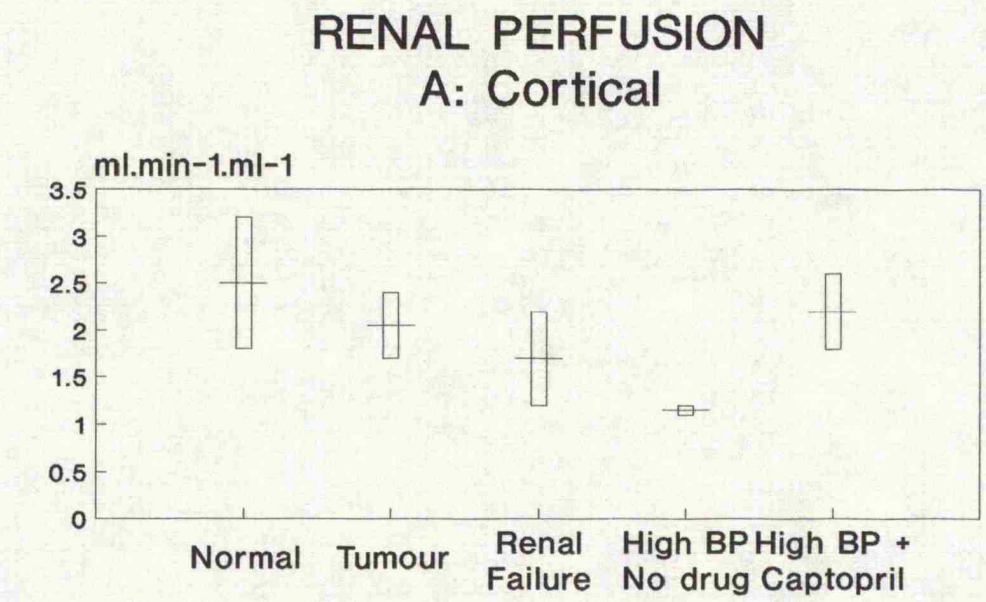

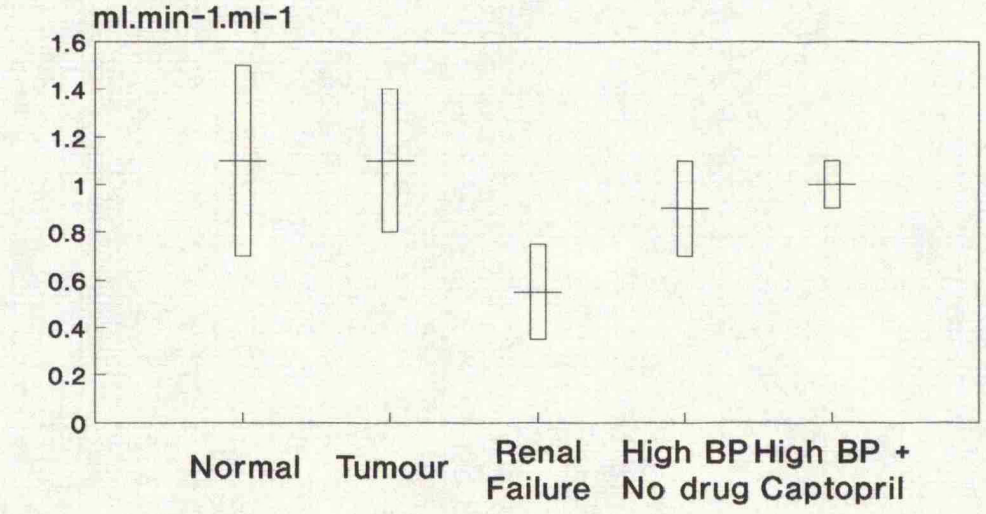

Figure 4.2: Data from IGE 8800

Discussion:

Quantitative assessment of renal cortical and medullary perfusion can be derived from data from regions of interest using the analysis described in section 3.3. No direct validation of the values has been obtained as this is not readily performed non-invasively. However, the mean value of 1.1 $ml.min^{-1}ml^{-1}$ for medullary perfusion in normal kidneys corresponds closely to the accepted value of 1.3 $ml.min^{-1}ml^{-1}$ derived from studies using intra-arterial xenon [68] but the CT derived value of 2.5 $ml.min^{-1}ml^{-1}$ for cortical perfusion is significantly lower than the accepted value of 4.1 $ml.min^{-1}ml^{-1}$ [68]. This is likely to be due to the low sampling rate (i.e. 1 data acquisition every 8 seconds) which will tend to lead to underestimation of the rate of change of enhancement, particularly when this is rapid (as for the renal cortex). Peak aortic enhancement will also tend to be underestimated which would, to some extent, offset the effect of underestimating the maximal rate of tissue enhancement. It should be remembered that the values obtained using Xenon are derived using compartmental analysis identifying a physiological rather than an anatomical compartment. To date it has not been possible to non-invasively study the human renal cortex and medulla with separate anatomically defined regions and hence no true reference values are available.

The reduction in cortical perfusion, and hence the change in the cortico-medullary perfusion ratio, occurring in renal

failure is in accordance with Gruenewald [69] using radio-isotope renography with deconvolutional analysis. Renal failure is also known to reduce overall renal blood flow and the CT study has confirmed that this comprises a reduction in both cortical and medullary perfusion.

Contrast medium is known to cause a transient increase in renal blood flow followed by a more prolonged decrease [44]. It has been suggested that such a reduction in cortical blood flow may be the mechanism for contrast nephrotoxicity. This reduction may be related to changes in the renin-angiotensin system. The fact that a reduction in cortical perfusion can be reversed by captopril, as measured with contrast and dynamic CT, is evidence that captopril is potentially of value in prevention of contrast nephrotoxicity. This may be so not only in patients where cortical perfusion is reduced, such as patients with hypertension, but also possibly in patients with renal failure (a high risk group for contrast nephrotoxicity) where dynamic CT has also demonstrated some reduction in cortical perfusion.

4.2 Functional Imaging: Normal Kidneys:

This section describes the application of the technique for obtaining functional images of perfusion, as described in section 3.5, to a series of normal human kidneys.

Technique:

The Siemens Somatom Plus CT system situated at Addenbrooke's hospital, Cambridge was used. After a 50 ml intravenous bolus of Iopamidol 300 $mg.ml^{-1}$ (Niopam, Merck) given as rapidly as possible by hand, a series of 1 s data acquisitions was performed without table movement at 0, 6.5, 9.5, 12.5, 15.5, 20.5, 25.5, 30.5, 37 and 43.5 seconds (slice thickness 10mm) with the patient breathing gently. The calculation of perfusion values and subsequent creation of functional images were as described in sections 3.3 and 3.5. All functional images were scaled identically as follows:

Black: 0 $ml.min^{-1}ml^{-1}$
Red: 5 $ml.min^{-1}ml^{-1}$
White: > 5 $ml.min^{-1}ml^{-1}$

Patients:

Thirteen kidneys were studied in eight patients without known or suspected renal disease who were undergoing dynamic CT for investigation of the liver (in three patients only one kidney was present on the slice selected for enhancement). The fourteenth kidney studied was the contralateral kidney in a

patient with renal carcinoma (Case A below). Regional variations in perfusion within the kidney were observed and quantified by inspection of the images and construction of profiles 1 pixel wide drawn from the cortex into the medulla. The profiles were drawn with a radial orientation avoiding cortical columns of Bertin and used to determine the maximal cortical and minimum medullary perfusion.

Results:

Typical cortical and medullary time-density data obtained using the Siemens Somatom Plus system are displayed below (Fig 4.Supp).

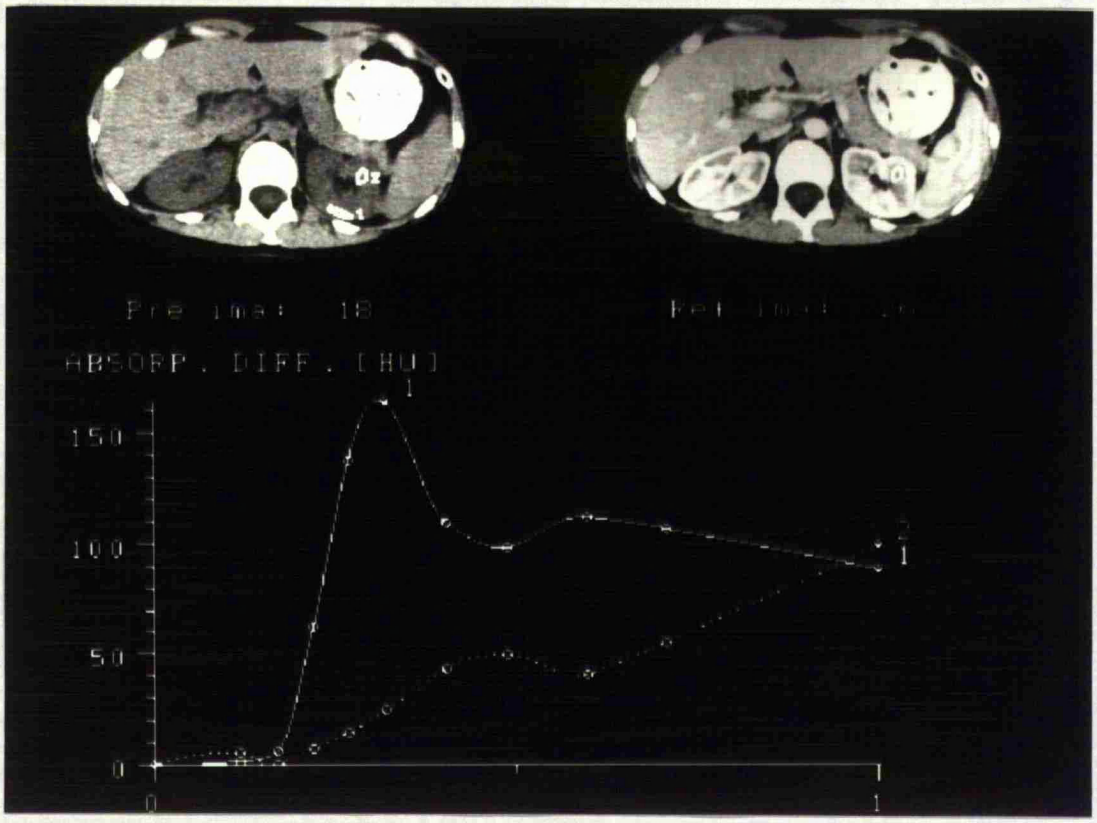

Figure 4.Supp: Renal cortical and medullary TDCs from the Siemens Somatom Plus CT system (Addenbrooke's Hospital).

Perfusion maps were successfully obtained in all cases. A typical perfusion image from a normal kidney is shown in Figure 4.3. Areas of high and low perfusion clearly corresponding with renal cortex and medulla were seen in all 14 normal kidneys. Values for cortical and medullary perfusion are given in Table 4.1. The ratio of mean cortical to mean medullary perfusion was 4.3:1 (4.7 $ml.min^{-1}ml^{-1}$: 1.1 $ml.min^{-1}ml^{-1}$)

Figure 4.3 demonstrates a normal perfusion profile derived from the line shown in Figure 1a, showing the change in perfusion between cortex and medulla. The change was seen to be gradual in 12 of the 14 normal kidneys (as shown in Fig 4.3) with a relatively sharp demarcation between cortex and medulla in the remaining two examples.

TABLE 4.1

Patient No.	Kidney	Cortex	Medulla
1	R	4.0	0.8
1	L	5.0	0.6
2	R	4.2	1.2
2	L	4.8	1.0
3*	R	4.6	1.7
4	R	5.8	0.9
4	L	3.8	1.0
5	R	4.1	1.5
5	L	5.6	1.3
6	L	5.2	1.3
7	R	3.8	1.2
8	L	4.8	1.3
9	R	5.9	1.0
9	L	4.2	1.2
MEAN		4.7	1.1
STANDARD DEVIATION		0.72	0.28

Values for cortical and medullary perfusion ($ml.min^{-1}ml^{-1}$) for the 14 normal kidneys derived from radial profiles. (R = right, L = left, * = the contra-lateral kidney the patient with a renal carcinoma, case A.)

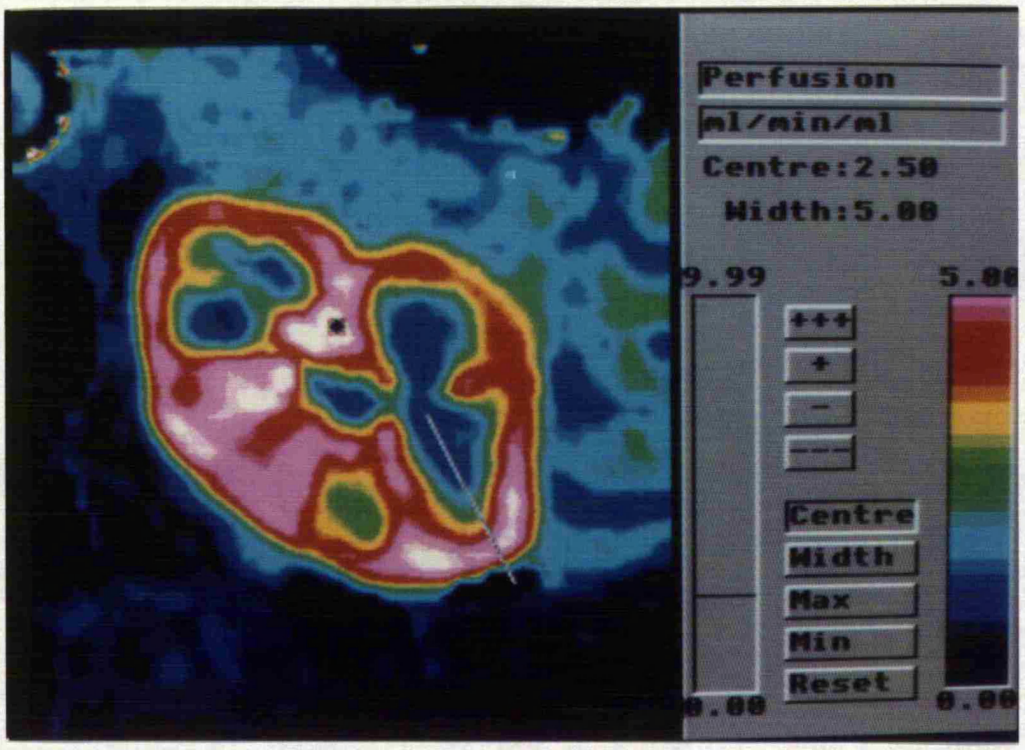

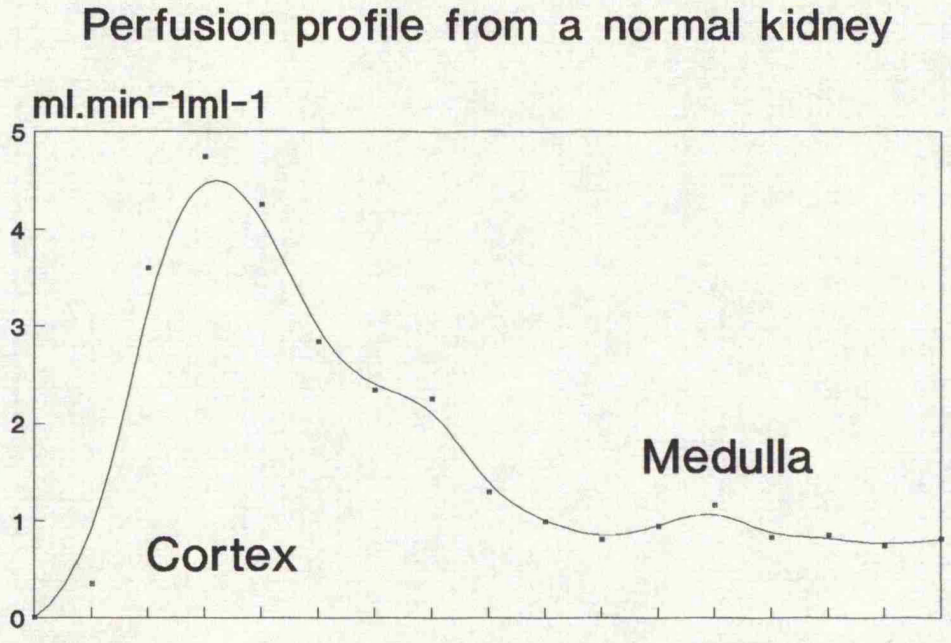

Figure 4.3 Perfusion image and profile from a normal kidney.

Discussion:

The technique successfully generates functional images with high spatial resolution consistently demonstrating regional variations of perfusion within the kidney with areas of high perfusion corresponding with the cortex and low perfusion with the medulla. Once again, the absence of a non-invasive method of measuring renal cortical and medullary perfusion in humans has prevented direct validation of the CT technique in our human subjects. The ratio of mean cortical to mean medullary perfusion obtained using our technique (i.e. 4.3:1) is close to that obtained from renal scintigraphy with iodohippuran using deconvolutional mathematics [69]. Unlike the results obtained using the IGE 8800 (section 4.1), the absolute values for both cortical and medullary perfusion obtained in our normal cases correspond closely with those for the physiological compartments assumed to be cortex and medulla derived from compartmental analysis of the wash-out of radioactive xenon injected into the renal artery [68]. To date, no direct anatomical localisation of these compartments has been made. The values for canine renal cortical and medullary perfusion obtained by Jaschke [29,30] using ultrafast CT are in concordance with our results.

As compared with the IGE 8800, the superior time resolution of the Siemens system with shorter and more frequent data acquisitions (Compare Figures 4.1 & 4.Supp) will have significantly reduced the likelihood of errors resulting from

underestimation of either the maximal slopes of tissue TDCs or the peak value of aortic enhancement.

The creation of functional images has a further advantage over region of interest analysis as such regions are created with reference to anatomical features and therefore assumptions about the location of any areas of high or low perfusion have to be made before the analysis is performed. No such assumptions are required when producing a functional image of perfusion where analysis is performed on a pixel by pixel basis.

The lack of a clear separation between cortical and medullary perfusion demonstrated in 12 of the 14 normal kidneys using the profiles constructed from the perfusion images has several possible explanations. It may indicate spatial overlapping between physiological compartments such as those observed on Xenon washout studies [68]. Partial volume effects or movement of the patient may also have smoothed out any true separation. Furthermore, partial volume effects could account for smoothing of the abrupt change that would be expected between outer cortex and perirenal fat and could alter values derived from cortex or medulla in individual cases. Movement of the patient has rarely been a problem using gentle respiration during the study as long as careful instruction and warning of the flushing induced by the contrast medium is given to the patient.

4.3 Functional Imaging: Case Histories:

This section describes the application of the technique applied to a series of normal human kidneys in section 4.2 to three cases with renal impairment.

Case 1: Renal Carcinoma

A 63 year old man presented with haematuria and left loin pain. An ultrasound examination demonstrated a mass with appearances consistent with a carcinoma in the left kidney. The patient was referred for CT to stage the tumour during which the flow study was performed.

Pathological examination of the resected kidney confirmed a renal carcinoma with tumour invasion into the renal vein but without involvement of the inferior vena cava.

Figure 4.4A illustrates the perfusion image of the renal carcinoma with perfusion profiles (figure 4.4B) from the tumour lying anteriorly and the apparently normal renal tissue posteriorly. There is derangement of the normal arrangement of the columns of Bertin with generally increased perfusion (8 $ml.min^{-1}ml^{-1}$ maximum) but demonstrating lower perfusion centrally (2-3 $ml.min^{-1}ml^{-1}$). The perfusion of the normal portion is within normal limits despite the presence of thrombus within the renal vein.

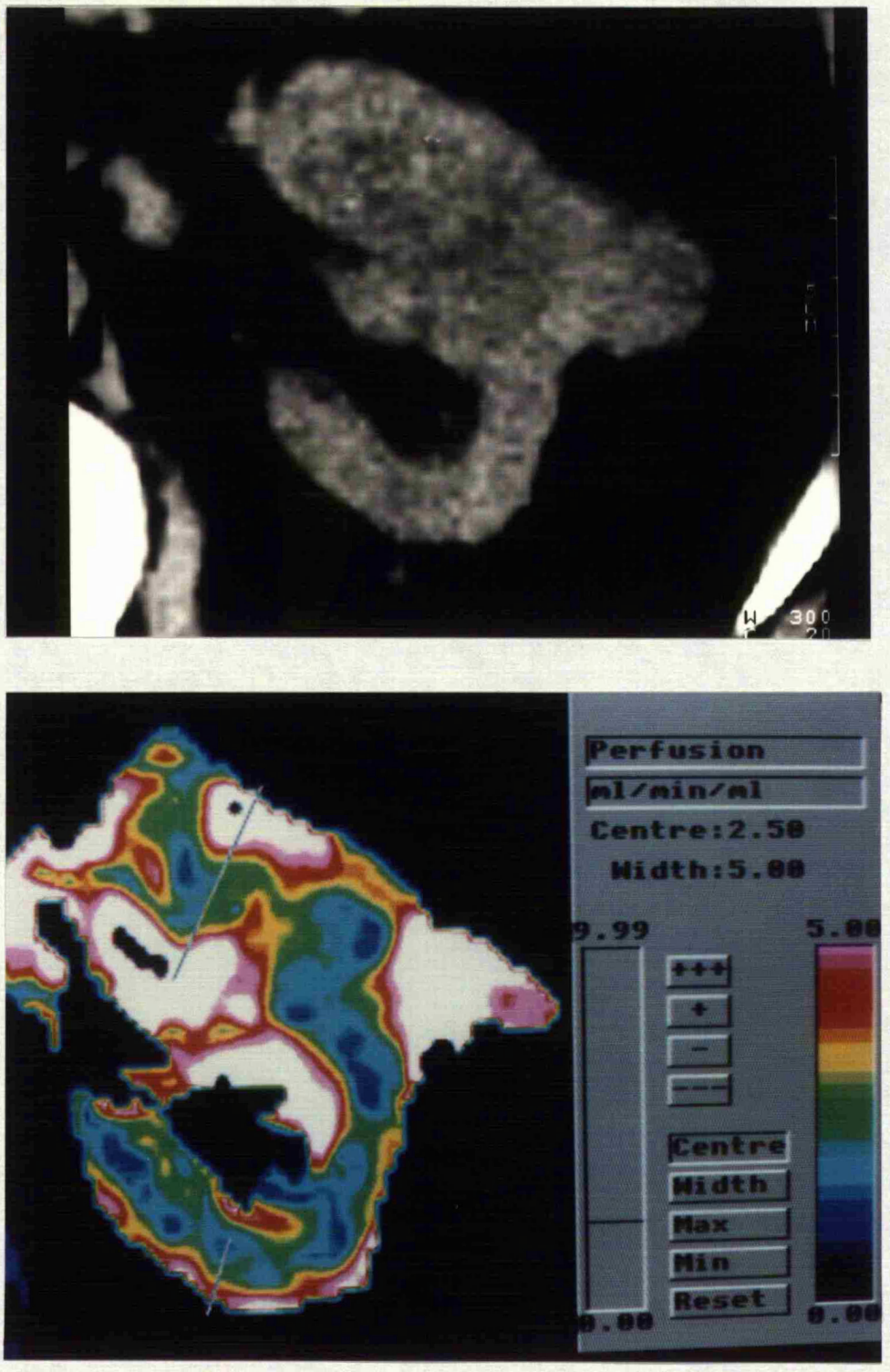

Figure 4.4A Unenhanced CT (above) and perfusion image (below) of a kidney containing a renal carcinoma.

Perfusion profiles from renal tumour and normal portion of kidney.

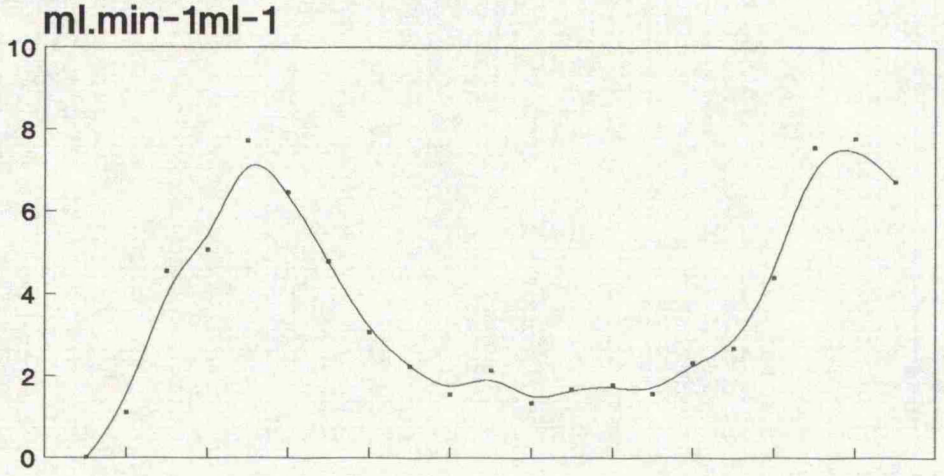

Tumour

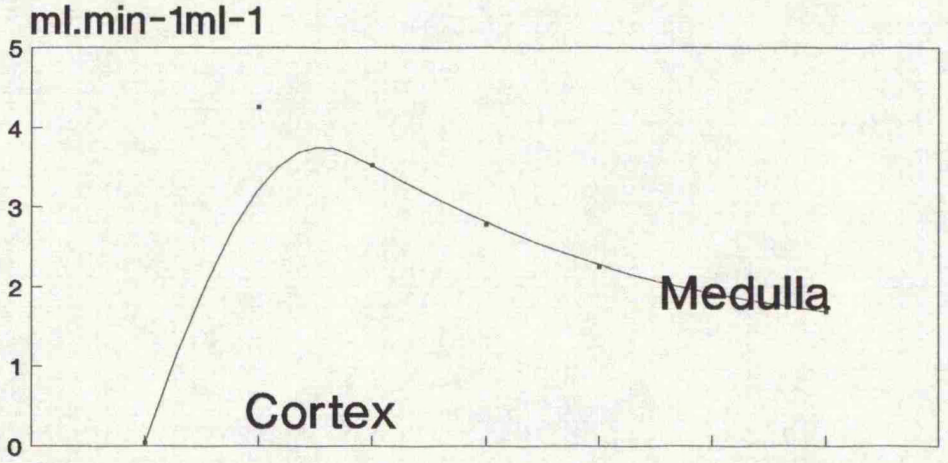

Normal portion of kidney

Figure 4.4B

Case 2: Non-functioning renal allograft

A 22 year old man had undergone renal transplantation 3 years previously for chronic glomerular nephritis. Nine months previously, the transplant function had deteriorated and haemodialysis was commenced. The patient now presented with haematuria and was referred for CT to exclude a tumour within the transplant, during which the perfusion study was performed. No tumour was demonstrated and the allograft was subsequently excised. Pathological examination revealed infarction of the transplant.

Figure 4.5A demonstrates the perfusion image and figure 4.5b the perfusion profile from the infarcted renal allograft. There is a marked reduction in perfusion through the transplant kidney, being lowest centrally (0.2 $ml.min^{-1}ml^{-1}$) with slightly higher perfusion peripherally (1.1 $ml.min^{-1}ml^{-1}$).

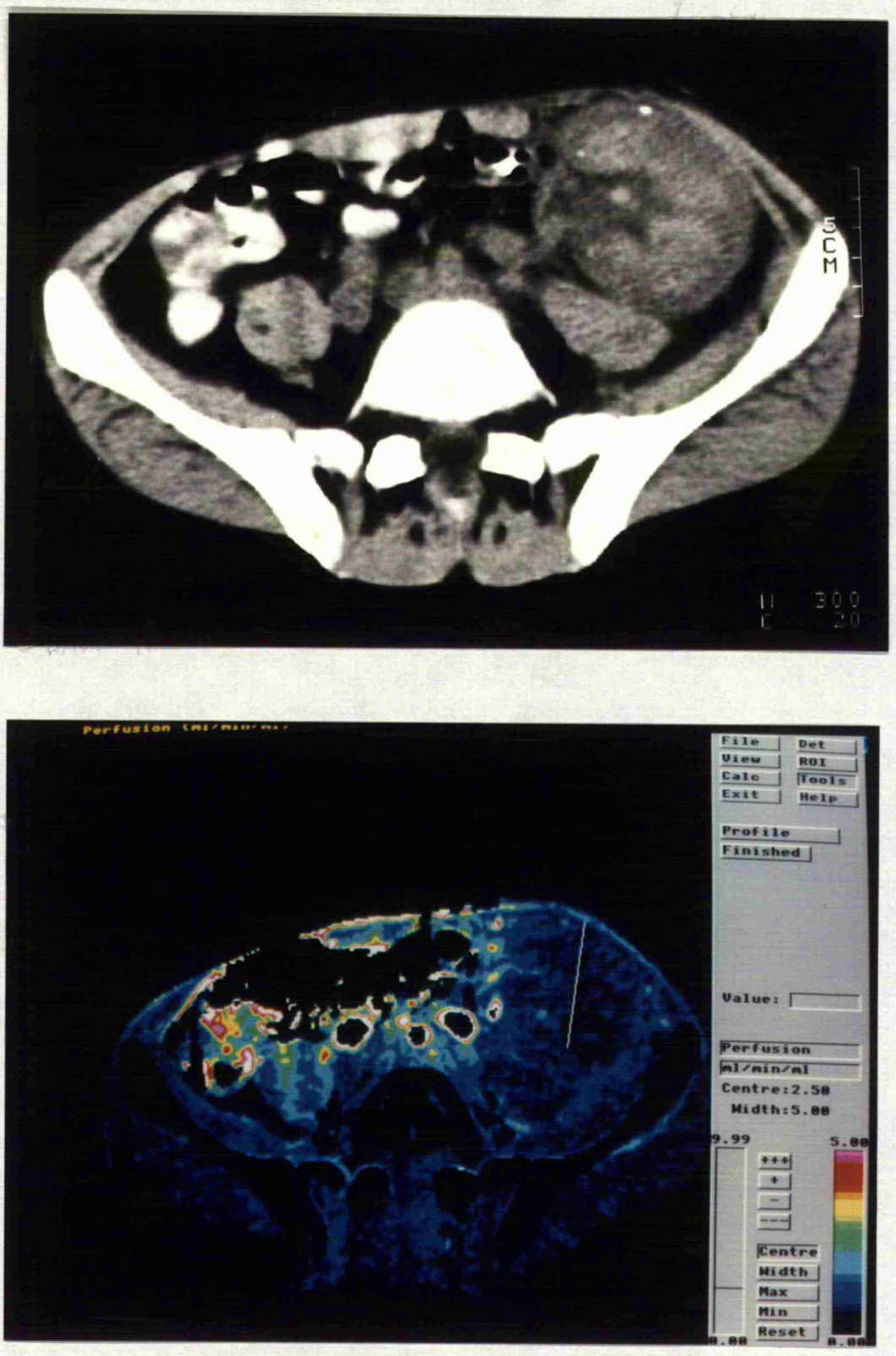

Figure 4.5A Unenhanced CT (above) and perfusion image (below) of the infarcted renal allograft.

Perfusion profile from an infarcted renal transplant.

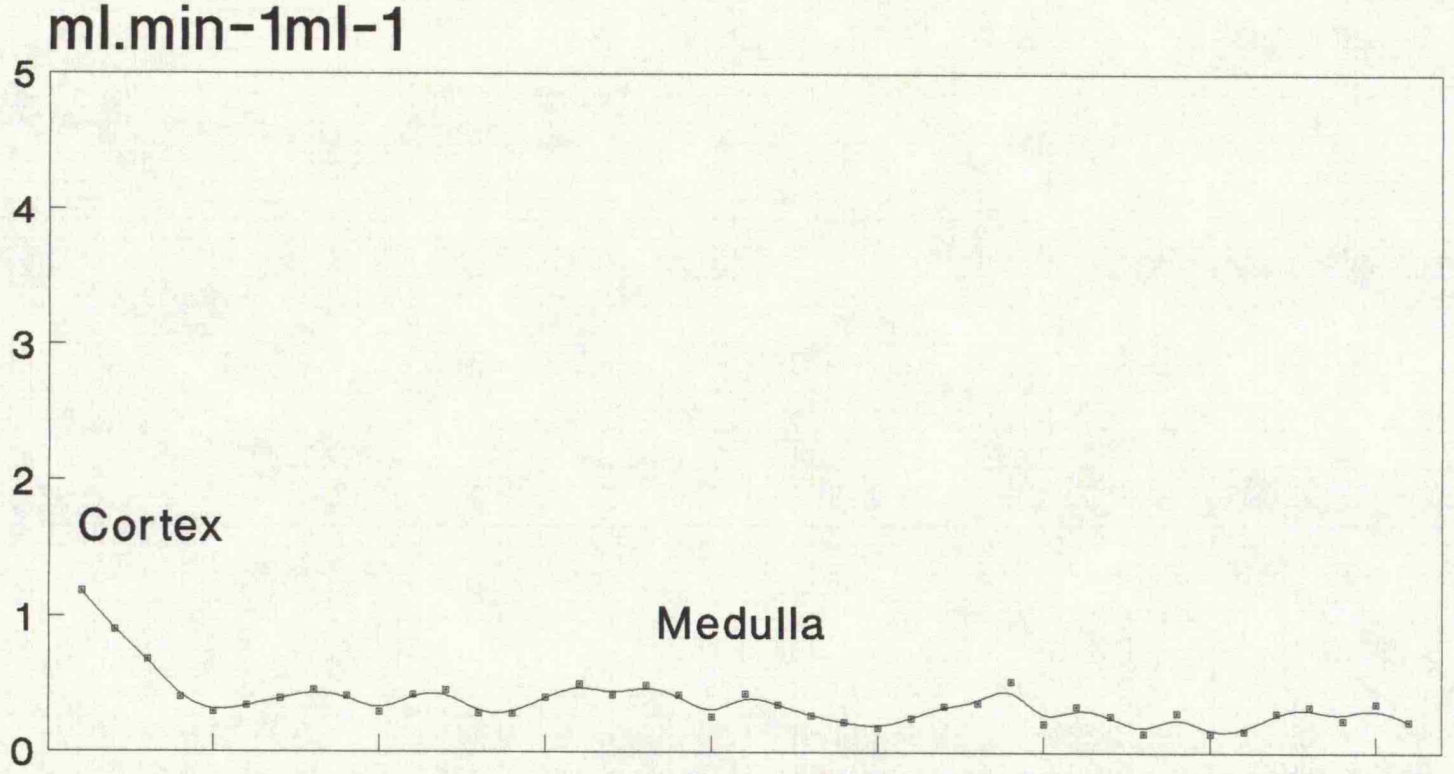

Figure 4.5B

Case 3: Cyclosporin Toxicity

A 23 year old man who had undergone hepatic and pancreatic transplantation 5 years previously presented with worsening renal function. Serum creatinine was 139 $mmol.l^{-1}$ and the glomerular filtration rate measured using ^{51}Cr Chromium labelled EDTA and timed blood samples was reduced at 58 (+/- 2) $ml.min^{-1}$ (expected from surface area: 116 $ml.min^{-1}$). His drug treatment comprised daily doses of 400 mg of cyclosporin, 7.5 mg of prednisolone, 75 mg of azathioprine and 21 units of insulin. Trough levels of serum cyclosporin concentration were 290 $ug.l^{-1}$.

The cyclosporin dose was subsequently reduced to 300mg daily with a concomitant fall in serum creatinine implicating drug toxicity as the likely cause of the renal impairment.

The results from the patient with cyclosporin toxicity are given in figure 4.6. The perfusion image demonstrates that the normal arrangement of cortex and medulla is preserved but cortical and medullary perfusion are reduced (3.3 $ml.min^{-1}ml^{-1}$ and 0.5 $ml.min^{-1}ml^{-1}$ respectively).

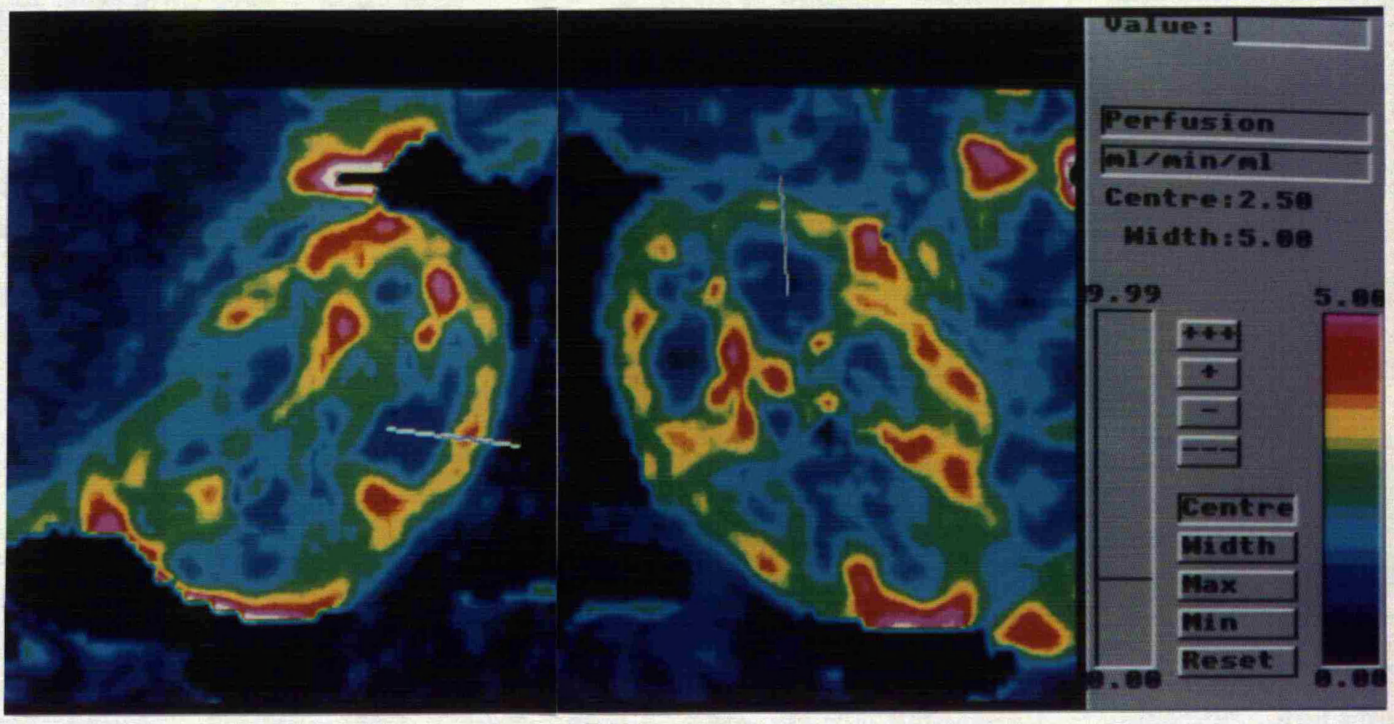

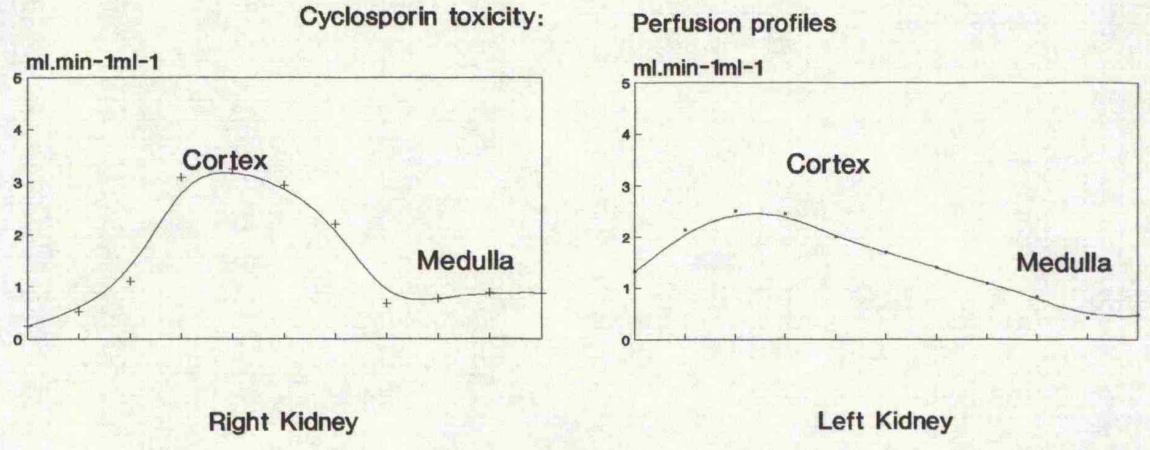

Figure 4.6 Perfusion images and profiles from the kidneys in a patient with cyclosporin toxicity.

Discussion:

The changes observed in the abnormal kidneys are consistent with the recognised pathophysiologies of these conditions, thus providing clinical validation and suggesting possible applications for the technique. It is well recognised that renal carcinomas have high perfusion as in Case A. The presence of normal perfusion within the apparently normal portion of kidney despite the presence of tumour thrombus within the the renal vein was also observed with one case in section 4.1. This may indicate adequate venous drainage either around the thrombus or via collateral vessels. It is also known that renal infarction will lead to virtually absent perfusion, although there may be some supply from capsular vessels; this is in keeping with our findings of slightly higher peripheral perfusion in Case B. Cyclosporin is known to reduce total renal blood flow, but separate quantification of cortical and medullary perfusion in such patients has not been previously performed. The CT technique has demonstrated a reduction in both cortical and medullary perfusion in the case studied (Case C).

5. LIVER:

5.1 Patients and methods

5.2 Validation against colloid scintigraphy

5.3 Right lobe perfusion in normals, metastases and cirrhosis

5.4 Differences in perfusion between right and left lobes

5.5 Perfusion of focal liver lesions

5.6 Perfusion imaging: Case studies

5.1 Patients and methods:

Patients:

Twenty four patients' livers were studied by dynamic CT as part of the CT assessment of known or suspected liver disease. One study was excluded due to excessive movement of the patient. Of the remaining twenty three patients, the liver was considered normal in five (controls), 10 had cirrhosis, 4 had hepatic metastases and there was a miscellaneous group of 4 patients. The controls included 3 patients investigated for suspected hepatic metastases in whom the liver was shown to be normal on CT and ultrasound examination and who remained well with normal liver biochemistry and follow-up CT examinations six months later. The other 2 controls were a patient in whom hepatic cirrhosis had been suspected but was not confirmed on subsequent liver biopsy and a patient with a benign islet cell tumour of the pancreas, normal liver biochemistry and a morphologically normal liver. All patients with cirrhosis had the diagnosis confirmed histologically following liver biopsy. The cause of cirrhosis was alcohol in three cases and biliary cirrhosis in four with the remainder comprising cases of idiopathic cirrhosis, Wilson's disease and Gaucher's disease. Two cirrhotic livers also contained a hepatocellular carcinoma; one confirmed following biopsy and the other from a raised alpha fetoprotein. In patients with metastases, the diagnosis had been confirmed at laparotomy in 3 with the fourth patient

having a progressive focal liver lesion following surgical excision of a colonic carcinoma. The miscellaneous group comprised two patients following liver transplantation, a case of post anaesthetic hepatitis (histological diagnosis) and a liver with an area of focal fat infiltration which had remained unchanged on serial examinations over 18 months.

Data Acquisition:

The Siemens Somatom Plus CT system located at Cambridge was used. A single location dynamic sequence with a 10mm slice thickness was performed at the level of the liver following a 50ml bolus of Iopamidol 300mg/ml injected as rapidly as possible by hand (8 to 10 seconds) into an antecubital vein. The data acquisition protocol was as for the renal studies (Section 4.2. i.e. 1 second acquisitions at 0, 6.5s, 9.5s, 12.5s, 15.5s, 20.5s, 25.5s, 30.5s, 37s and 43.5s) The patient was breathing as quietly as possible during the examination. The level for the sequence was chosen either to include a focal abnormality identified on unenhanced images or to include left and right lobes of the liver as well as spleen in the cases of diffuse liver disease. Some studies were from examinations performed to evaluate another organ e.g. pancreas where the liver happened to be included in the slice. The images were subsequently compressed into a 256 x 256 matrix and transferred to the Acorn Archimedes computer workstation. Patients had not been asked to starve beforehand.

Region of Interest (ROI) analysis:

Time-density curves (TDC) were created from circular ROIs with a minimum size of 50 pixels (256 x 256 matrix) drawn over the aorta, right lobe of liver, left lobe of liver and spleen. The ROIs were as large as possible to minimise noise but with a sufficient margin from the edge of the structure to avoid partial volume effects. The time of peak splenic enhancement was used to identify the separation of arterial and portal phases on the liver TDCs. When spleen was not included in the slice, the time of peak pancreatic or renal cortical enhancement was used. Using the methodology described in section 3.4, hepatic arterial, hepatic portal and total hepatic perfusion and the hepatic perfusion index (HPI) were calculated. The arterial perfusion of any focal abnormalities in the liver and splenic perfusion were determined as outlined in section 3.3.

5.2 Validation by comparison with dynamic colloid scintigraphy:

Eight of the above patients (2 with normal livers, 6 with cirrhosis) also underwent dynamic colloid scintigraphy with measurement of the ratio of arterial to total liver blood flow (Hepatic Arterial Ratio: HAR) within one week of the dynamic CT examination. A large field of view gamma camera was positioned posteriorly over the liver and spleen and, following a bolus injection of 150 - 350 MBq of ^{99m}Tc labelled colloid, a series of 2 second frames were acquired over 5 minutes into a 64 x 64 matrix. The splenic uptake method of analysis, as described by Wraight et al [70], was used to determine the hepatic arterial ratio (HAR) from a ROI over the right lobe of the liver. The value of HPI from the right lobe as derived from the CT method was compared with the scintigraphic value of HAR for each of the 8 patients.

So as to assess the likelihood of any inaccuracies in timing peak splenic enhancement affecting separation of arterial and portal phases, the times of maximal rate of enhancement in each phase for the right lobe ROI and the time of peak splenic enhancement were also noted for all 23 patients.

Results:

Figure 5.1 compares the results of dynamic colloid scintigraphy and dynamic CT. There was a significant

correlation (Pearson's correlation test, $p<0.001$, $r = 0.94$) between the HAR and the CT measurement of HPI from the right lobe of liver.

The mean values and ranges of the times to peak splenic enhancement and times to maximal rates of arterial and portal enhancement (and the intervals between these times) are given in table 5.1. The minimum time between the time of peak splenic enhancement and maximal rate of enhancement in either phase was 1.0 seconds.

Discussion:

The statistically significant correlation between dynamic colloid scintigraphy and dynamic CT has provided reasonable direct validation of the CT technique for determining the HPI. The CT method underestimates portal perfusion because there is some loss of contrast medium into the extracellular space of the spleen and gut during its first pass through these organs prior to passage to the liver in the portal blood. Thus, CT values for HPI are generally higher than the corresponding HAR value from scintigraphy.

Inaccuracies in the timing of peak splenic enhancement could falsely separate arterial and portal phases, and this was a problem for early radionuclide methods using non-extracted tracers [60]. However, unlike the radionuclide techniques which integrate the slope over several seconds, the CT method

requires the maximum slope to be measured. This occurs some seconds before (mean 9.1 s) and after (mean 6.2 s) peak splenic enhancement (Table 5.1) and so errors in timing of the peak will need to be large before affecting the measurements. In practice, this does not seem to occur.

TABLE 5.1

	Mean (s)	Range (s)
Time of maximal slope during Arterial phase.	15.3	10.5 - 25.9
Time of maximal slope during Portal phase	30.6	20.7 - 36.8
Time of peak splenic enhancement	24.4	15.4 - 33.4
Time from maximal arterial slope to splenic peak	9.1	1.8 - 22.9
Time from splenic peak to maximal portal slope	6.2	1.0 - 21.3
Time between maximal arterial and maximal portal slopes	15.3	4.0 - 26.2

Time of maximal arterial and portal slopes of liver time-density curves and their relationship to the time of peak splenic enhancement.

Measurement of arterial/total perfusion: Comparison of nuclear medicine and CT

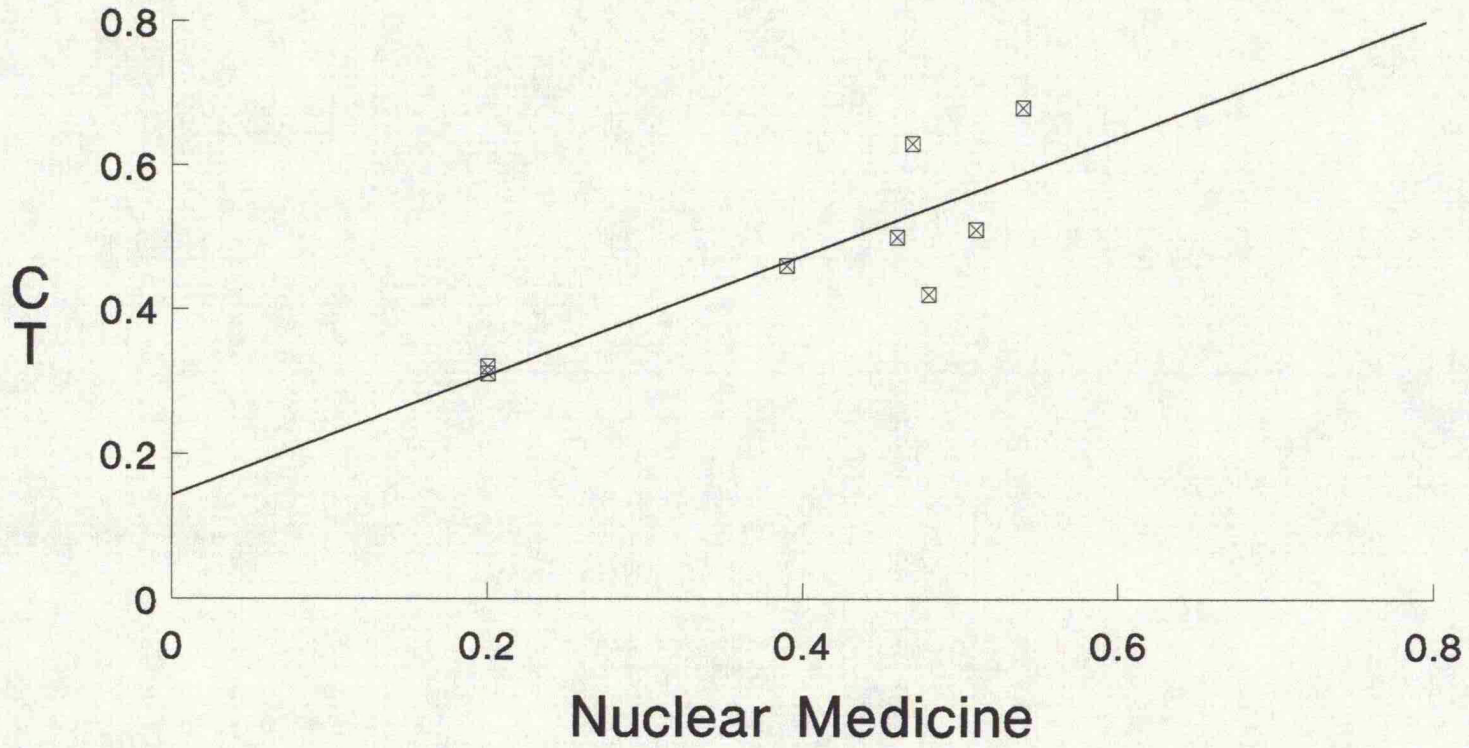

Figure 5.1

5.3 Hepatic perfusion in normality and disease:

Right lobe ROIs were available in all of the 23 patients successfully studied. The values of arterial, portal and total hepatic perfusion and HPI from the right lobe were compared for normal, cirrhotic, metastatic and miscellaneous groups using the Wilcoxon Rank-Sum test.

Results:

Figure 5.2 demonstrates the differences in right lobe arterial, portal and total perfusion and HPI derived from ROI analysis for the four groups of patients and the median values are listed in table 5.2. The median HPI was significantly higher in patients with cirrhosis (0.65), metastases (0.65) and the miscellaneous group (0.59) than in the controls (0.32; $P<0.005$, 0.05 & 0.05 respectively.) Portal perfusion was significantly lower in patients with cirrhosis (median: 0.17 $ml.min^{-1}ml^{-1}$) than in controls (median: 0.34 $ml.min^{-1}ml^{-1}$; $P<0.02$) but this was not so for the other groups. Arterial perfusion was significantly raised in patients with cirrhosis (median: 0.36 $ml.min^{-1}ml^{-1}$; $P<0.002$) or metastases (median: 0.50 $ml.min^{-1}ml^{-1}$; $P<0.02$) when compared with controls (median: 0.15 $ml.min^{-1}ml^{-1}$). The separation between the groups was clearest for arterial perfusion with portal perfusion demonstrating greater variability. There was no statistically significant difference in total hepatic perfusion between the four

groups, although there was a trend for total perfusion to be higher in livers containing metastases.

TABLE 5.2

	Normals	Cirrhosis	Metastases	Miscell.
Arterial Perfusion ($ml.min^{-1}ml^{-1}$)	0.15	0.36	0.50	0.23
Portal Perfusion ($ml.min^{-1}ml^{-1}$)	0.34	0.17	0.27	0.27
Total Perfusion ($ml.min^{-1}ml^{-1}$)	0.50	0.59	0.79	0.51
Hepatic Perfusion Index	0.32	0.65	0.65	0.59

Median values of liver perfusion parameters derived from the right lobe of liver for the four groups of patients.

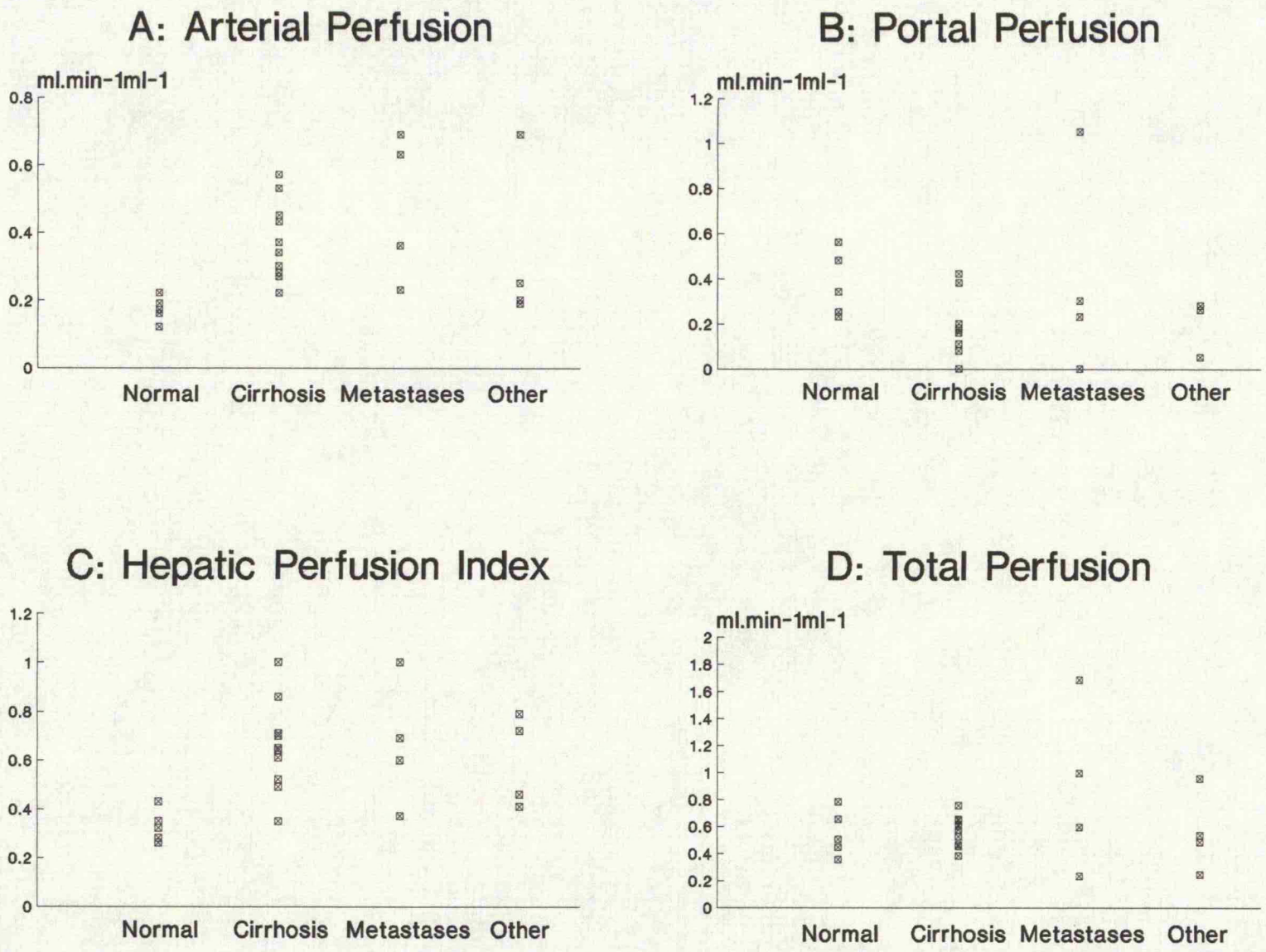

Figure 5.2 Perfusion values from the right lobe for various liver conditions.

Discussion:

Estimation of hepatic perfusion parameters in humans has yielded a wide range of results, both between individuals and the techniques used. Total perfusion is in the region of 1 $ml.min^{-1}ml^{-1}$, of which 20% is arterial [71]. Thus, the CT value of 0.15 $ml.min^{-1}ml^{-1}$ for arterial perfusion obtained from normal patients is close to the normal value of approximately 0.2 $ml.min^{-1}ml^{-1}$ derived from other techniques [71]. The portal perfusion and hence total perfusion are significantly underestimated by the CT technique (portal: 0.34 $ml.min^{-1}ml^{-1}$ vs. 0.8 $ml.min^{-1}ml^{-1}$ and total: 0.5 $ml.min^{-1}ml^{-1}$ vs. 1.0 $ml.min^{-1}ml^{-1}$ respectively). This could be due to either bolus spreading or loss of contrast medium from the circulation into the extravascular space during its passage through the gut and spleen.

The facts that CT arterial perfusion values in normals are close to reference ranges and that the CT technique has demonstrated appropriate changes in hepatic perfusion parameters in various diseases provides further clinical validation and indicates potential clinical uses of the technique. The increase in HPI that occurs in cirrhosis can be seen to be due to not only a fall in portal perfusion, as would be expected due to portal hypertension, but also to a rise in arterial perfusion (figure 5.2). This reciprocal relationship has been previously demonstrated using flow meters in the experimental dog [72] and the human at surgery

[73]. The increased arterial perfusion associated with hepatic metastases arises because these lesions have a predominantly arterial blood supply. The slight, but not statistically significant, fall in portal perfusion will be partially due to replacement of liver tissue by metastases that have no portal supply. Also, increased pressure with a liver segment containing metastases by increasing the resistance to portal flow causing a reduction in portal perfusion. The drop in total perfusion reported in cirrhosis using washout of radioactive xenon [74,75] was not seen with the CT technique. As the portal perfusion is underestimated by CT, the apparent magnitude of any fall in portal perfusion in cirrhotics will be less than the true extent and is likely to be swamped by the increase in arterial perfusion (which is measured more accurately).

5.4 Differences between right and left lobes:

The left lobe was included on the chosen slice in 18 of the 23 patients successfully studied, comprising 4 control patients, 4 with metastases, 8 with cirrhosis and 2 from the miscellaneous group. The values of arterial, portal and total perfusion for right and left lobe ROIs were determined and compared (Signed rank test for paired samples). The ratios of right to left perfusion values were calculated for three groups: control patients, cirrhotics and those with metastases. The ratios for the groups were compared using the Wilcoxon Rank-Sum test. The presence of any correlation between right or left lobe portal perfusion and splenic perfusion was also sought.

Results:

These are summarised in table 5.3 and figure 5.3. Taking all 18 patients as a single group, median arterial perfusion and total perfusion were higher in the left lobe ($P<0.02$ and $P<0.005$ respectively), but there was no statistically significant difference in portal perfusion. The raised arterial perfusion in patients with cirrhosis and metastases and the fall in portal perfusion in cirrhosis observed for the right lobe were much less apparent on the left, as there seemed to be much greater variability in perfusion measurements.

The ratio of portal perfusion between right and left lobes

was significantly different in cirrhotic livers as compared with controls ($p<0.05$). All four control patients had higher portal perfusion in the right lobe (Ratio Right/Left > 1.0) whereas this was only so for one patient with cirrhosis. Similar results were obtained for livers containing metastases but this did not reach statistical significance due to small numbers. This was also reflected in the HPI results where the median HPI was higher in the left lobe in control patients but higher in the right lobe for the other groups of patients. The right to left ratios for arterial and total perfusion showed no statistically significant differences between the three groups of patients.

8 patients had a left lobe arterial perfusion twice that of the right. They comprised 2 control patients, 3 patients with cirrhosis, one with a superadded hepatocellular carcinoma, 1 patient with metastases and 2 from the miscellaneous group; one of the miscellaneous patients was a patient with focal fat infiltration in the right lobe, the other had recurrent haemangioendothelioma within a liver transplant. In these patients, transient differences in attenuation between the lobes were visible on the standard enhanced CT images (figure 5.4).

There was a significant correlation (Pearson's correlation; $p<0.01$, $r=0.66$) between splenic perfusion and portal perfusion for the right lobe but not for the left. (figure 5.5)

TABLE 5.3

	Right Lobe	Left Lobe	Ratio (R/L)
Arterial Perfusion ($ml.min^{-1}ml^{-1}$)			
Controls	0.17	0.37	0.71
Cirrhosis	0.34	0.42	0.78
Metastases	0.50	0.69	0.63
All	0.28	0.58	0.63
Portal Perfusion ($ml.min^{-1}ml^{-1}$)			
Controls	0.41	0.33	1.27
Cirrhosis	0.17	0.31	0.55
Metastases	0.12	0.89	0.22
All	0.23	0.41	0.73
Total Perfusion ($ml.min^{-1}ml^{-1}$)			
Controls	0.58	0.74	0.89
Cirrhosis	0.59	1.08	0.74
Metastases	0.79	1.75	0.38
All	0.58	0.92	0.60
Hepatic Perfusion Index			
Controls	0.30	0.52	0.58
Cirrhosis	0.67	0.47	1.43
Metastases	0.65	0.59	1.10
All	0.57	0.55	1.03

Median values for perfusion parameters from right and left lobes and median right/left ratios for controls (n=4), patients with cirrhosis (n=8), patients with metastases (n=4) and all patients (n=18).

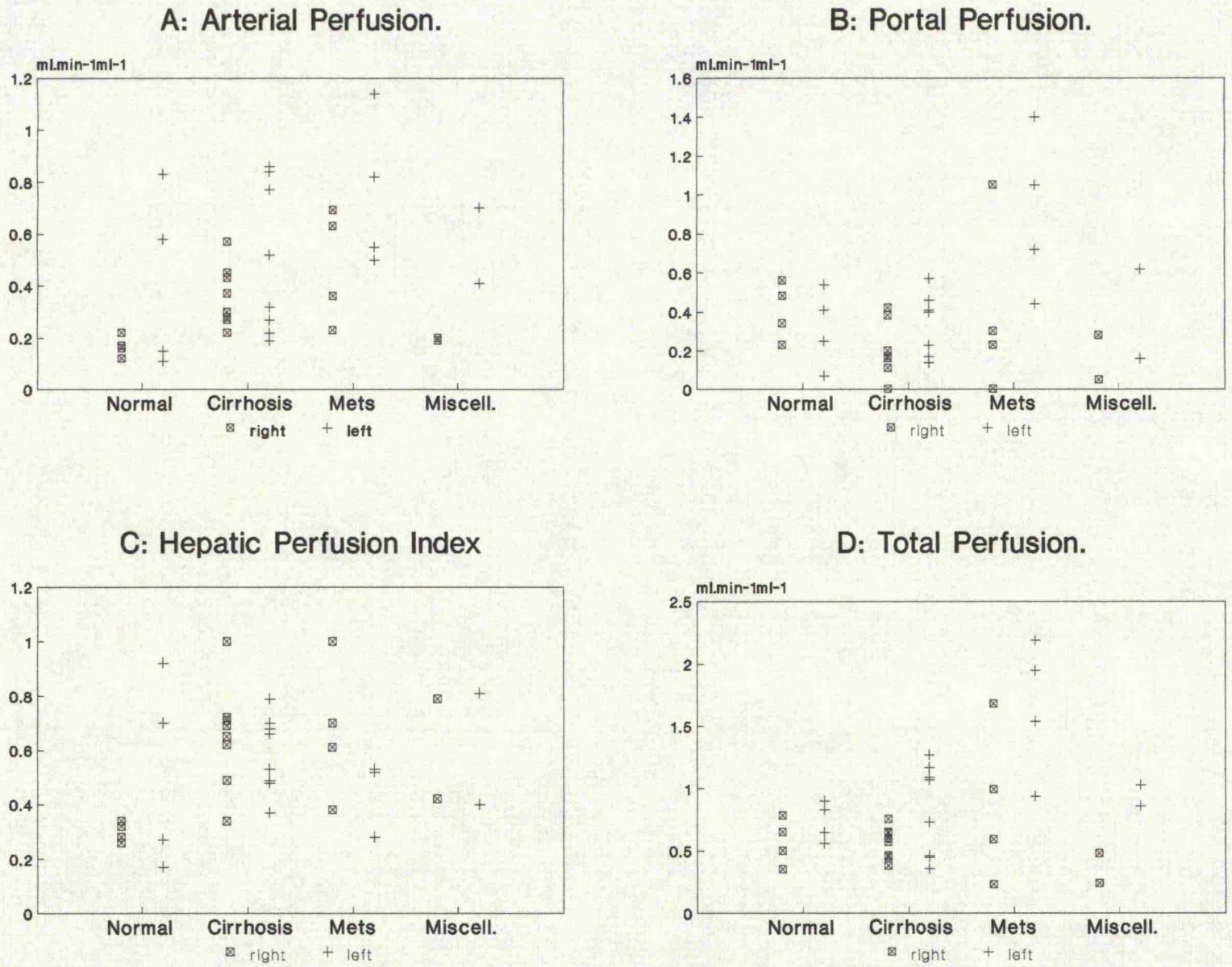

Figure 5.3: Perfusion parameters; differences between lobes.

Figure 5.4: Images from a single location dynamic sequence demonstrating a transient lobar difference in attenuation of the liver (greater enhancement in the left lobe).

Portal perfusion correlated against splenic perfusion.
A: Right Lobe

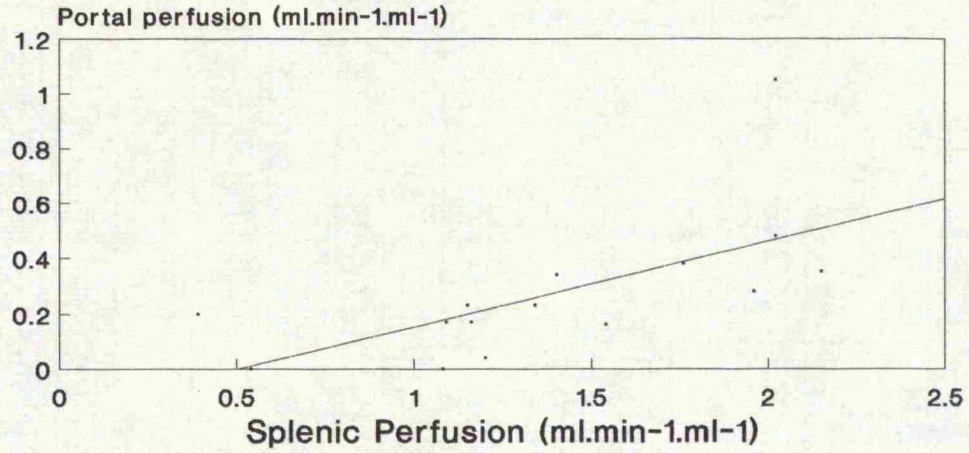

r = 0.66, p<0.01

B: Left lobe

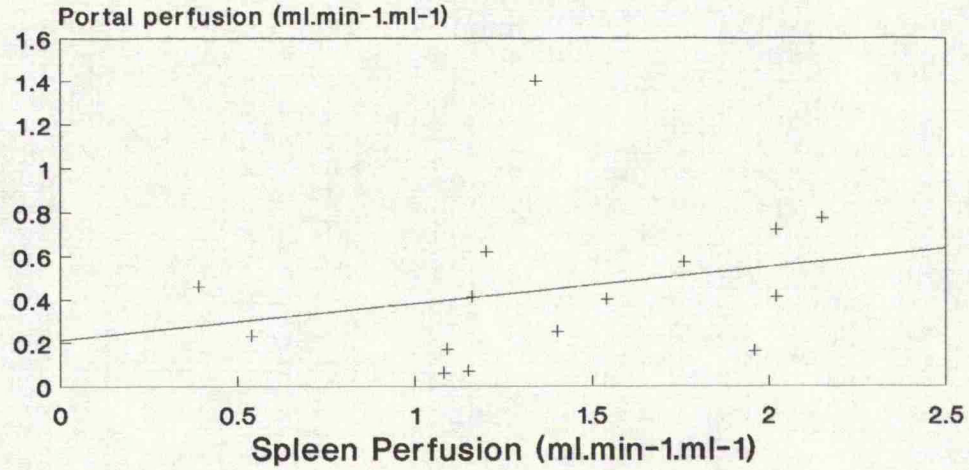

N.S.

Figure 5.5

Discussion:

The values for portal and total perfusion for the left lobe are higher and much closer to accepted normal values than the right lobe results. Great variability in regional liver perfusion has also been reported after radioactive xenon gas washout studies [76]. The fact that CT measurements of total perfusion are higher in the left lobe (although not reaching statistical significance) is discordant with the findings of Shiomi et al [75] using rectal xenon-133 gas. Although denied by some authors [77], streaming of blood within the portal vein has been hypothesised by others who propose that blood from the splenic, left gastroepiploic and inferior mesenteric vein predominantly passes to the left lobe of the liver and superior mesenteric blood to the right [78]. The time-dependent concentration of contrast medium returning to the liver from either the superior or inferior mesenteric circulations will depend upon the relative total blood flow of each circulation and, as discussed in section 5.2, the amount of bolus spreading and loss of contrast medium within gut and spleen. If any of these factors is different between the two circulations, then, as a result of streaming the portal vein, greater or lesser amounts of contrast medium may be returned in the portal blood going to either lobe.

The relative preservation of left lobe portal perfusion in cirrhotics is in keeping with similar findings for total left lobe perfusion by Shiomi et al [75] in such patients. Liver

mass is also thought to be related to portal perfusion [71,79] and this preservation of portal perfusion to the left lobe may be an important causal factor in the left lobe hypertrophy seen in many cases of cirrhosis.

Furthermore, portal vein streaming and the absence of a strict policy of fasting prior to the examination could account for the greater variability of perfusion values within the left lobe. A recent meal will cause an increase in hepatic blood flow (arterial or portal) in response to the increased metabolic demand placed upon the liver. If blood from the stomach passes predominantly to the left lobe, then left lobe perfusion could be raised in those patients who have eaten recently.

The possibility of a technical cause for greater variability of perfusion parameters in the left lobe must also be considered. The left lobe may be more susceptible to respiratory movement than the right with varying partial volume effects adding noise to the TDCs. However, the fact that in many cases transient differences in lobar attenuation were visible on the unprocessed enhanced images suggests that such artefacts cannot account for right-left differences in all patients.

The correlation between portal perfusion and splenic perfusion would be expected but the fact that right, but not left, lobe portal perfusion correlated with splenic perfusion

cannot be explained in terms of portal vein streaming with splenic blood passing predominantly to the left lobe. It is more likely that any correlation with left lobe portal perfusion is masked by the greater variability observed in left lobe perfusion parameters.

Transient regional variations in liver attenuation after intravascular contrast medium injection have been observed in portal vein branch thrombosis and focal liver lesions [80-83]. With portal vein occlusion, the fall in portal perfusion will be associated with a rise in arterial perfusion causing increased attenuation in the arterial phase. With focal liver lesions, a mass effect may compress portal vein branches thereby reducing portal perfusion with a reciprocal increase in arterial perfusion, as in portal venous thrombosis. Alternatively, a vascular focal lesion may increase the arterial supply to a large liver area due to a "steal" effect. Focal biliary obstruction or regional variations in the severity of cirrhosis could also create lobar differences in perfusion. More severely affected areas will have a lower portal and higher arterial perfusion than less affected or unaffected areas. Of the 8 patients with the most marked lobar differences in arterial perfusion, such focal abnormalities were not apparent in 4, including 2 control patients. The cause in these 4 patients remains obscure but could possibly be related to a recent meal.

5.5 Focal liver lesions:

ROIs were also created over focal liver lesions and the arterial perfusion calculated using the general equation for perfusion outlined in section 3.1.

Table 5.4 lists the arterial perfusion values observed in the seven focal liver lesions studies. As would be expected, hepatocellular carcinomas had the highest perfusion values. Metastases demonstrated a wide range of perfusion values and the case of focal fat had low perfusion. The hepatocellular carcinoma and all but one of the metastases had values greater than the arterial perfusion of supposedly normal hepatic parenchyma in the control patients. These findings are consistent with current knowledge concerning the blood supply to malignant lesions within the liver.

TABLE 5.4

LESION	ARTERIAL PERFUSION ($ml.min^{-1}ml^{-1}$)
HEPATOCELLULAR CARCINOMA	0.70
HEPATOCELLULAR CARCINOMA	0.59
METASTASIS	0.63
METASTASIS	0.56
METASTASIS	0.38
METASTASIS	0.19
FOCAL FAT	0.10

Arterial perfusion measurements from focal liver lesions (Normal hepatic arterial perfusion = 0.15 (range:0.12-0.22) $ml.min^{-1}ml^{-1}$.)

5.6 Functional Images:

These were created by calculating perfusion parameters from TDCs created for each pixel as outlined in section 3.5. These values were then used to create functional images of each parameter displayed using a 256 element colour scale. Rather than scaling the images to the maximum value, all functional images were displayed using the following colour scales to enable direct comparisons:

Hepatic Perfusion index: Black = 0% arterial,

Red = 100% arterial.

Arterial, Portal & Total Perfusion:

Black = 0 $ml.min^{-1}ml^{-1}$

Red = 2.5 $ml.min^{-1}ml^{-1}$

Any tissues with perfusion values greater than 2.5 ml/min/ml would therefore appear as white.

The images were evaluated visually to detect regional variations in hepatic perfusion parameters and to characterise focal abnormalities.

Results:

Functional images of arterial, portal and total perfusion and HPI were successfully obtained in all patients except the one excluded due to artefacts caused by marked respiratory movement. Perfusion parameters were calculated for all voxels in the image except air, fat and bone, which were eliminated by excluding pixels with initial attenuation values less than 0 or greater than 400. Thus perfusion values for voxels containing non-hepatic structures are also displayed. Although values for portal and total perfusion and HPI for such pixels have little physiological significance, they were included to maintain spatial orientation. Three cases studies are described below.

Case 1. Normal

A 60 year old man presenting with epigastric pain, diarrhoea and weight loss, was found to have a carcinoma of the sigmoid colon on a barium enema examination. A CT examination, performed to exclude metastases, was normal. Subsequent laparotomy confirmed a colonic carcinoma, which was resected, and a normal liver. The patient was well and had normal liver function tests 6 months later.

Figure 5.6 demonstrates the unenhanced CT image and the normal arterial, portal, total perfusion and HPI images. In this patient, the mean values in the right lobe for these parameters are 0.17 $ml.min^{-1}ml^{-1}$, 0.48 $ml.min^{-1}ml^{-1}$, 0.65 $ml.min^{-1}ml^{-1}$ and 0.26 respectively.

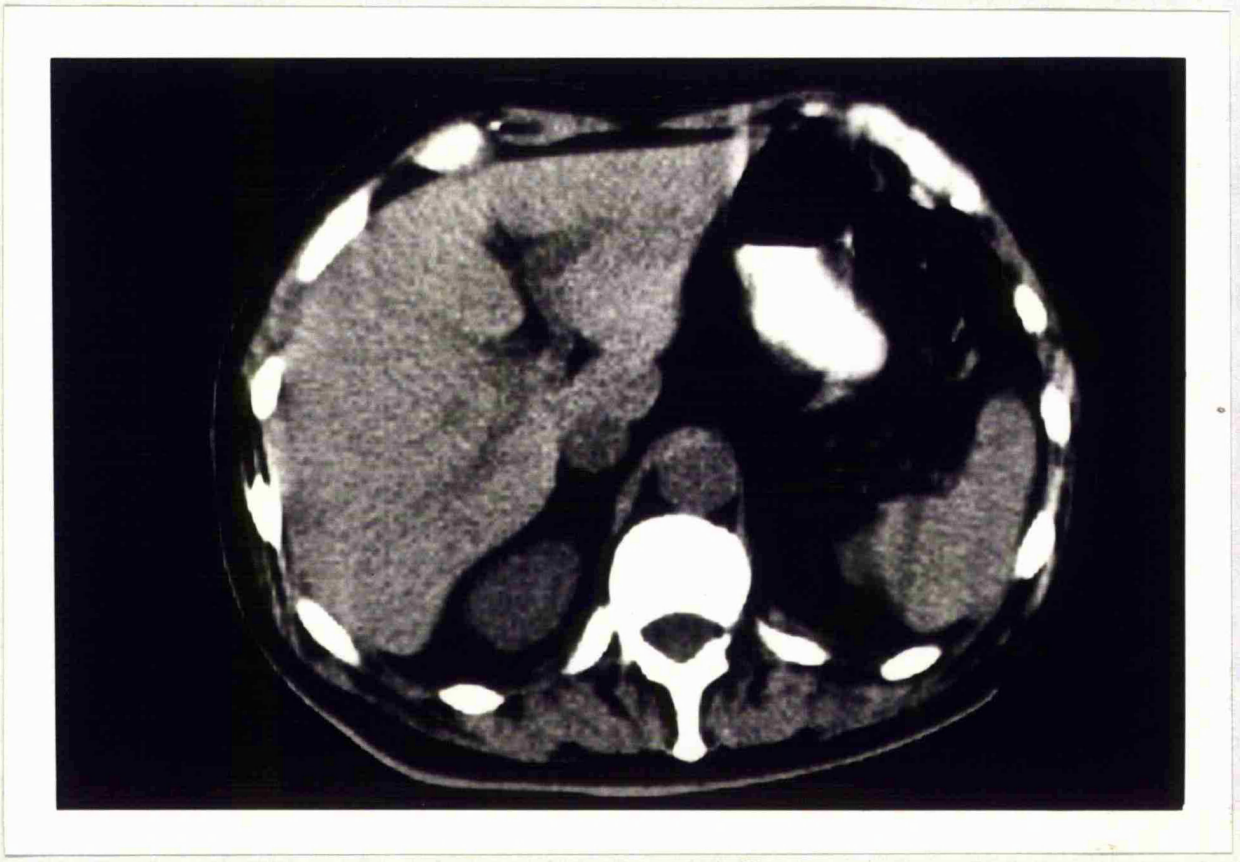

Figure 5.6A: Unenhanced CT from case 1: normal liver.

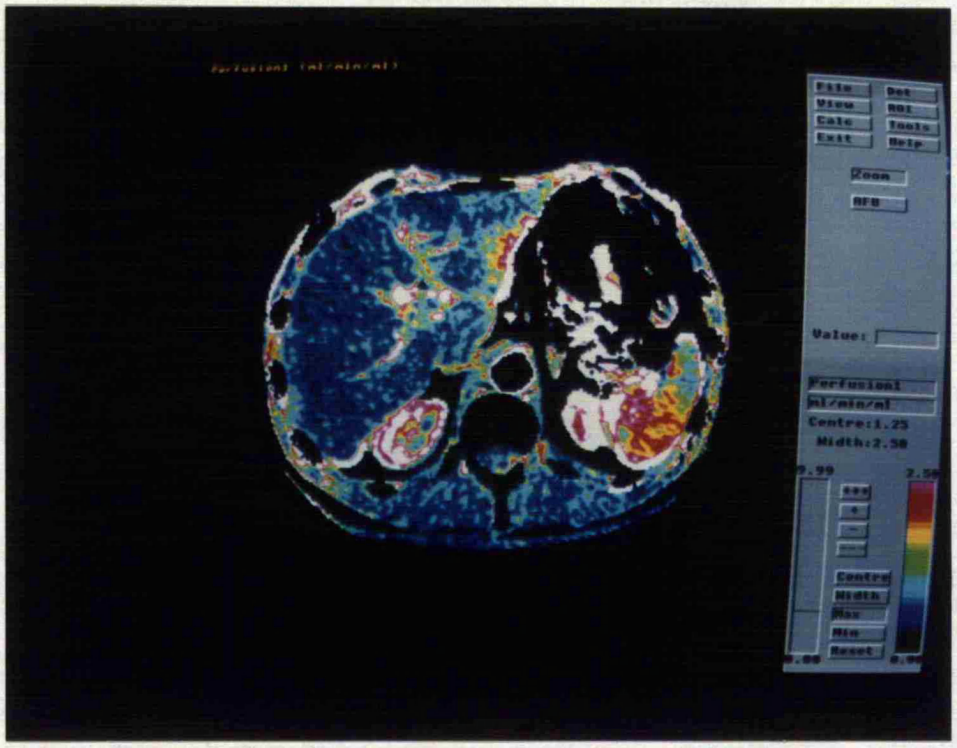

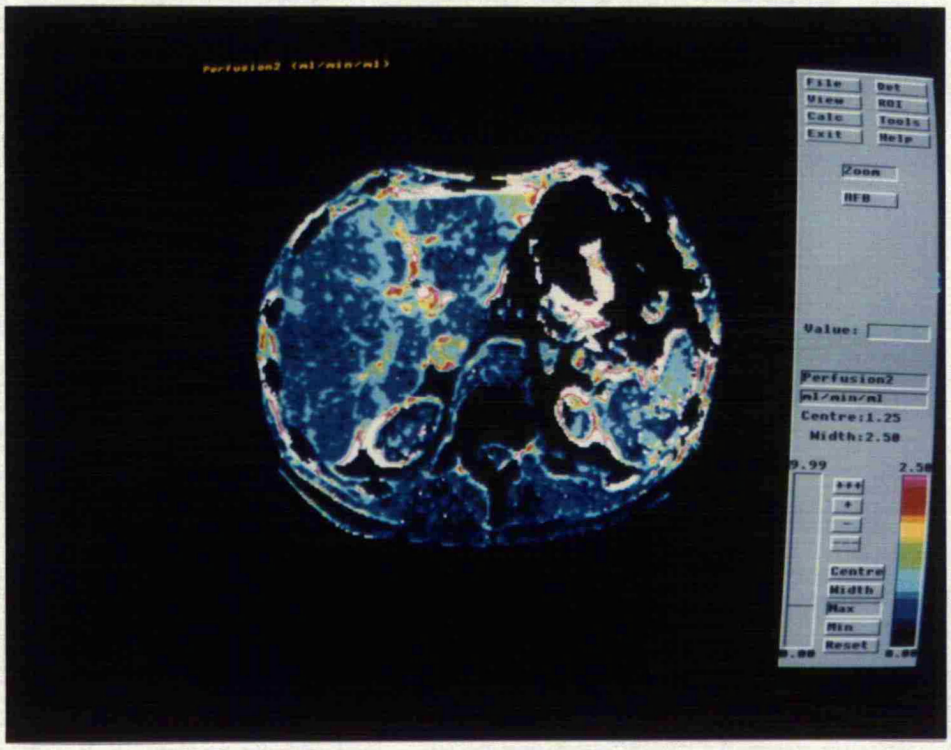

Figure 5.5B: Arterial (above) and portal (below) images from case 1: normal liver.

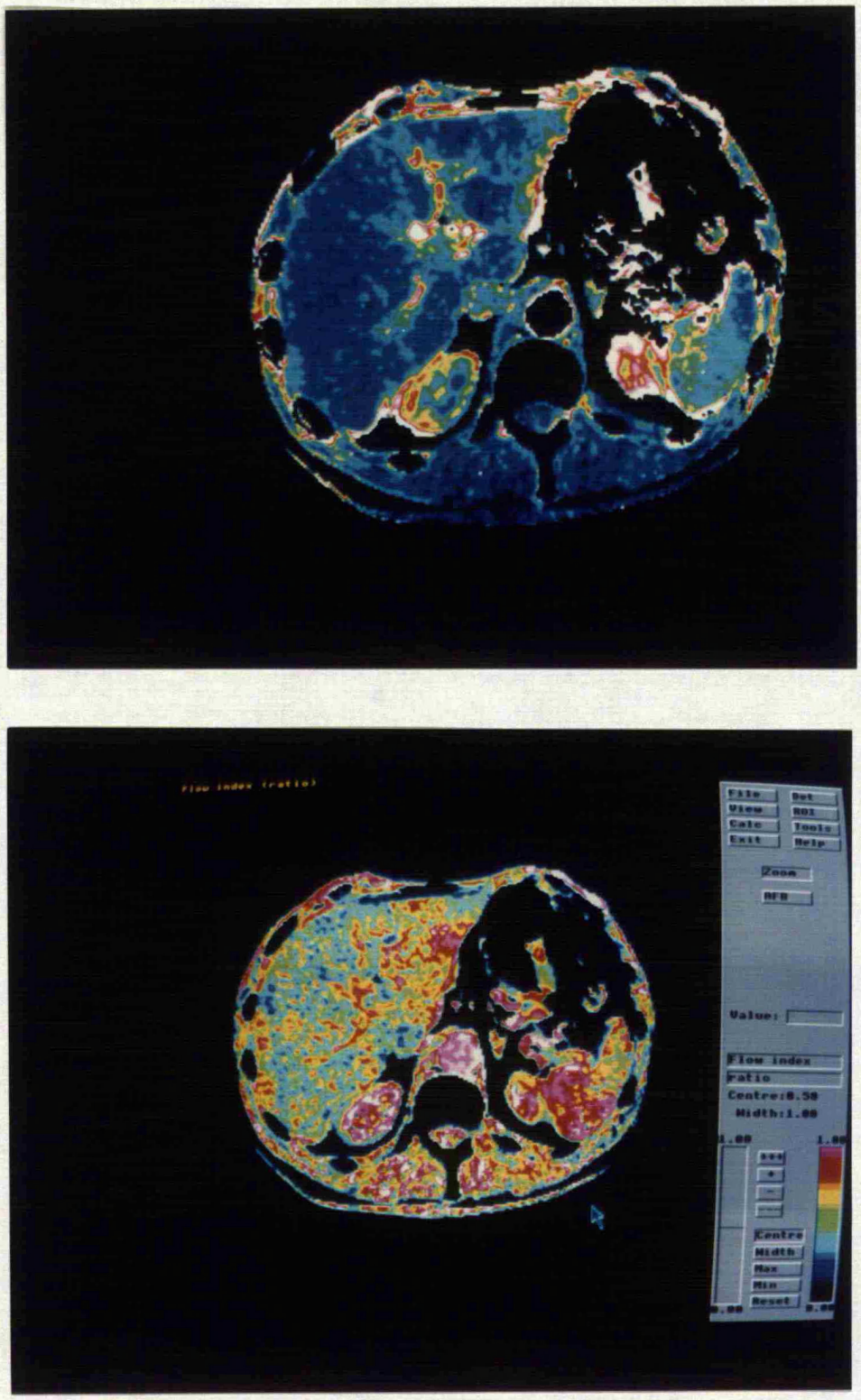

Figure 5.5C: Total perfusion (above) and HPI (below) images from case 1: normal liver.

Case 2: Idiopathic Cirrhosis and Hepatocellular Carcinoma.

A 68 year old lady with histologically proven idiopathic cirrhosis presented with bleeding oesophageal varices. The haemorrhage settled with conservative management but investigations revealed a raised serum alpha fetoprotein at 34 kUnits.l^{-1} (Normal <10). The standard CT images demonstrated typical features of cirrhosis with a hepatocellular carcinoma in the right lobe (figure 5.7A).

Figures 5.7B-C demonstrate the perfusion images. The HPI is increased throughout the liver (typically 0.67), including the hepatocellular carcinoma, with raised arterial (0.4 $ml.min^{-1}ml^{-1}$) and reduced portal (0.2 $ml.min^{-1}ml^{-1}$) perfusion. The hepatocellular carcinoma showed greatest perfusion peripherally with low values in the presumed necrotic centre (mean perfusion of whole lesion: 0.65 $ml.min^{-1}ml^{-1}$).

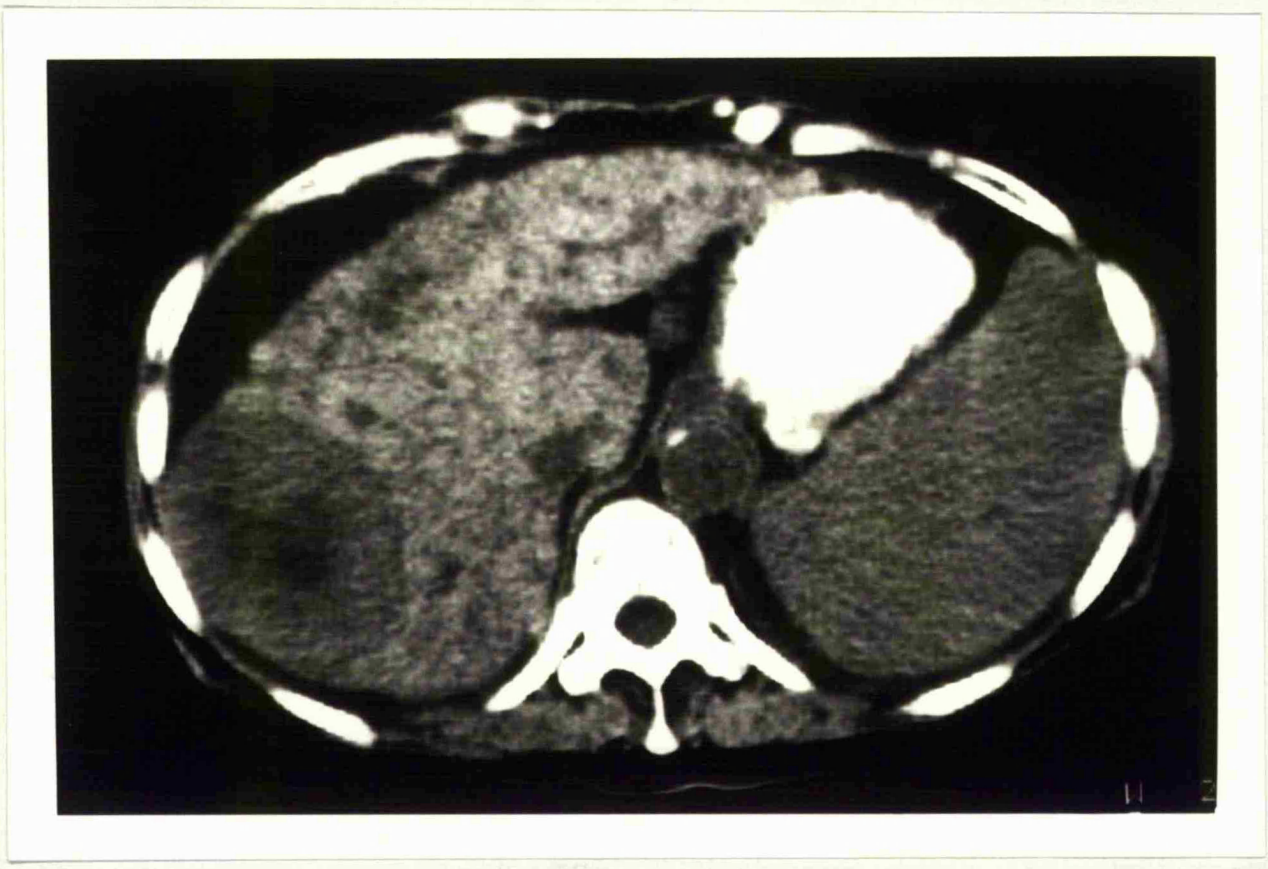

Figure 5.7A: Unenhanced CT from case 2: cirrhosis with hepatocellular carcinoma in the right lobe.

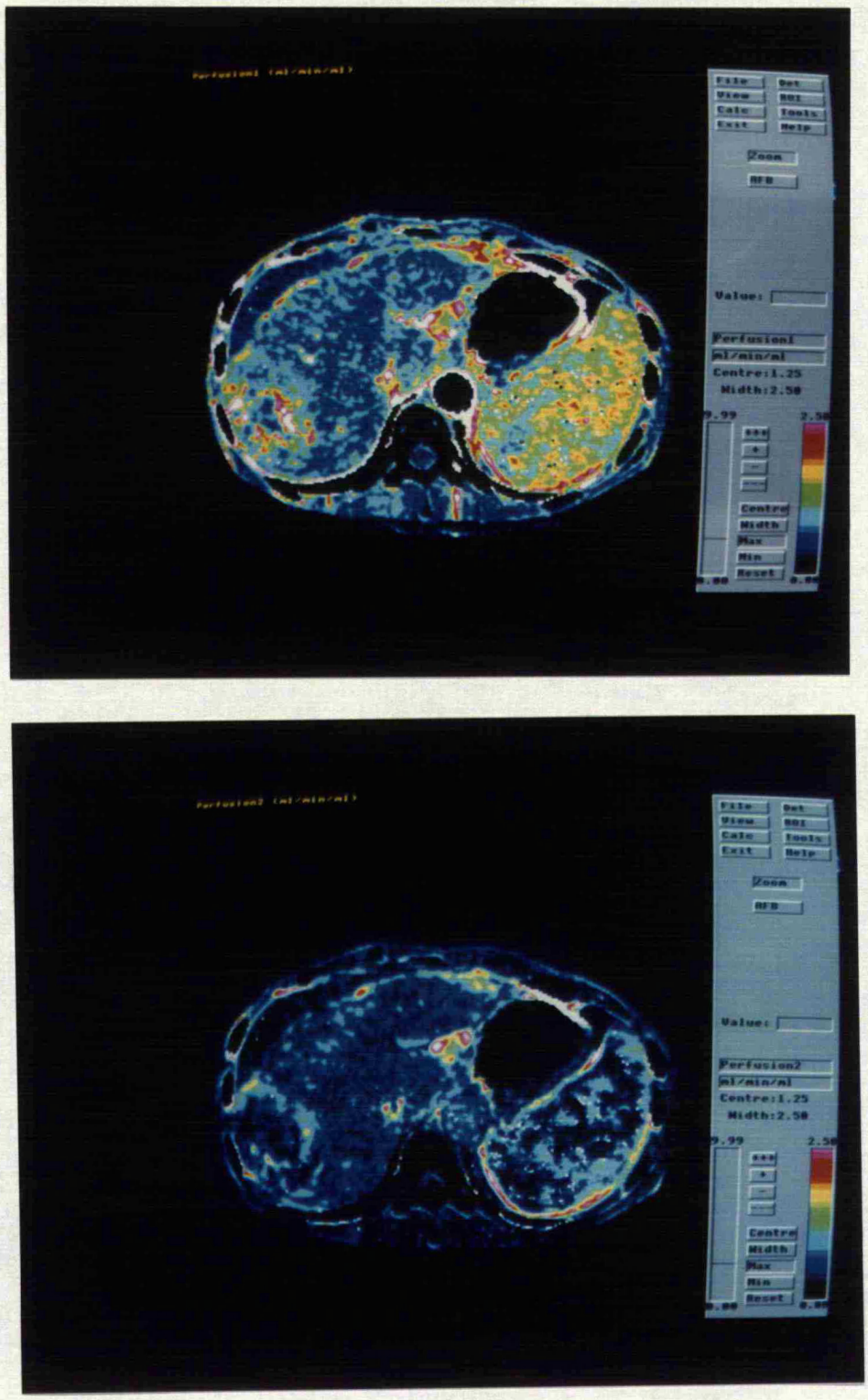

Figure 5.7B: Arterial (above) and portal (below) images from case 2: cirrhosis with hepatocellular carcinoma in the right lobe.

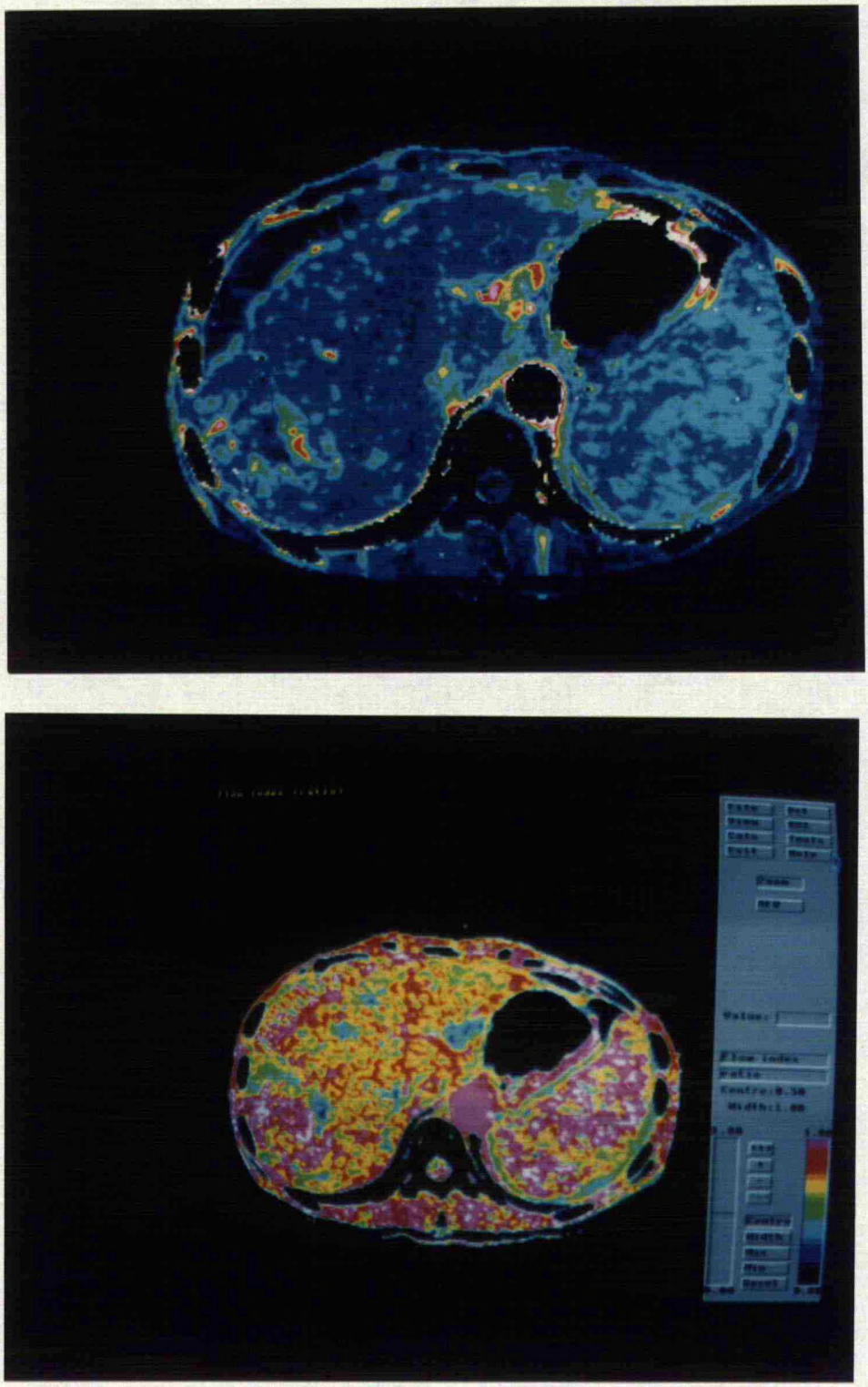

Figure 5.7C: Total perfusion (above) and HPI (below) images from case 2: cirrhosis with hepatocellular carcinoma in the right lobe.

Case 3: Hepatic Metastases

A 47 year man, presenting with upper abdominal pain, was found to have a gastric ulcer from which endoscopic biopsies revealed adenocarcinoma. At laparotomy, an antral carcinoma was confirmed and a liver metastasis was seen. A partial gastrectomy was performed. CT was requested to document disease extent prior to chemotherapy.

Figure 5.8A demonstrates an unenhanced CT slice and figures 5.8B-C the subsequent perfusion images. The metastasis is seen as a region of high value on the HPI but low value on the portal perfusion image. The perfusion is also abnormal in the areas which do not appear to contain metastases on the standard CT image, with raised HPI (0.4 to 0.55) and arterial perfusion (0.6 to 0.85 $ml.min^{-1}ml^{-1}$).

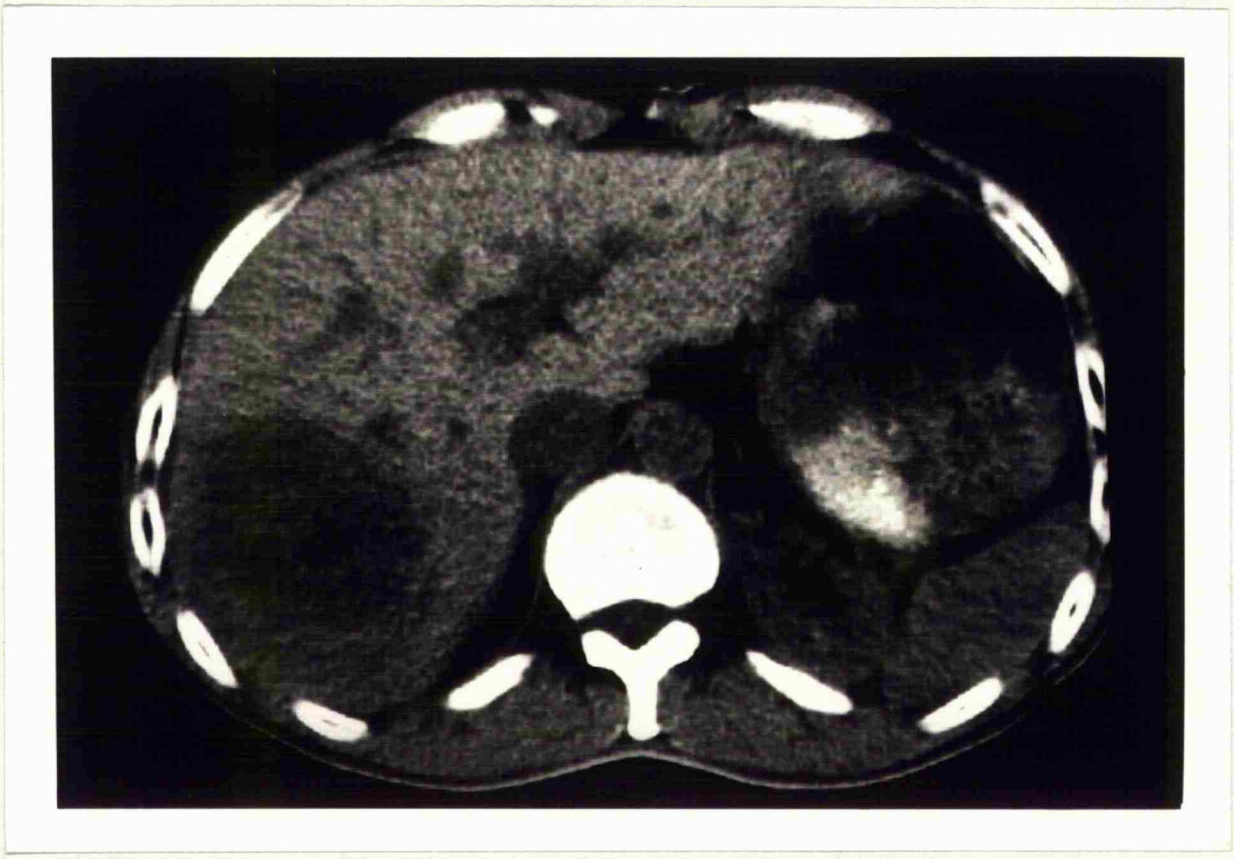

Figure 5.8A: Unenhanced CT from case 3: hepatic metastases.

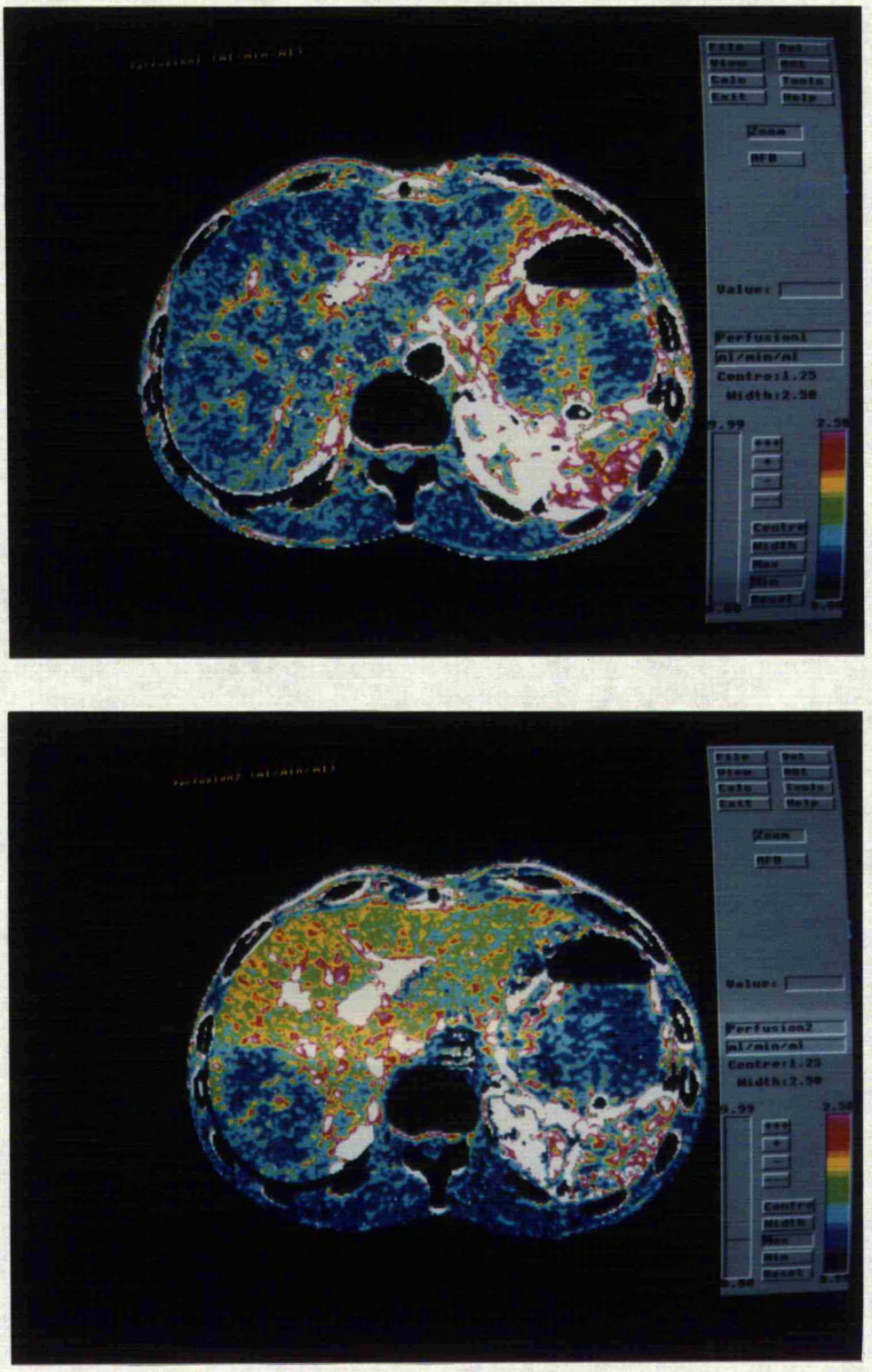

Figure 5.8B: Arterial (above) and portal (below) images from case 3: hepatic metastases.

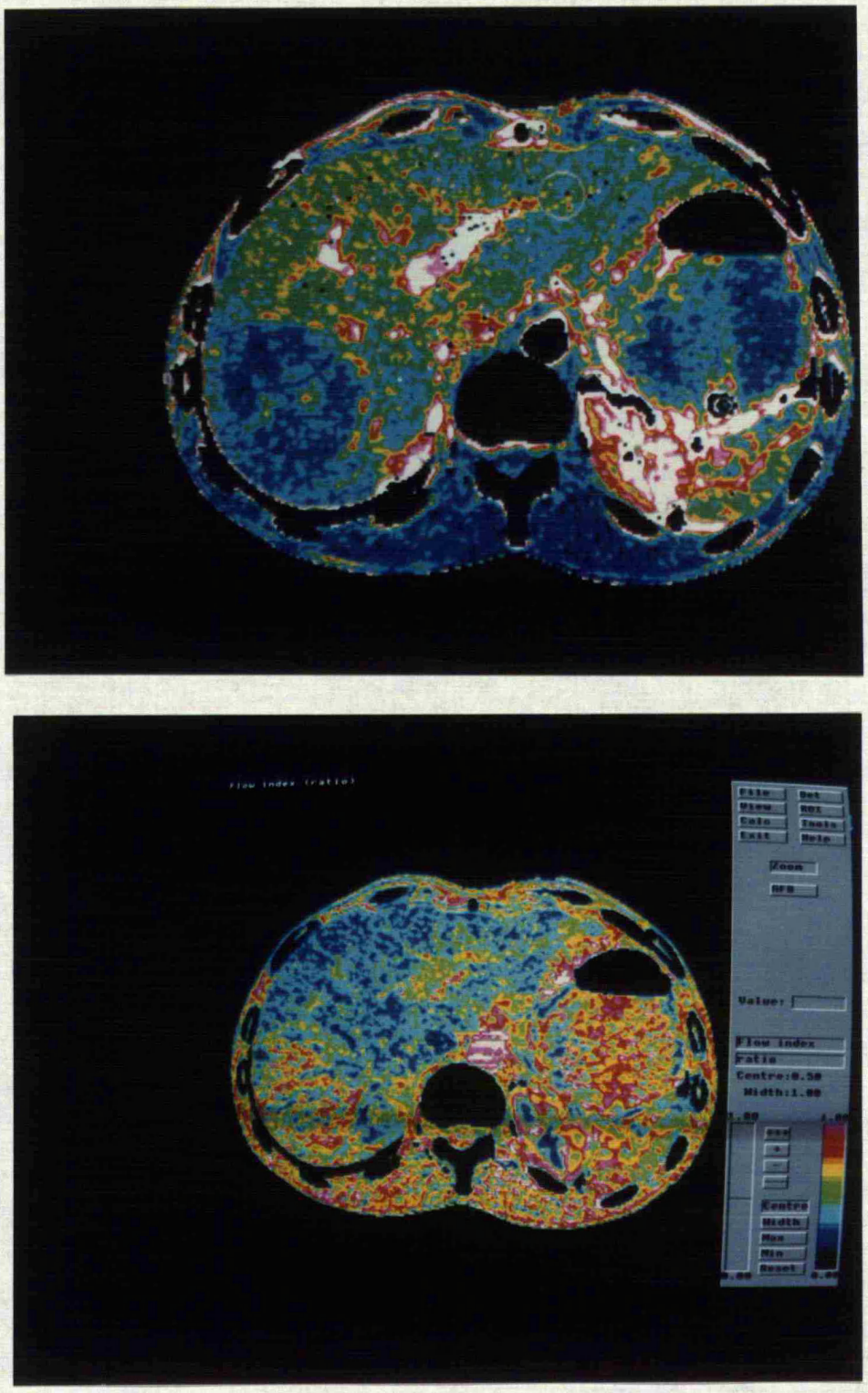

Figure 5.8C: Total perfusion (above) and HPI (below) images from case 3: hepatic metastases.

Discussion:

The functional images visually confirmed the findings from region of interest analysis in sections 5.2 and 5.3: arterial perfusion and HPI were increased in patients with metastases and cirrhosis whilst portal perfusion decreased. As liver tumours, whether primary hepatocellular carcinoma or metastatic deposits, have a blood supply derived almost exclusively from the arterial rather than portal circulation, they appear as areas of raised arterial perfusion and HPI on the functional images. In livers that contain metastases, the areas that appear morphologically unaffected display abnormal haemodynamics with an increased arterial perfusion and HPI. There are many possible explanations for this. Radionuclide studies of liver blood flow in patients with colonic cancer have demonstrated a group of patients with a raised HPI in whom metastases are not visible on imaging or at surgery [62]. Such patients have a greater probability of subsequently developing hepatic metastases than those with normal flow characteristics and it is proposed that the presence of "micrometastases", too small to visualise, cause alterations in liver haemodynamics. Thus, in patients with visible metastases, the apparently unaffected portions of liver could contain micrometastases. Other possible explanations are those proposed for transient lobar attenuation differences in patients with focal liver lesions as discussed in section 5.4.; a hypervascular lesion may increase arterial flow to the whole of a liver region on

account of a steal phenomenon or increased pressure within a liver segment reducing portal flow with a reciprocal rise in arterial perfusion.

6. SPLEEN

6.1 Normal splenic perfusion using region of interest analysis.

6.2 Assessment of the splenic microcirculation.

6.3 Functional images of splenic perfusion: case studies.

6.1 Normal splenic perfusion using region of interest analysis

Patients and Methods:

a) IGE 8800

Splenic perfusion was studied in twelve patients undergoing dynamic CT for staging of renal carcinoma, diagnosis of renal vein thrombosis in the nephrotic syndrome or diagnosis of renal artery stenosis where the spleen was included on the slice studied. In all cases the spleen appeared normal on unenhanced and contrast enhanced images and in the patients with renal carcinoma, no splenic abnormality was found at laparotomy.

The CT machine used was the IGE 8800 situated at the Leicester Royal Infirmary. A single location dynamic sequence was performed with data acquisitions performed as rapidly as possible, i.e. six second data acquisitions every eight seconds, during quiet breathing. 50 ml of iopamidol 370 $mg.ml^{-1}$ was injected intravenously by hand as rapidly as possible and time-density curves (TDCs) were derived from regions of interest (ROIs) constructed over the abdominal aorta and spleen. ROIs were made as large as possible to reduce the effects of photon noise whilst avoiding partial volume effects. Splenic perfusion was calculated using the formula derived in Chapter 3.3.

b) Siemens Somatom Plus

Splenic perfusion was studied in nine patients undergoing dynamic CT for assessment of the liver. In seven patients, the indication for CT was suspected metastases. In three of these patients, metastases were not found and liver biochemistry and follow up CT examinations remained normal 6 months later. Of the remaining two patients, one was found to have focal fat infiltration of the liver and a further patient was investigated for suspected hepatic cirrhosis but a subsequent liver biopsy proved to be normal. In all patients, no focal abnormality was seen in the spleen either on unenhanced or enhanced images.

The Siemens Somatom Plus CT system situated at Addenbrooke's hospital, Cambridge was used. The data acquisition protocol was as for the studies of kidney (section 4.2) and liver (section 5.1). ROIs were constructed over the aorta and spleen and splenic perfusion was calculated as described in section 3.3.

Results:

The mean value of splenic perfusion amongst the twelve patients studied using the IGE 8800 was 1.2 $ml.min^{-1}ml^{-1}$ with a standard deviation (SD) of 0.4 $ml.min^{-1}ml^{-1}$ as

compared with 1.4 $ml.min^{-1}ml^{-1}$ with a SD of 0.3 $ml.min^{-1}ml^{-1}$ in the nine patients studied using the Siemens Somatom Plus.

Discussion:

Clearly, there is good agreement in the measured value of splenic perfusion for the two CT systems. The poorer time resolution of the IGE is likely to underestimate the perfusion as the maximal slope of tissue enhancement will not be measured quite so accurately. However, this error is likely to be greatest at high perfusion values and comparison of renal perfusion values measured using the two CT systems (section 4) showed a large discrepancy for the renal cortex (IGE: 2.5 $ml.min^{-1}ml^{-1}$, Somatom Plus: 4.7 $ml.min^{-1}ml^{-1}$) but close agreement for the medulla (1.1 $ml.min^{-1}ml^{-1}$ for both systems).

Human splenic perfusion has been determined previously by a number of authors using various methods. Washout studies using Xenon-133 or Krypton-85, either by intra-arterial injection or inhalation, are likely to be more accurate than methods using labelled blood cells, such as platelets or erythrocytes, as blood cells may be sequestered within the spleen in view of its reticulo-endothelial and blood filtering functions. The values for human splenic perfusion from washout studies range from 0.96 $ml.min^{-1}g^{-1}$ to 1.19 $ml.min^{-1}g^{-1}$ [84-88] (figure 6.1).

It has not been possible to validate the CT splenic perfusion values directly by comparison with another method in individual patients. However, the CT results are in close agreement with the values derived from gas washout studies but give slightly higher results. One reason for CT overestimating perfusion is that the results are expressed in $ml.min^{-1}ml^{-1}$ rather than $ml.min^{-1}g^{-1}$. The density of the spleen is greater than $1g.ml^{-1}$ and thus converting to $ml.min^{-1}g^{-1}$ will yield slightly lower perfusion values. Assuming a typical soft tissue density of the spleen of 1.05 $g.ml^{-1}$, the error would be in the region of 5%. It should also be remembered that rare gas techniques will be affected by the fat content of the spleen due to the high affinity of such gases for lipids. It is estimated than such an error could be in the region of 10% [87]. The CT technique is unaffected by splenic fat.

For the patients studied using the Siemens Somatom Plus, it is assumed that the presence of hepatic metastases does not influence splenic perfusion. However, as discussed in section 4, changes in portal perfusion may occur in patients with hepatic metastases and splenic perfusion was found to correlate with right lobe portal perfusion. Thus, it is possible that the presence of hepatic metastases could be associated with a reduction in splenic perfusion. On the other hand, the presence of splenic metastases too small to

be seen on the images could possibly increase splenic perfusion. Nevertheless, no significant difference in splenic perfusion was observed between those without (mean: 1.45 $ml.min^{-1}ml^{-1}$) and those with metastases (mean: 1.33 $ml.min^{-1}ml^{-1}$).

Figure 6.1
Values for normal splenic perfusion

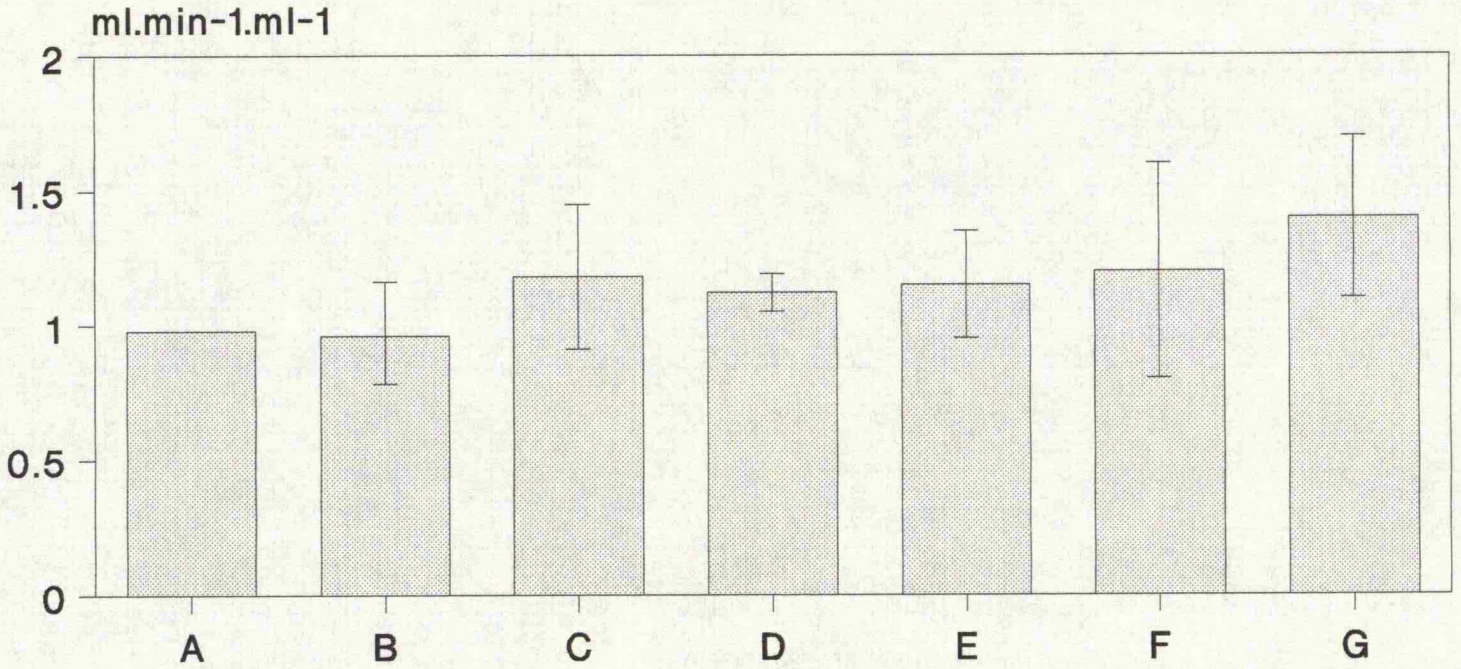

A:Williams et al; B:Gitlin et al;
C:Ueda et al; D:Huchzermeyer et al;
E:Takahashi et al; F:IGE 8800 G: Siemens

6.2 Assessment of the splenic microcirculation

Patients and Methods:

Twenty two patients were studied comprising the 9 control patients examined using the Siemens unit as described in section 6.1 above and 13 patients with diffuse liver disease. These comprised 10 patients with biopsy proven hepatic cirrhosis, two patients post liver transplantation and one patient with biopsy proven anaesthetic hepatitis.

All patients were examined with the Siemens Somatom Plus CT system using the imaging protocol described in section 6.1. Functional images of perfusion and time to peak enhancement were created as outlined in section 3.6. So as to study in greater detail the patterns of uneven enhancement often seen during dynamic CT of the spleen (e.g. case 1 in section 6.3 below), a further analysis of data from a region of interest created over the spleen (mean number of pixels: 503, range 113 to 1373) was performed as follows: The pixels were divided into two populations on the basis of time to peak enhancement using an automated statistical method. By an iterative process, this method identified the time to peak value that separated the two populations such that the sum of their variances (v^2) was the minimum (equation 6.1)..ls1

$$v^2 = \frac{n_1(\bar{x}_1 - \bar{x}_t)^2}{n_t} + \frac{n_2(\bar{x}_2 - \bar{x}_t)^2}{n_t} \qquad 6.1$$

where $n_{1,2,t}$ and $\bar{x}_{1,2,3}$ are then number and means of each group and the total respectively.

The number of pixels, the perfusion value and the time to peak was determined for each population. The mean perfusion for the whole splenic ROI was also calculated.

Considering all 22 patients as one group, the perfusion values of the two populations were compared using the signed rank-sum test for paired samples. The values of mean splenic perfusion, perfusion of each population, early and late enhancing, and the proportion of pixels from the splenic ROI that fell into the early enhancing population were compared between controls and patients with diffuse liver disease using the Wilcoxon rank sum test. A scatter plot of the proportion of early enhancing pixels against mean splenic perfusion was made and a statistical correlation sought.

Results:

Although more marked in some, functional images of the spleen demonstrated intrasplenic variations in perfusion in all cases, often with dramatic whorled patterns. An early impression from the functional images was that the areas of high perfusion appeared as equivalent areas of early enhancement on the time to peak enhancement images (see case 1 in section 6.3 below).

The results from the splenic region of interest analysis are summarised in table 6.1 and in figures 6.2-3. Considering all patients as one group, perfusion was significantly lower in the late enhancing population (Early: 1.32 $ml.min^{-1}ml^{-1}$, Late: 1.03 $ml.min^{-1}ml^{-1}$, $p<0.005$). In patients with cirrhosis, perfusion was reduced in both the early and late enhancing populations and in the whole splenic ROI, but this was most marked in the late enhancing population where the difference reached statistical significance ($p<0.05$).

The scatter plot showing the relationship between the relative size of the early phase population and the mean perfusion from the whole splenic ROI (figure 6.3) demonstrated a significant correlation (Pearson's correlation: $r=0.58$, $p<0.005$); With a lower splenic perfusion, the size of the early enhancing population was relatively smaller with an increase in the size of the late enhancing population.

The time to maximum enhancement of both phases was slightly later for spleens in patients with hepatic cirrhosis. This was more apparent for the late enhancing population but did not reach statistical significance in either case. Such minor differences may reflect changes in cardiac output or blood volume in cirrhosis rather than any change in splenic haemodynamics.

TABLE 6.1

	Controls	Cirrhosis	All Patients
Early Phase:			
Time to Maximum Enhancement (s)	24.5	25.8	25.3
Perfusion ($ml.min^{-1}ml^{-1}$)	1.44	1.22	1.32
Percentage of pixels from ROI	77	65	70
Late Phase:			
Time to Maximum Enhancement	33.8	36.0	35.0
Perfusion ($ml.min^{-1}ml^{-1}$)	1.24	0.89	1.03
Percentage of pixels from ROI	23	35	30
Whole ROI:			
Perfusion ($ml.min^{-1}ml^{-1}$)	1.40	1.13	1.24

Differences in perfusion and time of enhancement of the early and late populations of pixels and whole spleen for controls and patients with cirrhosis.

Early & late phase & total splenic perfusion in normals and cirrhosis

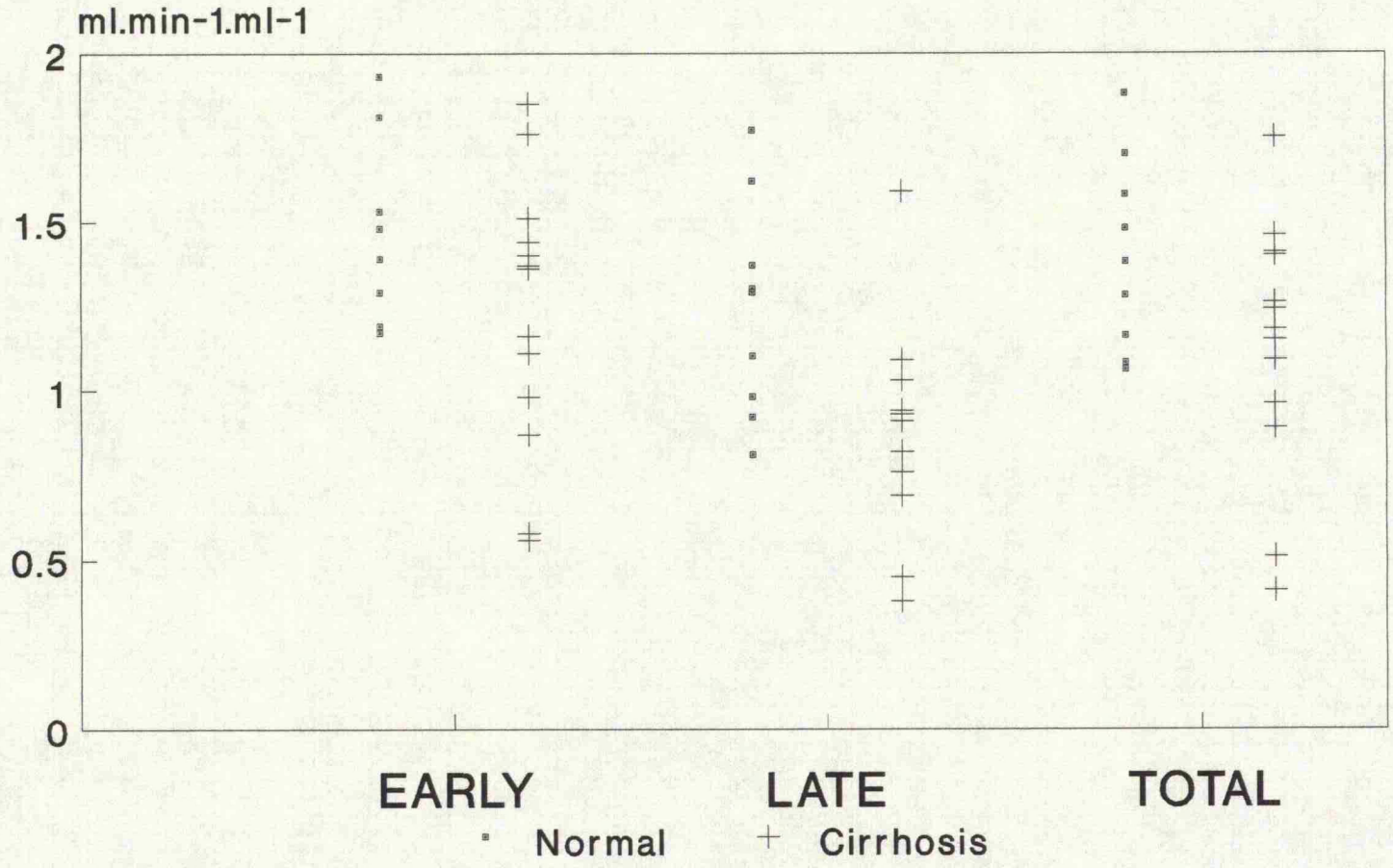

Figure 6.2

Relationship between size of early enhancing population & total perfusion.

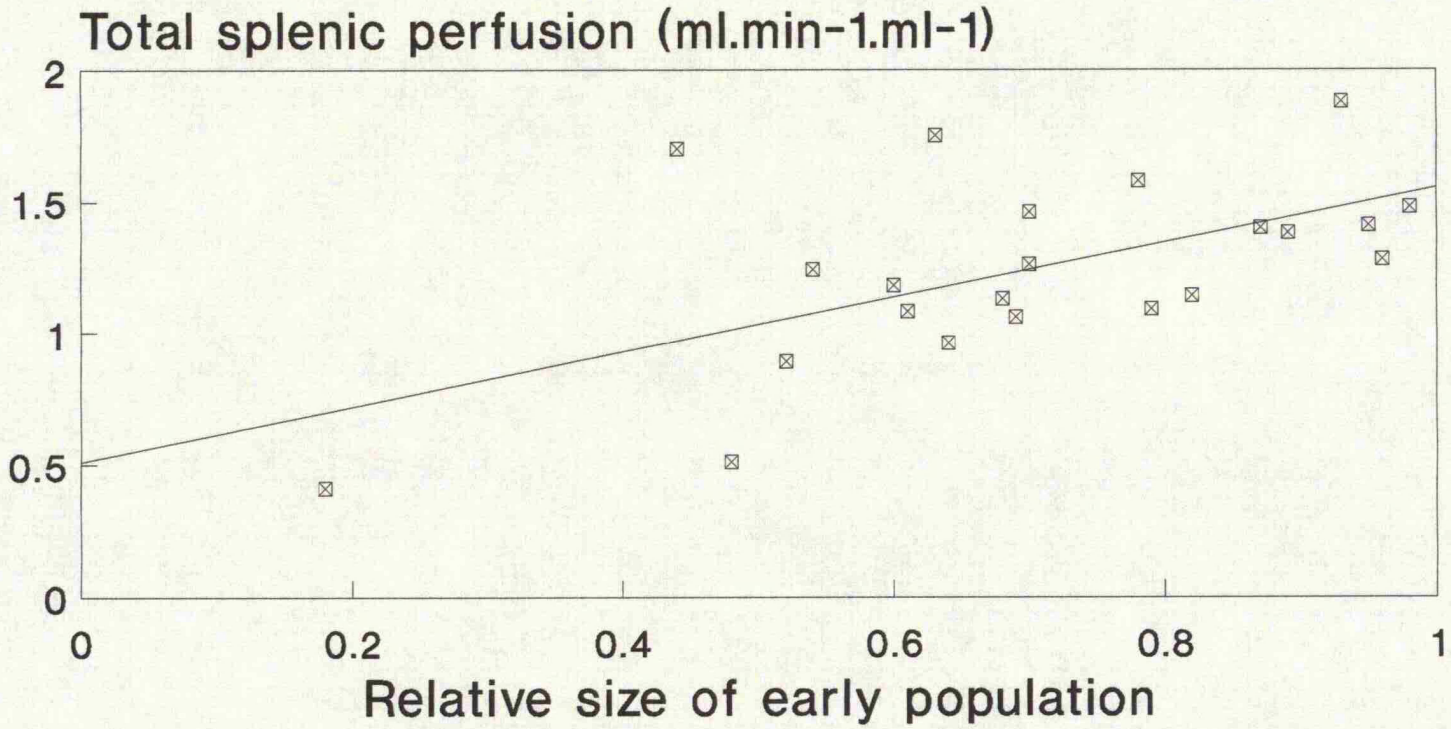

r=0.58, p<0.005

Figure 6.3

Discussion:

The spleen is essentially a lymphatic organ but is the only organ of the lymphatic system specialised to filter the blood, selectively weakening abnormal or senescent red cells prior to their destruction in the circulation ("conditioning"). Its venous outflow is into the portal vein and thus any increase in the vascular resistance in the liver (e.g. cirrhosis) will lead to an increase in venous pressure within the portal vein and the spleen itself.

Structurally, the spleen comprises white pulp and red pulp. The white pulp is a sheath of lymphatic tissue surrounding the arteries and is thickened in places to form lymphatic nodules. The red pulp occupies most of the parenchyma and is the site of the organs filtration function.

There has been much interest in the microcirculation of the spleen and its relationship to the organ's filtration function and the perfusion CT findings are consistent with current knowledge of the subject. Studies of the washout of plasma from the spleen show a biexponential curve suggesting two vascular pathways; fast and slow. Similar studies using red cells demonstrate a third component, not seen with plasma, reflecting sequestration of red cells within the spleen. About 90% of splenic flow is via the fast pathway with 10% passing through the slow pathway [89].

Corrosion casting and in vivo microscopy have been used to search for morphological counterparts for these physiological compartments [89]. The findings are summarised in figure 6.4. Blood flows through the white pulp and then the red pulp in series. Within the lymphoid follicles, capillaries may connect directly with the venous sinuses. This is known as the closed system. Alternatively, some capillaries terminate within the marginal zone of a lymphoid follicle close to open ended venous sinuses whilst others open into the reticular meshwork of the red pulp. Blood then passes from reticular meshwork into the venous sinuses through endothelial slits. These later two routes are known as open systems. The fast blood flow pathway comprises the direct capillary-venous connections (closed system) and the route via open ended sinuses in the marginal zone (part of the open system). The slow flow pathway is via the reticular meshwork of the red pulp (part of the open system) and this pathway is associated with the filtration function of the spleen.

The results of the dynamic CT studies above are in concordance with the model described above and provide new insights into the alterations in the splenic microcirculation that occur in hepatic cirrhosis. Within blood, contrast medium is virtually totally distributed to the plasma, and thus the results CT investigations of the spleen would be expected to parallel the plasma washout results. This is

indeed so in that two pathways are seen and in the normal spleens the fast pathway was the larger but comprising only approximately 77%.

Perfusion imaging allows anatomical localisation of the two flow compartments and there is a great variety in the arrangements of the two compartments, occasionally forming dramatic whorled patterns (figure 5.5). Contrast angiography of the dog spleen has shown similar regional variability in enhancement with late opacification not only of the splenic pulp but also the marginal sinuses [90].

Washout studies using rare gases have demonstrated a drop in overall splenic perfusion in cirrhosis but predominantly in the absence of splenomegaly [84-88]. The CT studies above demonstrated a drop in splenic perfusion in some but not all patients and, as a group, the results did not reach statistical significance. However, the presence or absence of splenomegaly was not noted. A perfusion value below 1 $ml.min^{-1}ml^{-1}$ only occurred in patients with cirrhosis and this result has potential value in clinical diagnosis. Yet, a fall in splenic perfusion has also been observed in Hodgkin's disease [87].

The drop in splenic perfusion in hepatic cirrhosis occurred in both the fast and slow pathways but reached statistical

significance in the slow pathway, implying a greater effect in the latter. Furthermore, there was a change in the relative sizes of the compartments with a shift towards the slow pathway in the presence of lower perfusion. These findings may in part indicate the mechanism for hypersplenism with increased red cell destruction seen in hepatic cirrhosis. There would be a greater proportion of blood passing through the reticular meshwork of the red pulp and a lower perfusion may be associated with a longer transit allowing more time for "conditioning".

Schematic representation of the splenic microcirculation.

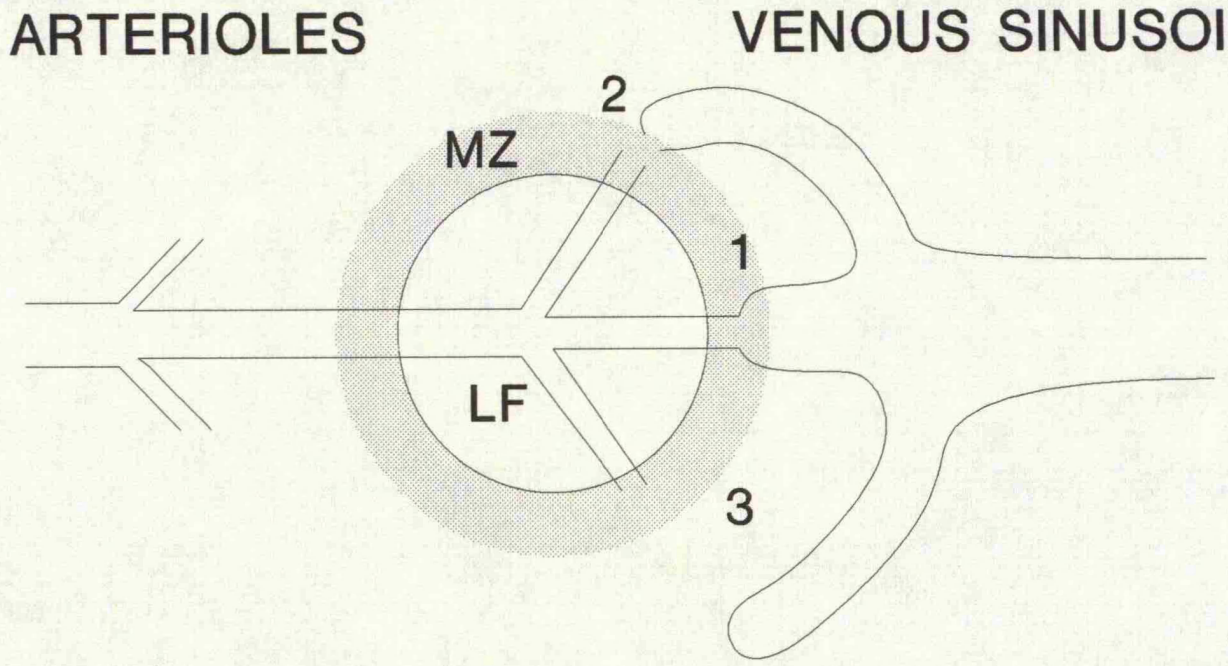

LF: LYMPHOID FOLLICLE

MZ: MARGINAL ZONE

1. Closed system, rapid transit
2. Open system, rapid transit
3. Open system, slow transit (red cell conditioning)

163

Figure 6.4

6.3 Functional images of splenic perfusion: Case studies.

The data acquisition protocol was as described in section 6.2 above. All functional images were displayed with identical windows as follows:

Colour	Perfusion	Time to Peak
Black	0 $ml.min^{-1}ml^{-1}$	0 seconds
Pink/red	3 $ml.min^{-1}ml^{-1}$	60 seconds
White	>3 $ml.min^{-1}ml^{-1}$	>60 seconds

Case 1. Prominent regional variations in splenic enhancement in a patient with cirrhosis without portal hypertension.

A 20 year old lady presented with generalised pruritus. Investigations demonstrated deranged liver function tests and subsequently liver biopsy revealed primary sclerosing cholangitis. There were no clinical features of portal hypertension and portal venous Doppler ultrasound traces were normal. The patient was referred for CT for assessment of the liver.

Mean splenic perfusion was 1.46 $ml.min^{-1}ml^{-1}$. The conventional CT images demonstrated a transient but marked pattern of high and low areas of enhancement following contrast medium administration (figure 6.5A). Perfusion imaging (figure 6.5B) confirms alternating areas of high (1.76 $ml.min^{-1}ml^{-1}$) and low (0.76 $ml.min^{-1}ml^{-1}$) perfusion. The time to maximum enhancement image (figure 6.5B) demonstrates a similar pattern with high perfusion areas corresponding with early enhancement and low perfusion with late enhancement.

This case demonstrates a marked example of a striped pattern of regional variations in splenic perfusion. Also, a normal splenic perfusion is noted in a case of cirrhosis but without portal hypertension.

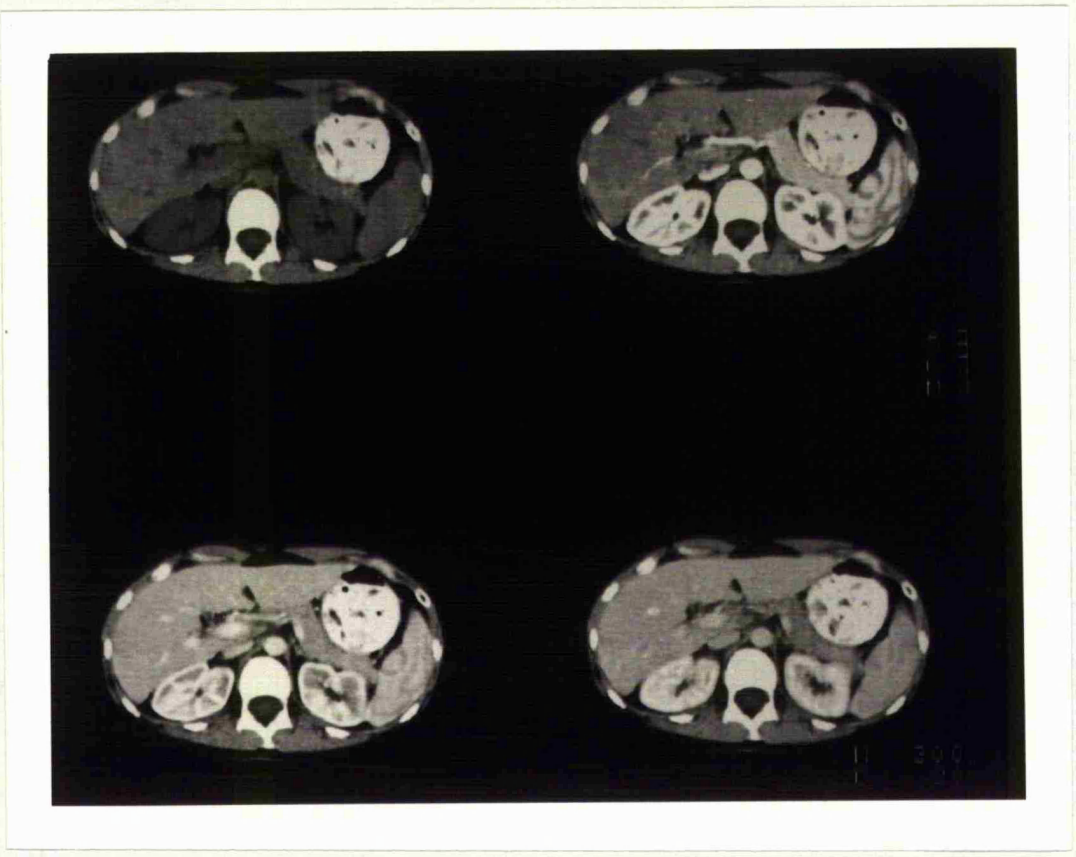

Figure 6.5A: Conventional CT images from a single location dynamic sequence demonstrating dramatic regional variations in splenic enhancement.

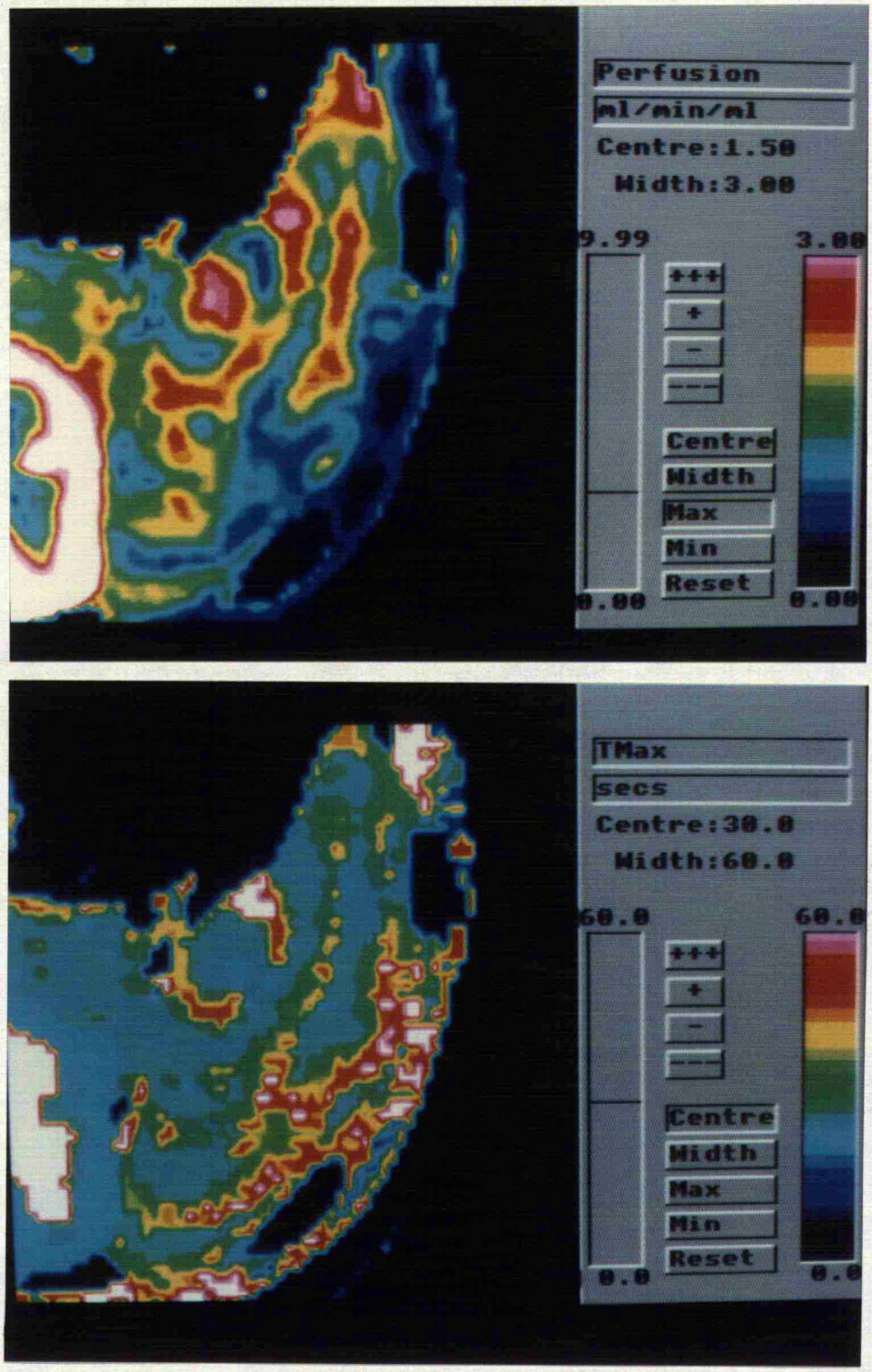

Figure 6.5B: Perfusion (above) and time to maximum enhancement (below) images from case 1. The high perfusion areas correlate with areas of early enhancement and vice versa.

Case 2: Normal Spleen

A 46 year old man presented with a months history of upper abdominal pain. Ultrasound examination, colloid scintigraphy and unenhanced CT images demonstrated hepatic metastases but no focal splenic abnormality. No primary tumour was found. CT was performed to stage the extent of disease prior to chemotherapy.

Mean splenic perfusion is 1.38 $ml.min^{-1}ml^{-1}$. The pattern of high perfusion/ early enhancement is present on the functional images (figure 6.6) but is less well seen than in case 1. (High perfusion: 1.39 $ml.min^{-1}ml^{-1}$; low perfusion: 1.3 $ml.min^{-1}ml^{-1}$). The majority of the spleen (89%) demonstrates the higher perfusion and early time to maximum enhancement values.

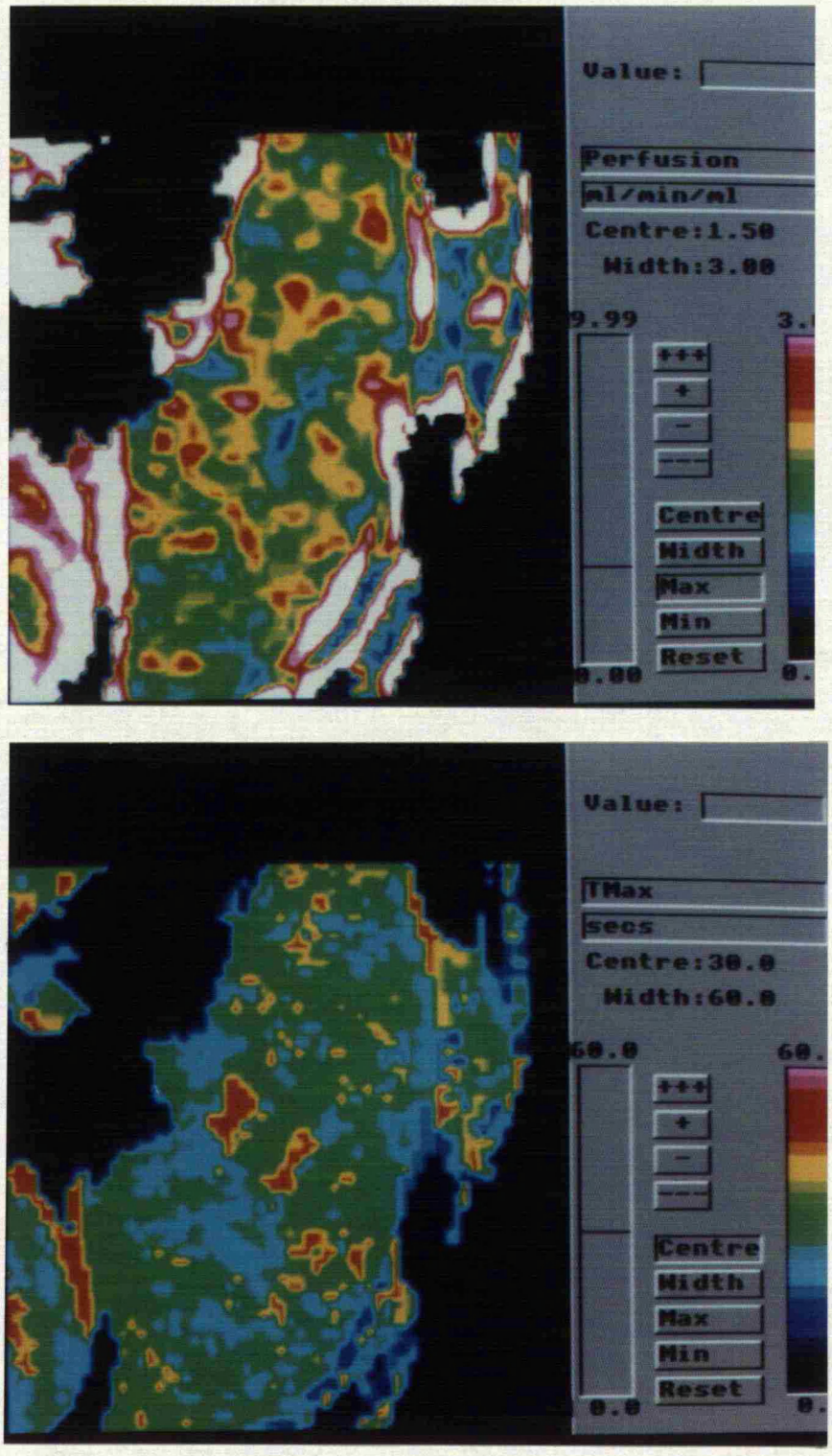

Figure 6.6: Perfusion (above) and time to maximum enhancement (below) images from case 2: normal spleen.

Case 3. Cirrhosis with portal hypertension.

A 56 year old man who had presented 4 years previously with abdominal pain and diarrhoea was referred for assessment prior to liver transplantation. A liver biopsy had demonstrated cryptogenic cirrhosis. Portal venous thrombosis was demonstrated on ultrasound examination, magnetic resonance imaging and superior mesenteric angiography. Oesophageal varices were also present.

Mean splenic perfusion is markedly reduced at 0.41 $ml.min^{-1}ml^{-1}$. Functional images (figure 6.7) show that most of the spleen (72%) is comprised of pixels with low perfusion and late enhancement. (High perfusion: 0.56 $ml.min^{-1}ml^{-1}$; low perfusion 0.38 $ml.min^{-1}ml^{-1}$)

This example demonstrates the typical changes in regional splenic perfusion with portal hypertension. Overall splenic perfusion is reduced, with a fall in both early and late enhancing regions. There is also a redistribution of perfusion from the high perfusion/early enhancing pathway to the low perfusion/late enhancing route.

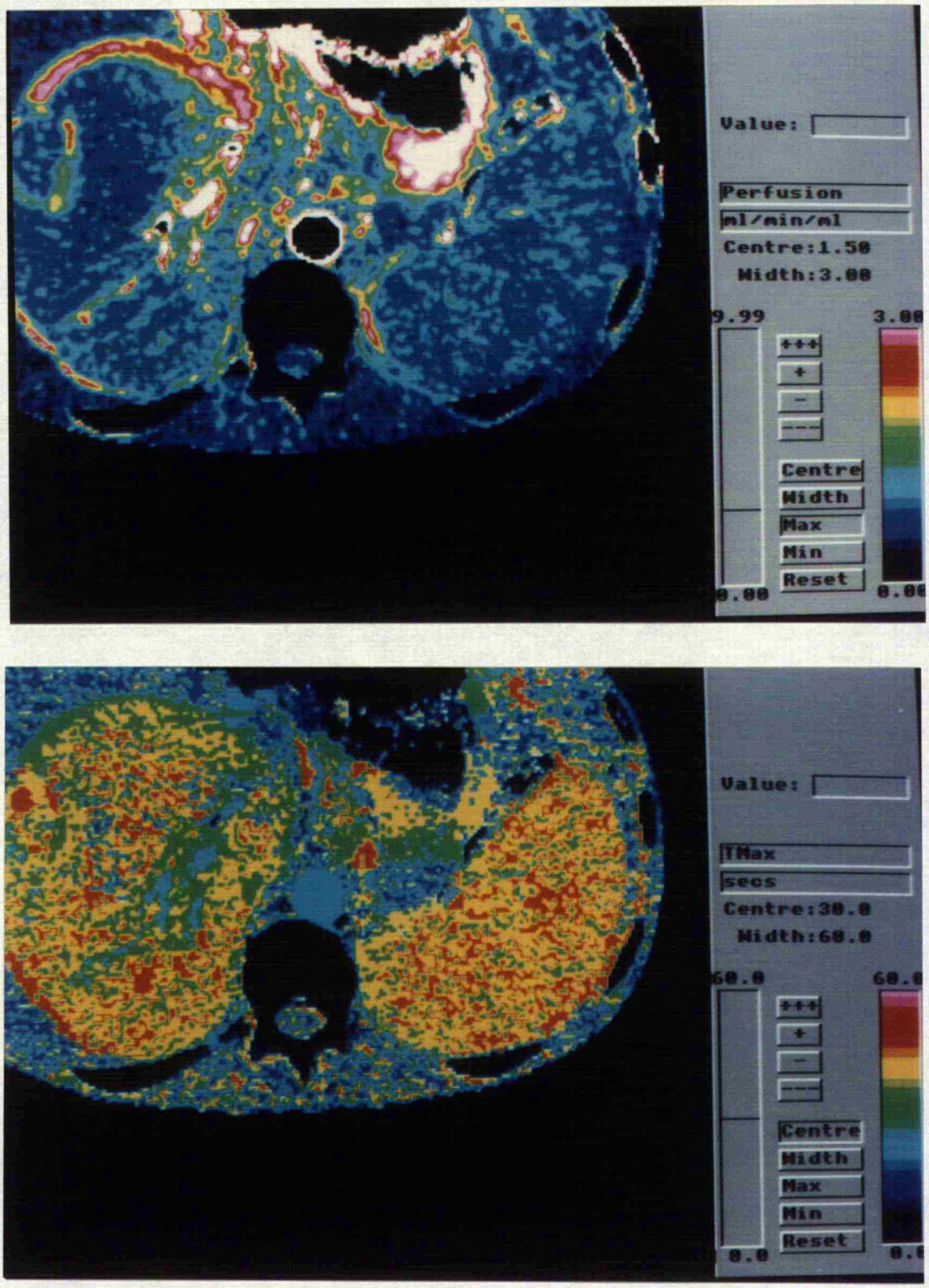

Figure 6.7: Perfusion (above) and time to maximum enhancement (below) images from case 3. Note the low splenic perfusion and the greater proportion of late enhancing pixels.

7. PANCREAS

7.1 Normal pancreatic perfusion.

7.2 Perfusion imaging: case studies

7.1 Normal Pancreatic Perfusion:

Patients and Methods:

Pancreatic perfusion was studied in eleven patients. These included 5 patients undergoing CT for investigation of hepatic cirrhosis and 4 patients investigated for suspected hepatic metastases (confirmed in only two). None of these patients had a focal pancreatic abnormality apparent on unenhanced or enhanced images. A further patient underwent CT for assessment of a pancreatic tumour, subsequently found to be a benign islet cell tumour on histological examination. Time-density data from a normal portion of pancreas were used in this study. The final patient had undergone pancreatic transplantation for diabetes and was excluded from this section but appears as a case study in section 7.2.

All patients were studied using the Siemens Somatom Plus CT system (sited at Addenbrooke's hospital) using the data acquisition protocol as for renal studies (section 4.2).

Results:

Mean pancreatic perfusion was found to be 1.7 $ml.min^{-1}ml^{-1}$ (standard deviation: 0.6). The mean and standard deviation were increased by a single value of 3.43 $ml.min^{-1}ml^{-1}$ recorded in a patient with Wilson's disease. The remainder of values fell within a narrow range of 1.25 to 1.66 $ml.min^{-1}ml^{-1}$ (Mean:1.5 $ml.min^{-1}ml^{-1}$, SD.: 0.14).

Discussion:

The author has been unable to find a study reporting an absolute value for normal pancreatic perfusion in man. A perfusion index method using Oxygen-15 water and positron emission tomography (PET) has been reported in man and perfusion was found to be reduced in pancreatic carcinoma [91]. The value of PET measurements of pancreatic perfusion is questionable as the spatial resolution is not sufficient to reliably separate pancreas from splenic vein.

Measurements of pancreatic perfusion in animals vary depending upon species and technique used with a range of 0.35 to 1.73 $ml.min^{-1}g^{-1}$ with no variation in perfusion between the head, body and tail [92]. Excluding the single high reading, the CT results in humans are entirely in accordance with these values.

The cause for the single high value of 3.43 $ml.min^{-1}ml^{-1}$ in the patient with Wilson's disease and hepatic cirrhosis is unclear. Technical factors do not appear to be the cause as sudden marked enhancement was apparent on the unprocessed images. Inflammation of the pancreas or a vascular tumour (e.g. insulinoma) would increase pancreatic perfusion [13] but pancreatic disease is not widely recognised as a clinical feature of Wilson's disease. Neither was this suggested by

the clinical findings in this patient and no focal abnormality was seen in the pancreas. The process of copper deposition in the tissues that occurs in Wilson's disease may have affected the pancreas but whether this would alter pancreatic perfusion is merely speculative. Interestingly, a fall in pancreatic perfusion has been observed in dietarily copper-deficient rats (inducing atrophy) [93] but whether the converse is true with copper deposition is unknown.

The validity of using patients with cirrhosis as normal subjects can be questioned as a raised portal pressure will increase pressure in the splenic vein into which the venous drainage of the pancreas enters. Thus, reduced pancreatic perfusion might be expected in cirrhosis. Excluding the patient with the unusually high reading, pancreatic perfusion was slightly lower amongst patients with cirrhosis (1.43 $ml.min^{-1}ml^{-1}$ vs. 1.57 $ml.min^{-1}ml^{-1}$) but numbers were insufficient to achieve statistical significance.

7.2 Perfusion imaging: Case Studies:

Technique:

The data acquisition protocol is as described in section 7.1 above. The method for production of perfusion images is described in section 3.6. All images were displayed with identical colour scales as follows:

Perfusion	Colour
0 $ml.min^{-1}ml^{-1}$	Black
5 $ml.min^{-1}ml^{-1}$	Pink/red
>5 $ml.min^{-1}ml^{-1}$	White

Case 1. Normal Study

A 20 year old lady with known primary sclerosing cholangitis underwent dynamic CT for assessment of the liver with the pancreas fortuitously appearing on the slice under study. There was no clinical evidence of portal hypertension or pancreatic disease. Doppler ultrasound studies of the portal vein were normal and no focal pancreatic abnormality was present in the pancreas either on ultrasound or unenhanced CT.

Perfusion images (figure 7.1) demonstrate even perfusion throughout the pancreas with a mean value of 1.47 $ml.min^{-1}ml^{-1}$.

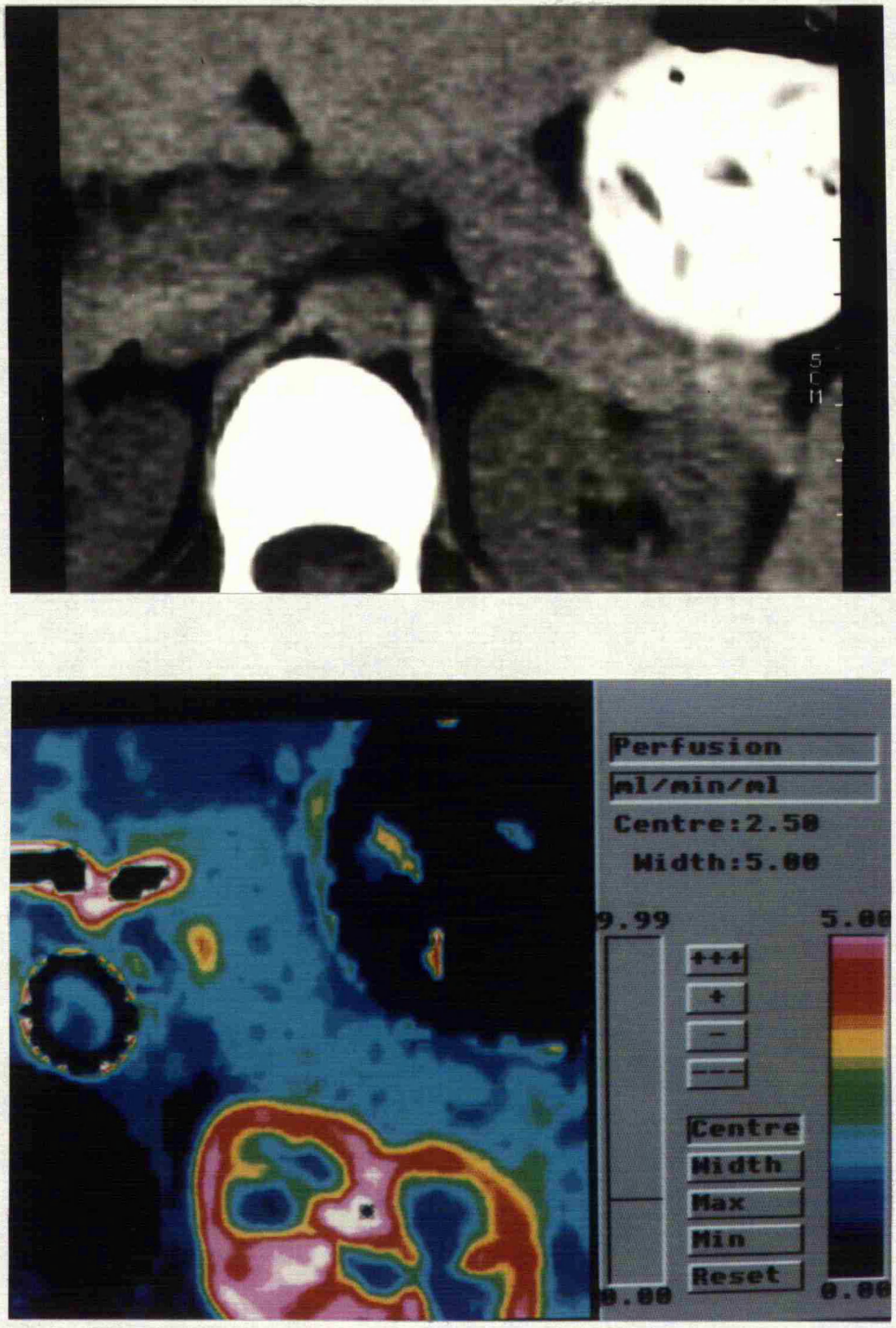

Figure 7.1: Conventional unenhanced CT (above) and perfusion (below) images from Case 1: Normal study.

Case 2. Islet cell tumour.

A 19 year old girl with a strong family history of Von Hippel-Lindau disease presented with a 2 month history of headache and early papilloedema on examination. Cranial CT revealed a 1cm nodule in the right parietal area which was found to be a haemangioblastoma on subsequent excision. The patient was referred for abdominal CT to search for renal tumours. However, a pancreatic mass and pancreatic cysts were found (figure 7.2). Histological examination of the subsequently excised pancreas demonstrated an islet cell tumour.

Perfusion images (figure 7.2) demonstrate high perfusion within the periphery of the tumour and low perfusion in the necrotic centre (overall perfusion 2.11 $ml.min^{-1}ml^{-1}$). The remainder of the pancreas demonstrates normal perfusion (1.42 $ml.min^{-1}ml^{-1}$).

Islet cell tumours are a recognised feature of Von Hippel-Lindau disease. They are typical hypervascular as demonstrated by CT whereas adenocarcinomas generally are hypovascular [13]. This case demonstrates the potential of CT perfusion imaging in enabling some degree of tissue characterisation.

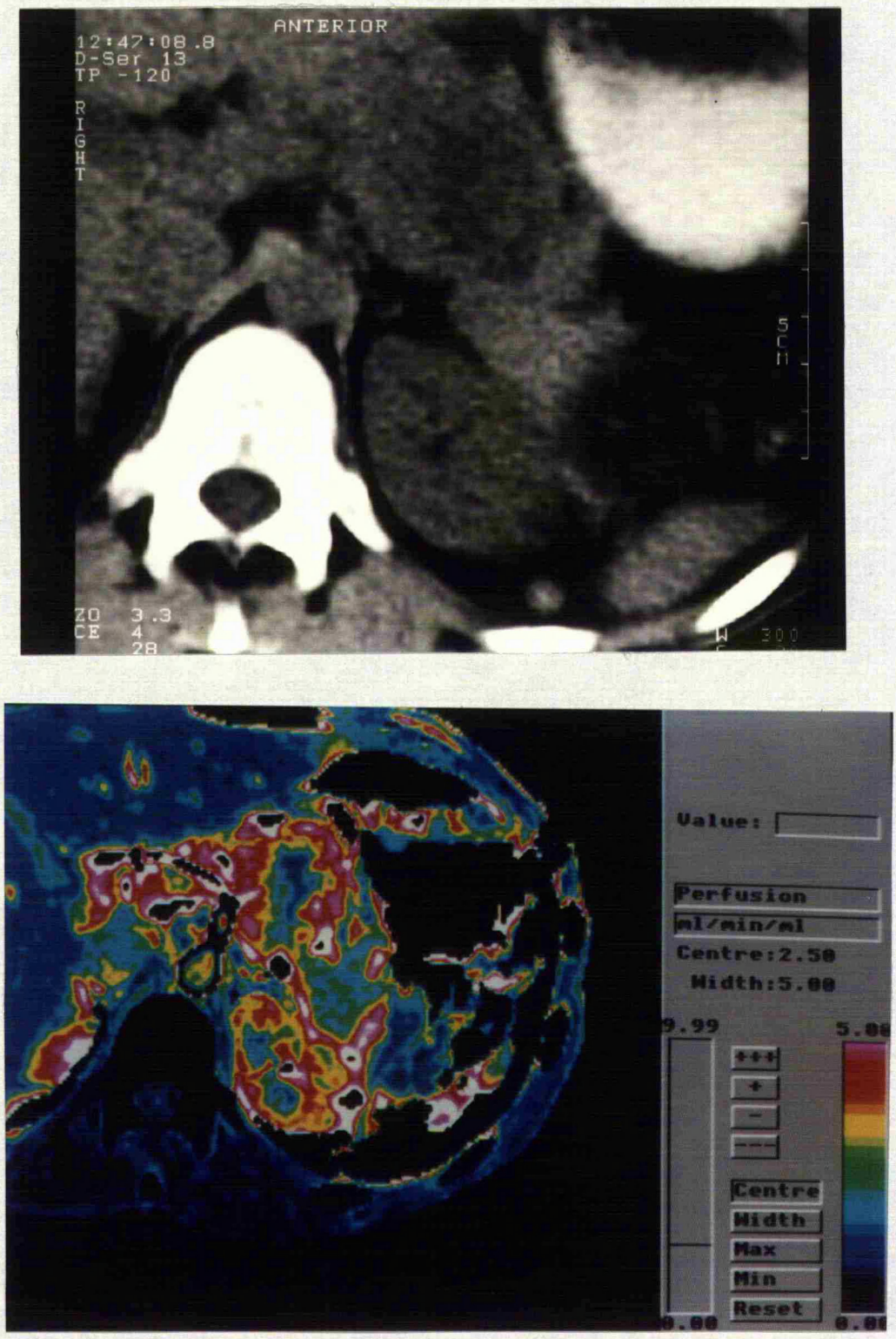

Figure 7.2: Conventional unenhanced CT (above) and perfusion images (below) of case 2: Islet cell tumour

Case 3. Diabetes and pancreatic transplant

A 23 year old man who had undergone liver and pancreatic transplantation 4 years previously had redeveloped insulin dependence over the previous 6 months. His drug therapy also included cyclosporin 400mg, prednisolone 7.5 mg and azathioprine 75mg (daily doses). The original surgical procedure involved a segmental pancreatic graft where the donor splenic artery was anastomosed with the donor splenic vein, creating an arterio-venous fistula. On transplantation, the donor splenic artery was anastomosed to the aorta, the splenic vein to the portal vein and the pancreatic duct to the gastric antrum. CT was requested to assess the perfusion of the transplanted pancreas.

Perfusion images (figure 7.3) demonstrate the native pancreas (large arrow) and the transplant pancreas and supplying vessels (small arrow). Pancreatic perfusion is markedly reduced in the native pancreas (0.60 $ml.min^{-1}ml^{-1}$). Perfusion in the transplant is less than normal (0.97 $ml.min^{-1}ml^{-1}$) but higher than that of the native pancreas.

The failure of the pancreatic transplant was subsequently attributed to islet cell exhaustion. The relationship between pancreatic perfusion and diabetes in man is unclear due to the difficulties in measuring pancreatic perfusion. In rats, an age related fall in pancreatic perfusion associated with

reduced islet cell mass has been observed [94] and thus it would be reasonable to expect reduced pancreatic perfusion in diabetes and in the transplant with islet cell exhaustion. However, cyclosporin may also affect pancreatic perfusion [95,96]. The patient in this study did indeed have evidence of renal cyclosporin toxicity (see section 4.3, case 3) and the possibility of an effect of the drug on perfusion of the native pancreas and/or transplant should also be considered. Animal studies have given mixed results with a cyclosporin induced increase in perfusion found in sheep [95] but a decrease in rats [96] and thus the response may be species specific.

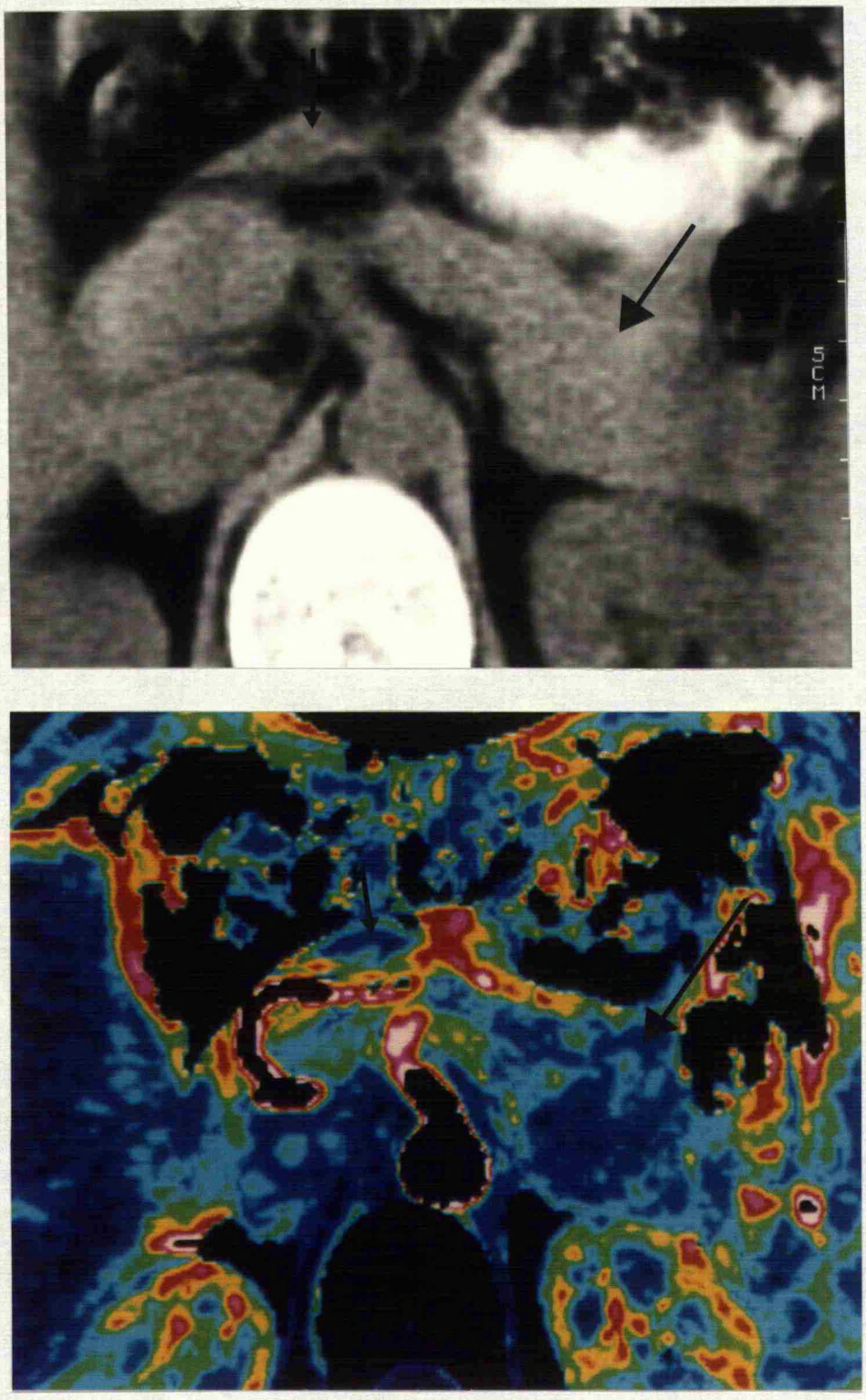

Figure 7.3: Conventional unenhanced CT (above) and perfusion (below) images from case 3. Large arrow: native pancreas; small arrow: transplant pancreas.

8. DISCUSSION

8.1 Relationship of CT perfusion imaging to other imaging techniques.

8.2 Advantages and limitations of CT as a technique for measuring perfusion.

8.3 Further research and potential applications.

8.4 Summary

8.1 Relationship of CT perfusion imaging to other imaging techniques:

Non-invasive assessment of blood flow and tissue perfusion in man until recently has been achieved largely using nuclear medicine techniques. However, not only computed tomography, but also other newer imaging modalities, such as ultrasound (US), magnetic resonance imaging (MRI) and digital subtraction angiography (DSA) are being increasingly applied to the evaluation of haemodynamics. Unlike standard radiography, these techniques all produce quantifiable data which can be processed by computers thus facilitating the derivation of functional information.

Blood flow can be assessed either within blood vessels or within the organs or tissues themselves. The two measurements will be the same only when the organ has a single supplying artery which is frequently not the case. Assessment of flow or perfusion at the tissue level benefits over evaluation of vessel flow by being more directly related to the metabolism of the tissue. Furthermore, evaluation of vessel flow is limited by being unable to assess regional variations of flow within the organ supplied by that vessel. For instance, measurement of renal arterial flow cannot separately determine flow within renal cortex and medulla.

Within vessels, flow is either measured in volume per unit

time (e.g. $ml.min^{-1}$), which is the strict definition of the term "blood flow", or in units of blood velocity which is displacement per unit time (e.g. $cm.sec^{-1}$). There is usually a variation in blood velocity across the cross section of a vessel (velocity profile) with higher velocities centrally and lower velocities peripherally. However, mean blood velocity is proportional to flow divided by the cross sectional area of the blood vessel. Thus, within a vessel with a large cross sectional area it is possible to have high flow (in terms of volume) but low blood velocity, such as may occur in an hepatic cavernous haemangioma.

For whole organs, flow is usually expressed in terms of volume of blood per unit time whereas the term "perfusion" describes blood flow per unit volume or mass of tissue (e.g. $ml.min^{-1}ml^{-1}$ or $ml.min^{-1}g^{-1}$). The methods that evaluate organ flow or tissue perfusion broadly fall into two categories. The assessment can be either at the capillary level, as when using a non-diffusible tracer, or at the cellular level where uptake of a tracer depends not only upon perfusion of the tissue but also upon intact metabolism. It can be argued that techniques assessing cellular uptake measure more than just blood flow as the metabolic state of the tissue will also affect the measurement.

A summary of the level of flow assessment for different

imaging techniques is given in table 8.1. Washout techniques using xenon or krypton and magnetic resonance diffusion/perfusion imaging also depend upon the physical properties of the tissue under study (e.g. partition coefficient) but have not been classified under "cellular" mechanisms because no metabolic process is involved. Dynamic CT techniques have been applied to evaluation of flow within vessels, for instance measurement of cardiac output [21] and semi-quantitative assessment of aortic flow in aortic dissection [9]. Myself and others [20] have also assessed renal vein flow in patients with renal carcinoma. However, xenon CT techniques and CT perfusion measurements with iodinated contrast media evaluate flow at the more metabolically relevant tissue level. The other methods which can be applied to non-invasive assessment of blood flow are briefly discussed below.

TABLE 8.1

	Vessel	Capillary	Cellular
Nuclear Medicine	Non-diffusible Tracers	Non-diffusible Tracers	"Chemical microspheres"
		Radioactive* Xenon/Krypton	
			Clearance Methods
	Most tracers during 1st pass	Most tracers during 1st pass	
Ultrasound	Doppler	Ultrasonic Contrast Media	--------
		(?Doppler)	
Magnetic Resonance Imaging	Phase Contrast	Paramagnetic contrast media	--------
	"Time of flight"	"Diffusion" MR*	
		Deoxyhaemoglobin Functional MR	
Digital Subtraction Angiography	Yes (quantitative)	(? semi-quantitative)	---------
Computed Tomography	Iodinated Contrast Media (semi-quantitative)	Iodinated Contrast Media	---------
		Xenon CT*	

* also depends on physical properties of tissue.

Comparison of techniques for assessing blood flow.

Nuclear Medicine Techniques:

1. First Pass Studies

Cardiac output can be determined from an arterial time-activity curve using the Stewart-Hamilton equation and left to right intracardiac shunting can be quantified using first pass studies by measuring the amount of early recirculation within the lungs. The first pass through an organ of an intravenous bolus of many radiopharmaceuticals can be used to evaluate blood flow. The perfusion index of Hilson is used routinely to give a semi-quantitative measure of blood flow through renal transplants. Absolute quantification in terms of percentage cardiac output is provided by the method of Peters et al [58]. The first pass of radiotracers, such as radiolabelled colloid, through the liver enables determination of the ratio of hepatic arterial and portal blood flow [60-62,70]. Such techniques have been of value in studying patients with liver metastases, hepatic cirrhosis and following liver transplantation [60,63-65]. Limb blood flow can be assessed under conditions of reactive hyperaemia by studying the inflow of a blood pool marker, such as labelled Human Serum Albumen, on release of the tourniquet [97].

2. Radiolabelled microspheres

These are non-diffusible tracers which are now rarely used except for imaging regional lung perfusion and quantification

of right to left intracardiac or intrapulmonary shunts. To determine organ blood flow they need to be injected intra-arterially and hence the technique is invasive. The microspheres lodge in small blood vessels and organ blood flow is determined from the organ uptake and the dose of microspheres injected. This technique is considered the "gold standard" for evaluation of organ blood flow but its application is limited due its relatively invasive nature. It is most accurate when the radioactivity is measured in tissue samples which is clearly inappropriate in human studies which rely on gamma camera imaging.

3. "Chemical microspheres"

A number of radiopharmaceuticals can be considered as "chemical microspheres" in that, when injected intravenously, they have high extraction within the organs and thus uptake is similar to that which would have been obtained with microspheres. ^{99m}Tc hydroxymethylpropylamineoxime (HMPAO) is routinely used for imaging cerebral perfusion and has been used to study tumour blood flow. ^{201}Tl thallous chloride and ^{99m}Tc Methoxyisobutylisonitrile (MIBI) are routinely used for assessing myocardial perfusion and can be used for evaluating leg muscle blood flow. One benefit of such agents is that they can be injected under conditions of stress (e.g. exercise) and images acquired later will reflect the organ perfusion at the time of injection.

4.Clearance measurements:

The clearance from blood of a radiotracer with high extraction in one organ system can be used to determine an "effective" plasma flow. The best known example of this is radiolabelled hippuran which is cleared by tubular uptake and secretion within the kidney; the blood clearance thus giving effective renal plasma flow (ERPF). The individual kidney ERPF can be determined from the relative function measured from an iodohippuran renogram.

5.Washout studies

The rate of washout of radioactive Xenon or Krypton from an organ will be dependent upon the mean perfusion. Compartmental analysis enables assessment of regional variations of perfusion within an organ (e.g. cerebral grey and white matter) but the compartments cannot be localised anatomically. Assumptions about the partition coefficient of xenon between blood and tissues are necessary but these may not be valid in diseased tissues. The technique may require intra-arterial injection rendering it invasive.

The radiation doses from nuclear medicine investigations are frequently lower than comparable radiological techniques. Although the gamma camera is a highly sensitive device, nuclear medicine techniques have low spatial resolution as compared with CT perfusion measurements, even when using

positron emission tomography (PET: maximum resolution approximately 4mm). With the conventional gamma camera, absolute quantification is frequently difficult, especially when using emission tomography, due to problems with attenuation and scatter corrections. This is much less of a problem with PET were a transmission scan allows accurate attenuation corrections. (With CT, the concentration of contrast medium can be determined directly from Hounsfield Unit measurements.)

With the planar gamma camera, regional variations in perfusion within an organ cannot be readily evaluated due to spatial overlapping of anatomical compartments. For instance, the renal cortex overlies renal medulla in all projections. Transaxial imaging can overcome this problem but the time resolution of emission tomographic and PET equipment cannot match the 1 second data acquisition times of CT without large increases in image noise. For these reasons and due to limited spatial resolution, nuclear medicine techniques evaluating regional variations of perfusion within an organ rely upon compartmental analysis. Examples of this are the curve stripping techniques used to identify different compartments with the kidney using radioactive xenon washout data [68] and the deconvolutional analysis of renographic data using I-123 iodohippuran [69] to compare renal cortical and medullary blood flow. Such analyses merely identify physiological compartments which may or may not have

anatomical correlates whereas CT perfusion imaging allows direct spatial localisation of regional variations of perfusion.

Many of the first pass techniques developed in nuclear medicine have been applied to dynamic CT including measurement of cardiac output [21], evaluation of intracardiac shunts [98] and the perfusion index [27]. As described in Section 3, the Peters technique for determination of organ blood flow from first pass data method and slopes ratio method for determining the ratio of hepatic arterial to total blood flow provide the basis of the CT perfusion techniques developed in this thesis.

Due to the limited resolution of the gamma camera, radionuclide techniques for separate evaluation of hepatic arterial and portal blood flow methodology have merely been able to study data from large regions of interest (ROI) over the right lobe of the liver and although functional images of hepatic blood flow parameters have been produced [99], these have been of poor spatial resolution when compared with the CT perfusion images described in section 5. Also, techniques using the planar gamma imaging are unable to study the left lobe of the liver due to overlap of the aorta and inferior vena cava thereby including significant amounts of vascular activity within the left lobe ROI. This is not a problem for the transaxial format of CT. Furthermore, CT perfusion

techniques can quantify arterial and portal components separately whereas radionuclide methods are limited to determination of the arterial/portal ratio.

Ultrasound

1. Doppler studies:

The velocity of red cells moving within vessels can be determined from the shift in frequency of ultrasound waves reflected back to the probe from the cells. The signal can be represented as a wave form or displayed as a colour signal superimposed on the grey scale anatomical image. Mean velocity can be determined and comparison of systolic and diastolic velocities allow derivation of indices of pulsatility and vascular resistance. Volume flow can be estimated from the mean velocity and a measurement of the cross sectional area of the blood vessel but this may add significant errors as the velocity profile cannot be accurately determined by ultrasound. Colour Doppler imaging of tissues also enables an assessment of tissue haemodynamics. For instance, higher signals are obtained from the renal cortex than the renal medulla. But the signal is not readily quantifiable in physiological terms such as $ml.min^{-1}ml^{-1}$ and the precise relationship to true measurements of perfusion is not clear.

2. Ultrasonic contrast media.

Ultrasonic contrast media, such as sugar coated air bubbles, have recently become available. Experience with using such media for measurement of blood flow is limited. The main difficulty is determining the relationship between the concentration of contrast medium and a component of the complex ultrasound signal whilst still allowing for differing sound attenuation at different organ depths. Once this is achieved, the methods for measuring perfusion with dynamic CT potentially could be applied to ultrasound.

Ultrasonic studies use no ionising radiations and are generally considered to be safe. Ultrasound has, in the main, been applied to evaluating the intravascular flow effects of peripheral arterial and intracardiac disease, but renal and hepatic haemodynamics have also been studied. By evaluating the hepatic artery and portal vein using volume flow measurements, the changes in liver haemodynamics in the presence of hepatic metastases [100] or during drug infusions [101] can be demonstrated. However, the technique is largely limited to evaluating large and medium-sized vessels and thus the ability to demonstrate regional variations is somewhat limited (for example to the left and right hepatic arteries and portal veins).

Magnetic Resonance Imaging

Magnetic resonance has enormous potential for functional imaging and, although relative expensive, benefits from not using ionising radiation.

1. Vessel Flow:

Two MR techniques, namely time of flight and phase contrast studies, can be used to acquire flow images. Time of flight techniques use the inflow of unsaturated spins for differentiation from stationary spins [102] whereas phase contrast methods rely on the phase shift of spins moving along the direction of a bipolar velocity encoding gradient for differentiation from stationary spins [103]. Measurement of blood velocity is easier using phase contrast techniques and the high spatial resolution of MR allows accurate determination of the cross sectional area of the vessel and hence conversion to volume flow. Applications of such techniques includes measurement of renal arterial flow [104] with reasonable accuracy. However, potential errors include partial volume effects, especially for small vessels, and intravoxel phase dispersion, particularly with turbulent flow [105]. MR can assess the blood velocity profile within a vessel [106] more accurately than ultrasound and thus determination of volume flow from blood velocity is more readily performed. As for Doppler ultrasound, there is little

scope for studying regional variations in organ blood flow when studying vessel haemodynamics.

2. Diffusion Imaging:

Le Bihan et al [107] have developed MR sequences that can quantify random Brownian motion within a volume, known as intravoxel incoherent motions. When applied to a simple liquid, the signal corresponds to the diffusion coefficient of that liquid. However, the signal obtained from living tissue frequently yields a value somewhat greater than the diffusion coefficient of water. The authors postulated that this difference reflected tissue perfusion and the number of capillaries in the volume under study. The technique has so far only been used for studies of the brain and CSF and cannot easily identify the perfusion element within the signal nor express perfusion in physiological units such as $ml.min^{-1}g^{-1}$.

3. Paramagnetic Contrast Media.

Acquisition of a rapid sequence of images after a bolus of paramagnetic contrast medium, such as gadolinium dimethyltriethylpentacetic acid (DTPA) (dynamic MR) can be achieved using snapshot imaging sequences (e.g."TURBOFLASH" or "FAST GRASS") with typical acquisition times of 1 to 2 seconds. Such techniques potentially allow application of the CT techniques described in this thesis to magnetic resonance

imaging. The main benefit would be the avoidance of ionising radiation. This allows more frequent sampling than with CT and thus should improve the quality of data. However, a number of problems are associated with the application of dynamic CT techniques to MR. Most significant is the non-linear relationship between gadolinium concentration and signal intensity [102]. The relationship can be determined by imaging of a suitable phantom and measurement of signal intensities from different concentrations of gadolinium with the creation of a "look up" table. However, using such sequences, at higher concentrations of gadolinium, the signal intensity begins to fall again and thus for any given signal intensity there may be two possible gadolinium concentrations. Furthermore, there must also be no magnetic field or radiofrequency inhomogeneity as this will create non-uniformity of signal within the image. When using surface coils, this clearly will not be the case. The possibility of high concentrations of gadolinium within a structure creating susceptibility changes in surrounding tissues not containing gadolinium must also be considered. With all these variables, absolute perfusion measurements with dynamic MR will not be as straightforward as with dynamic CT.

4. Deoxyhaemoglobin or "functional" MR

Conventional anatomical MR imaging relies upon the contrast derived from the tissue relaxation parameters, T1 and T2. In the brain, this tissue relaxation can be influenced by the

oxygenation state of haemoglobin, local blood volume and tissue perfusion. It has been possible to demonstrate changes in these relaxation factors within the brain following stimulation of the motor and visual cortex [109,110]. It is believed that cortical activation leads to increased cerebral metabolism as well as blood flow and blood volume. There is an increase in delivery of oxygen to the tissue that exceeds the metabolic demand and thus the local concentration of paramagnetic deoxyhaemoglobin falls leading to a rise in signal intensity. Although this technique clearly has great potential to provide insights into brain function, there are considerable problems. Typically, a 2% change in signal relates to a change in perfusion of 0.5 $ml.min^{-1}ml^{-1}$ which is a major change when compared to a resting cortical perfusion of 0.75 $ml.min^{-1}ml^{-1}$. Thus noise is likely to be a problem. Furthermore, although in the intact brain, metabolism, perfusion and blood volume are functionally linked, this cannot be assumed to be so for disease states. Thus a definite relationship between signal change and perfusion as measured in physiological terms (e.g. $ml.min^{-1}ml^{-1}$) cannot be obtained.

Digital Subtraction Angiography

The ability of this technique to digitise and quantify changes in attenuation following intra-arterial or intravenous administration of contrast media provides opportunities to combine functional information with anatomical detail in a way somewhat similar to dynamic CT. One difficulty that arises when quantifying DSA data is that some of the signal from a given region will contain a component resulting from scattered radiation from structures outside of the area of interest. Another problem is that the two dimensional or planar orientation of the images means that a further component of the signal will arise from tissues anterior and posterior to the structure under study. Both these components will alter, to different degrees, following administration of contrast agents. Similar problems have been successfully addressed within the field of nuclear medicine and there is potential to apply this experience to DSA but, as yet, there is relatively little published work describing the application of DSA to functional imaging. Methods for determination of volume flow within vessels have been evaluated [111] and digital subtraction angiography with parametric imaging has been used to study regional variations in renal perfusion [112] but, as with the gamma camera, clear separation of cortex and medulla is not possible.

8.2 Advantages and limitations of CT as a technique for measuring perfusion:

The main advantage of using CT to assess perfusion is that the technique combines quantifiable functional information with good anatomical detail within one examination. Thus the problems of image registration that occur when combining the results of separate functional and anatomical imaging techniques are avoided. The methodology, which can be applied to most tissues, is simple and no special equipment is required. Hence, the technique could be performed on many of the existing CT systems currently installed in diagnostic radiology departments. Blood flow is assessed at the more metabolically relevant tissue level and regional variations of perfusion within an organ are readily studied.

Many of the limitations have already been discussed in earlier chapters, including the radiation burden, movement of the patient, the potential effect of contrast media on blood flow, the bolus quality and photon noise. For functional images, the effect of photon noise on the accuracy of perfusion measurements from an individual pixel will, in part, be dependent upon the value of perfusion itself; it is less important with higher perfusion. For the Siemens Somatom Plus CT system, using a 256 x 256 matrix, the error for an individual pixel with a perfusion of 0.32 $ml.min^{-1}ml^{-1}$ is +/- 0.06 $ml.min^{-1}ml^{-1}$ [42]. Of course, measurements from

regions of interest will be more accurate. A significant further limitation is that only one axial slice can be studied and thus craniocaudal variations in the distribution of perfusion cannot be visualised.

8.3 Further research and potential applications:

An important area for further research is validation of the measurements. The combined results of the studies presented in earlier chapters provide powerful evidence that the perfusion values are indeed accurate in that the normal values of perfusion agree closely with reference ranges for all of the organs studied. Furthermore, the changes observed in disease states are in accordance with known pathophysiology. However, direct validation in man is difficult and, in this work, has been limited to the comparison between the CT and scintigraphically derived hepatic arterial to total perfusion ratios. Animal studies to compare the technique with microspheres would strengthen the evidence further.

More recently, Blomley et al [113] have compared the Gould method, which in turn has been validated against microspheres below 2 $ml.min^{-1}ml^{-1}$ [32], with the analysis method described in this thesis. By processing data from human studies performed with ultrafast CT equipment using both analysis methods, they demonstrated close agreement for low perfusion rates, such as splenic perfusion, with a good correlation (slope 1.03, r= 0.78) for perfusion values less than 2 $ml.min^{-1}ml^{-1}$ [113a]. At high perfusion organs, such as renal cortex, the Gould method underestimated perfusion values confirming the greater dependancy of this technqiue on a long tissue transit time which may not present when

perfusion is high. The values obtained by Blomley et al [113] also correlate well with those presented in this thesis (Table 8.2).

TABLE 8.2

ORGAN	PERFUSION ($ml.min^{-1}ml^{-1}$)		
	This Thesis (Siemens)	Blomley (Gradient)	Blomley (Gould)
Spleen (Normal)	1.40	1.48	1.25
Liver (Arterial)	0.15	0.18	----
Renal Cortex	4.70	4.22	3.22

Comparison of CT perfusion values a) from this thesis using the Siemens Somatom Plus, b) from Blomley et al [113] using the analysis method as in this thesis (i.e. gradient) and c) from Blomley et al [113] using the Gould method.

The combined anatomical and functional information of CT perfusion imaging provides opportunities for research and clinical applications. In the case of the pancreas, no other imaging method is as straightforward and as readily available for providing absolute measurements of pancreatic perfusion in man and thus many questions such as the changes in pancreatic perfusion in diabetes can be addressed. The pancreatic work has also demonstrated a potential clinical role in tissue characterisation.

In the kidney, changes in intrarenal haemodynamics occur in

many conditions such as glomerulonephritis, outflow obstruction, hypertension and renal artery stenosis [114] and thus CT perfusion imaging creates opportunities for diagnosis of such conditions on functional grounds, even when the kidneys are morphologically normal. The effects of drugs on altered renal cortical or medullary blood flow in disease is also of interest. For instance, are the changes in intrarenal blood flow in diabetes reversed by drugs,such as captopril, that are used to treat diabetic nephropathy? The effects of cyclosporin on the human kidney and the potential to reverse them with pharmacological intervention could also be studied.

Similarly for the liver, cirrhosis can be diagnosed in the absence of morphological abnormalities. The quantification allows the severity of diffuse liver disease to be assessed and the results of studies before and after treatment could be compared. In patients investigated for possible hepatic metastases, there is also the possibility of detecting "micrometastases" from the change in arterial perfusion again when there is no visible structural abnormality. A group such patients with increased arterial to total liver blood flow ratio but a morphological normal liver has been already identified using scintigraphy. Such patients have a worse prognosis and develop overt metastases earlier than those patients within normal flow [62]. These patients could possibly benefit from adjuvent chemotherapy.

The CT studies of the spleen have provided some insight into the splenic microcirculation and its relationship to red cell destruction but conditions such as lymphoma have yet to be examined. On a clinical level, a splenic perfusion of less than $1ml.min^{-1}ml^{-1}$ suggests the presence of portal hypertension and individual values could provide a non-invasive measure of severity.

Other potential applications include studies of the brain (figure 8.1) and tumours. As yet, the author has had little experience of these applications. Tumour perfusion is of great interest to oncologists as modification of tumour flow (figure 8.2) by pharmacological means may render a tumour more susceptible to radiation or chemotherapy.

Generally, the clinical benefits are likely to be greatest where the functional data provides information about a disease state that could not be inferred from visual analysis of the unprocessed images. Examples presented in this thesis include cases of hepatic cirrhosis, renal cyclosporin toxicity and diabetes where the diagnosis and severity of disease could not be determined without perfusion measurements. Absolute quantification will be important in asessing disease severity and when diagnostic criteria include threshold values e.g. a splenic perfusion of less than $1ml.min^{-1}ml^{-1}$ implies portal hypertension.

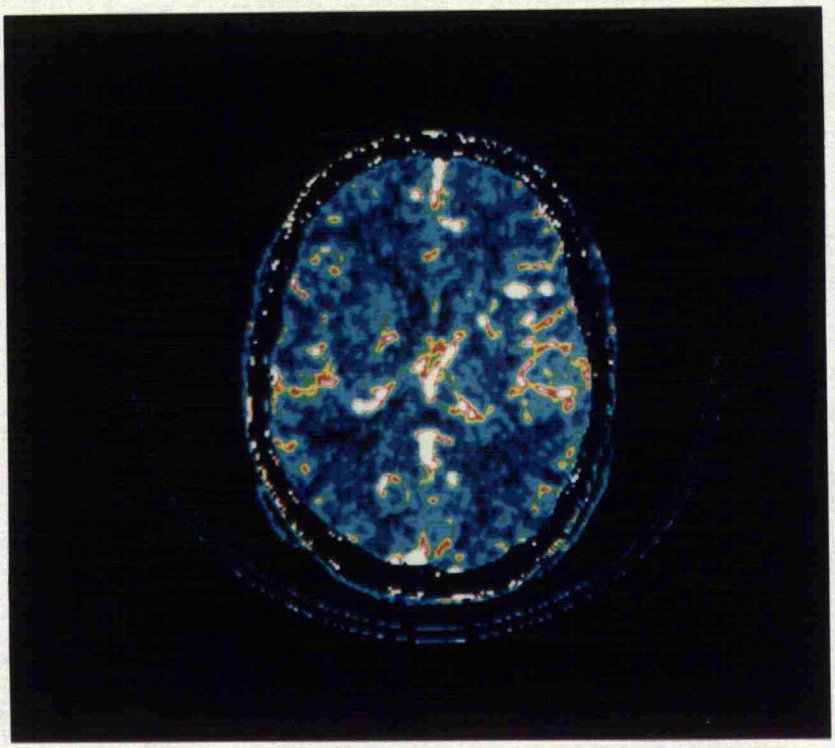

Figure 8.1: CT perfusion image of the brain in a patient with Moya-moya disease.

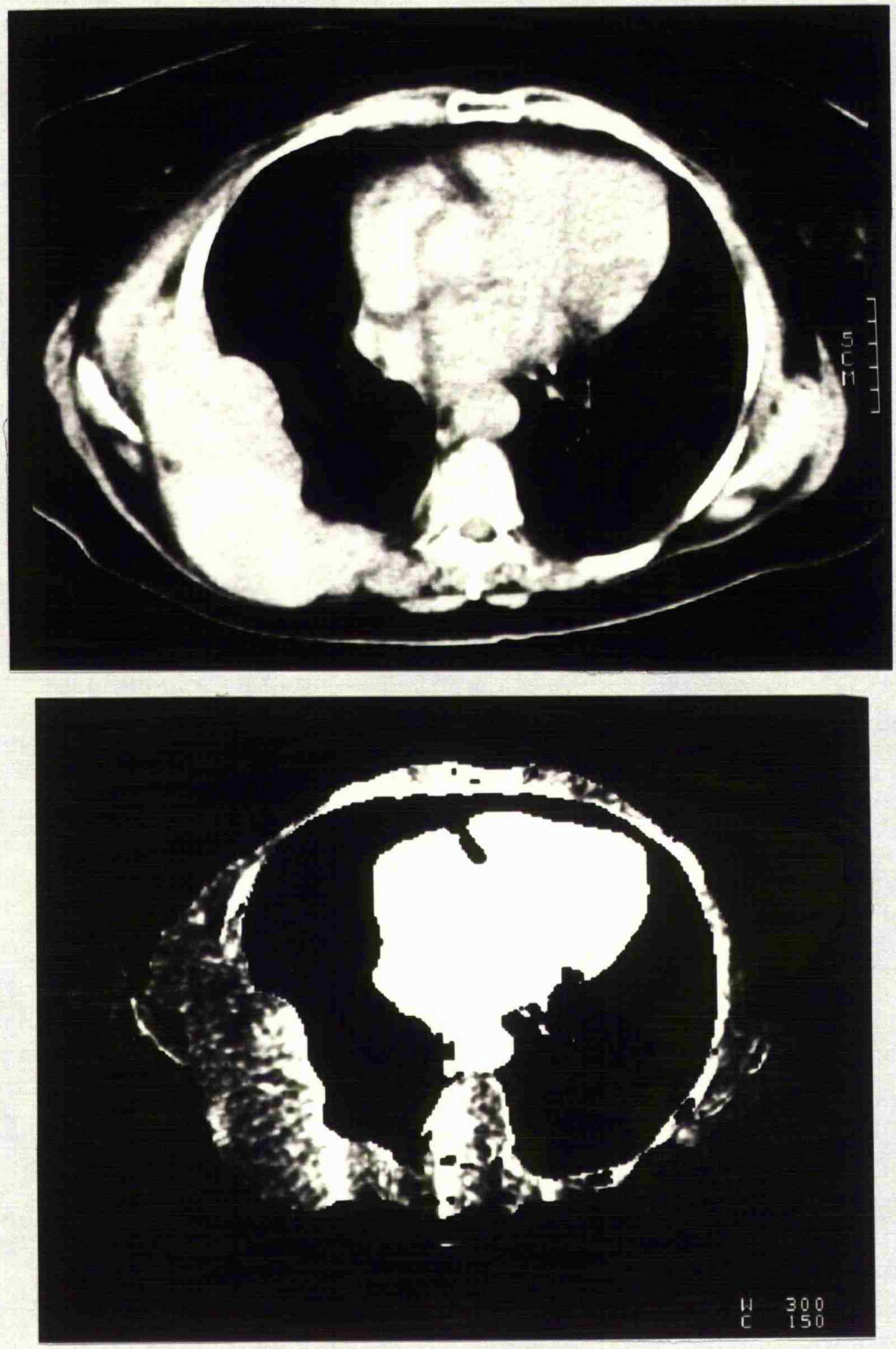

Figure 8.2A: Unenhanced CT (above) of the thorax in a patient with a metastasis in the right chest wall. Below: perfusion image created using the Siemens prototype software.

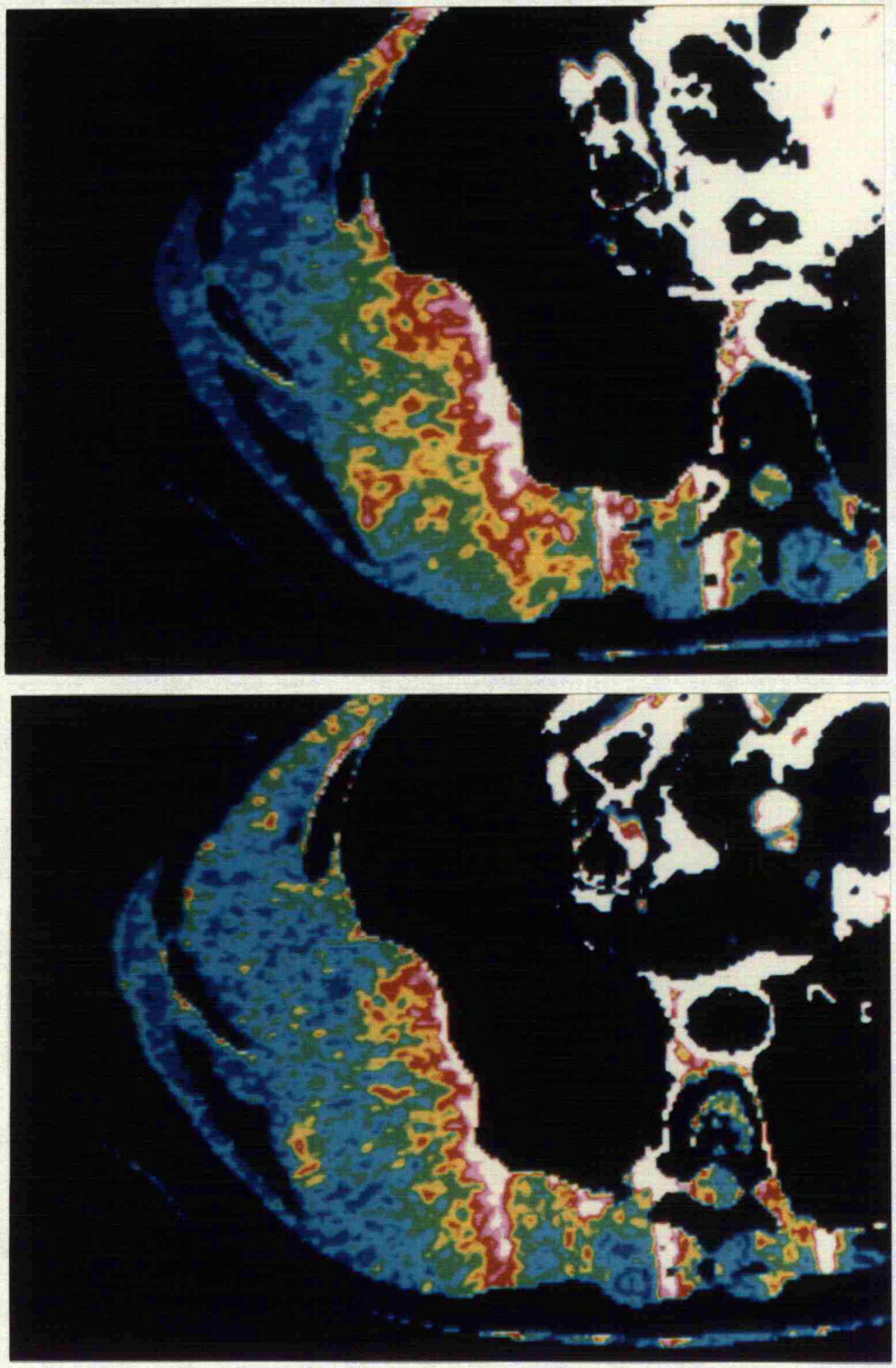

Figure 8.2B: Perfusion images of right chest wall metastasis before (above) and during (below) pharmacological intervention to reduce tumour blood flow. Note the fall in perfusion achieved.

8.4 Summary:

The technique of CT perfusion measurement and imaging developed and evaluated in this work has a number of advantages over previous CT methods and techniques that use other imaging modalities. CT perfusion imaging has not previously been described for the kidney, liver, spleen or pancreas. This technique, which provides a valuable combination of functional and anatomical information in one investigation, has many potential research and clinical applications.

9. ACKNOWLEDGEMENTS:

The technique and methods of analysis developed in this thesis have not been previously applied to CT and hence are novel applications. They have been derived by myself, being in the fortunate position of working in both Nuclear Medicine and Radiology. Nearly all the clinical studies were either performed or supervised by myself. Since starting the thesis, some aspects of the work have been published in refereed journals [33,115,116].

I am particularly grateful to and most keen to acknowledge the invaluable role of Mike Hayball (Department of Medical Physics, Addenbrooke's Hospital, Cambridge) whose computing expertise enabled my concept of CT perfusion imaging to become a practical reality. He has designed and written the software for calculation of perfusion from regions of interest and creation of functional images. The details of the computer programming and an evaluation of the noise characteristics of the Siemens Somatom Plus CT system installed at Addenbrooke's formed the basis of his own M.Sc. thesis (University College, London) [42]. There is no overlap between his thesis and the work presented here.

I also wish to thank Siemens U.K. for providing the Archimedes work station and the means of direct data transfer from the Somatom Plus CT system to the workstation. They have also installed prototype software for perfusion imaging based

on the methods presented in this thesis.

I am most grateful to the radiographers in the CT departments at the Leicester Royal Infirmary and Addenbrooke's Hospital, Cambridge for their patience and assistance in performing the studies. I would also like to thank Dr. D.C. James of the Radiology Department at the Leicester Royal Infirmary and Dr. A.K. Dixon of the University Department of Radiology, Cambridge for their encouragement and support in this project and also Dr. Dixon and my advisor, Professor D.H. Evans of the Department of Medical Physics, University of Leicester for their constructive criticisms during preparation of the manuscript. The Medical Illustration department at Addenbrooke's hospital and Michelle Deal of the University Department of Radiology, Cambridge have also been most helpful in production of the CT images included in the figures.

10. ABBREVIATIONS:

CT:	Computed Tomography
DSA:	Digital Subtraction Angiography
DTPA:	DimethyTriethylPentacetic Acid
ERPF:	Effective Renal Plasma Flow
HAR:	Hepatic Arterial Ratio
HMPAO:	HydroxyMethylPropylAmineOxime
HPI:	Hepatic Perfusion Index
MIBI:	MethoxyIsoButylIsonitrile
MRI:) MR:)	Magnetic Resonance Imaging
PET:	Positron Emission Tomography
ROI:	Region Of Interest
TDC:	Time-Density Curve
US:	UltraSound

11. REFERENCES:

1 Hounsfield G.N., Computerized transverse axial scanning (tomography): Part I. Description of system. British Journal of Radiology, 1973; 46:1016-22.

2 Pickering R.S., Hattery R.R., Hartman G.W. & Holley K.E. Computed tomography of the excised kidney. Radiology, 1974; 113: 643-7.

3 Zeman R.K., Cronan J.J., Rosenfield A.T., Lynch J.H., Jaffe M.H. & Clark L.R. Renal Cell Carcinoma: Dynamic thin section CT assessment of vascular invasion and tumour vascularity. Radiology, 1988; 167:393-396

4 Miles K.A., London N.J.M., Lavelle J.M., Messios N. & Smart J.G. CT staging of renal carcinoma: a prospective comparison of three dynamic computed tomography techniques. European Journal of Radiology 1991; 13:37-42

5 Husband J. Staging of bladder and prostate cancer. in CT Review (Churchill Livingstone, Edinburgh) 1989 p206

6 Kivisaari L., Somer K., Standertskjold-Nordenstan C.G., Shroder T., Kivilaasko E. & Lempinen M. A new method for the diagnosis of acute haemorrhagic-necrotizing pancreatitis using contrast enhanced CT. Gastrointestal Radiology 1984; 9(1):27-30

7 Block S., Maier W., Bittner R., Buchler M., Malfertheiner P. & Beger H.G. Identification of pancreas necrosis in severe acute pancreatitis: imaging procedures versus clinical staging. Gut 1986; 27:1035-1042

8 London N.J.M., Leese T., Lavelle J.M., Miles K.A., West K.P, Watkin D.F.L. & Fossard D.P. Rapid bolus contrast enhanced dynamic computed tomography in acute pancreatitis: a prospective study. British Journal of Surgery 1991; 78:1452-1456

9 Thorsen M.K., San Dretto M.A., Lawson T.L., Foley W.D., Smith D.F. & Berland L.L. Dissecting aortic aneurysms: Accuracy of computed tomographic diagnosis. Radiology 1983; 148:773-777.

10 Godwin D.J. & Webb W.R. Dynamic computed tomography in the evaluation of vascular lung lesions. Radiology 1981; 138:629-635.

11 Dean P.B., Kivisaari L. & Kormano M. The diagnostic potential of contrast enhancement pharmacokinetics. Investigative Radiology 1978; 13:533-540

12 Haertal M. Das kavernose Leberhamangiom im Computertomogramm. RoFo 1980; 133(4):379-381

13 Hosoki T. Dynamic CT of pancreatic tumours. American Journal of Roentgenology 1983; 140:959-965

14 Partanen K.P.L. Dynamic CT of liver cirrhosis. Investigative Radiology 1984; 19:303-308

15 Ishikawa I., Onouchi Z., Saito Y., Kitada H., Shinoda A., Ushitani K., Tabuchi M. & Suzuki M. Renal cortex visualisation and analysis of dynamic CT curves of the kidney. Journal of Computer Assisted Tomography 1981; 5(5): 695-701

16 Probst P., Mahler F., Roesler H. & Fuchs W.A. Renal artery stenosis and evaluation of the effect of endoluminal dilatation. Comparison of dynamic CT scanning and I-131-OIHA renogram. Investigative Radiology 1983; 3: 264-271

17 Mukai J. & Sabel P. Application of dynamic computed tomography to physiologic imaging of renal artery stenosis before and after angioplasty. Am. J. Physiol. Imaging 1986; 1:33-43

18 Ishikawa I., Masuzaki S., Saito T., Tateishi K., Kitada H., Yuri T., Shinoda A., Onouchi Z., Saito Y. & Futyu Y. Dynamic computed tomography in acute renal failure: Analysis of time-density curve Journal of Computer Assisted Tomography 1985; 9(6): 1097-1102

19 Fuld I.L., Matalon T.A., Vogelzang R.L., Neiman H.L., Kowal L.E., Hutchins W.W. & Soper W. Dynamic CT in the evaluation of physiologic status of renal transplants. AJR 1984; 142: 1157-1160

20 Miles K.A., London N., Messios N. & Smart J.G. Staging of renal carcinoma by dynamic computed tomography; A comparison of two techniques. Clinical Radiology, 1990; 42:122-127

21 Herfkens R.J., Axel L., Lipton M.J., Napel S., Berninger W. & Redington R. Measurement of cardiac output by computed transmission tomography. Investigative Radiology 1982; 17:550-553

22 Stewart G.N.J. Researches on the circulation time and on the influences which effect it. IV. The output of the heart. Journal of Physiology 1897;22:159-173

23 Moore J.W., Kinsman J.M., Hamilton W.F. & Spurling R.G. Studies on circulation. II. Cardiac output determinations; comparison of the injected method with the direct Fick procedure. American Journal of Physiology 1929;89:331-339

24 Axel L. Tissue mean transit time from dynamic computed tomography by a simple deconvolution technique. Investigative Radiology 1983;18:94-99

25 Partanen K. Dynamic computed tomography of the liver and the spleen. 1984; MD thesis. University of Kuopio, Finland.

26 Johnson D.W., Stringer W.A., Marks M.P., Yonas H., Good W.F. & Gur D. Stable xenon CT cerebral blood flow imaging: Rationale for and role in clinical decision making. American Journal of Neuroradiology 1991;12:201-213

27 Jansen V.O., Gmelin E., Burmester E., Rob P. & Weiss H.D. Analyse von dynamischen CT-kurven bei Nierentransplantaten mit Abstossungreaktion und Cyclosporin-A Intoxication. ROFO 1989;151(4):473-476

28 Axel L. Cerebral blood flow determination by rapid-sequence computed tomography; Theoretical analysis. Radiology 1980;137:679-686

29 Jaschke W.R., Gould R.G., Cogan M.G., Sievers R.S. & Lipton M.J. Cine-CT measurement of cortical renal blood flow. Journal of Computer Assisted Tomography 1987; 11:779-784

30 Jaschke W., Sievers R.S., Lipton M.J. & Cogan M.G. Cine-computed tomographic assessment of regional renal blood flow. Acta Radiologica 1989; 31:77-81

31 Wolfkiel C.J., Ferguson J.L., Chomka E.V., Law W.R., Labin I.N., Tenzer M.L., Booker M. & Brundage B.H. Measurement of myocardial blood flow by ultrafast computed tomography. Circulation 1987; 76:1262-1273

32 Gould R.G., Lipton M.J., McNamara M.T., Sievers R.E., Koshold S. & Higgins C.B. Measurement of regional myocardial blood flow in dogs by ultrafast CT. Investigative Radiology 1988; 22:348-353

33 Miles K.A., Hayball M. & Dixon A.K. Colour perfusion imaging: a new application of computed tomography. Lancet 1991; 337:643-645

34 Berninger W.H., Axel L., Norman D., Napel S. & Redington R.W. Functional imaging of the brain using computed tomography. Radiology 1981; 138:711-716

35 Handa J., Matsuda M., Nakasu Y., Nakasu S. & Morioka Y. Dynamic computed tomography and functional imaging in cerebral vascular anomalies. Surgical Neurology 1983; 19:497-507

36 Takahashi N., Kikuchi H. & Karasawa J. Dynamic CT in patients with superficial temporal-middle cerebral artery anastomosis. American Journal of Neuroradiology 1983; 4:454-457

37 Nakagomi T. & Takakura K. Dynamic computed tomography of brain tumor. Brain & Nerve 1984; 36:1031-1040

38 Nagata K. & Asano T. Functional image of dynamic computed tomography for the evaluation of cerebral hemodynamics. Stroke 1990; 21:882-889

39 Flower M.A., Husband J.E. & Parker R.P. A preliminary investigation of dynamic transmission computed tomography for measurement of arterial flow and tumour perfusion. British Journal of Radiology 1985; 58:983-988

40 Nishizawa K., Maruyama T., Takayama M., Okadu M., Hachiya J-I. & Furuya Y. Determination of organ doses and effective dose equivalents from computed tomographic examination. British Journal of Radiology 1991; 64:20-28.

41 Claussen C & Lochner B. Bolus geometry and dynamics: Contrast studies with intravenous contrast media. In: Dynamic computed tomography: Basic principles and clinical applications. Berlin: Springer-Verlag, 1985;33-37

42 Hayball M.P. The determination of perfusion images from dynamic single location X-ray computer tomography. MSc Thesis University of London 1992

43 Winkler S.S., Sackett J.F., Holden J.E., Flemming D.C., Madsen M. & Kimmel R.I. Xenon inhalation as an adjunct to computerized tomography of the brain: preliminary study. Investigative Radiology 1977;12:15-18

44 Good W.F. & Gur D. Xenon-enhanced CT of the brain: effect of flow activiation on derived cerebral blood flow measurements. American Journal of Neuroradiology 1991;12:83-85

45 Hindmarsh T. Elimination of water-soluble contrast media from the sub-arachnoid space. Investigation with computed tomography. Acta Radiologica 1975; 346:45-50

46 Steiner R.M., Grainger R.G., Menon N., Weiss D., Kanofsky P.B. & Menduke H. The effect of contast media of low osmolarity on the peripheral arterial blood flow in the dog. Clinical Radiology 1980; 31:621-627

47 Russel S.B. & Sherwood T. Monomer/dimer contrast media in the renal circulation: experimental angiography. British Journal of Radiology 1974; 47:268-71

48 Almen T. & Aspelin P. Cardiovascular effects of ionic monomeric, ionic dimeric and non-ionic contrast media. Investigative Radiology 1975; 10:557-563

49 Aspelin P. Effects of ionic and non-ionic contrast media on the morphology of human erythrocytes. Acta Radiologica (Diagn) 1978; 19:675-687

50 Grainger R.G. Intravascular contrast media. in "Diagnostic Radiology: An Anglo-American textbook of imaging". Ed Grainger R.G. & Allison D.J. (Churchill Livingstone, Edinburgh) 1986 pp105

51 Dean PB, Kivisaari L & Kormano M. The diagnostic potential of contrast enhancement pharmacokinetics. Investigative Radiology 1978; 13:533-540

52 Dean PB, Kivisaari L & Kormano M. Contrast enhancement pharmacokinetics of six ionic and non-ionic contrast media. Investigative Radiology 1983; 18:368-374

53 Kalender W.A., Polacin A., Eidloth H., Kashiwagi S., Yamashita T. & Nakano S. Brain perfusion studies by xenon-enhanced CT using washin/washout study protocols. Journal of Computer Assisted Tomography 1991; 15:816-22.

54 Kashiwagi S., Yamashita T., Nakano S., Kalender W., Polacin A., Tagasago T., Eguchi Y. & Ito H. The wash-in/washout protocol in stable xenon CT cerebral blood flow studies. American Journal of Neuroradiology 1992; 13:49-53

55 DeWitt D.S., Faturos P.P., Wist A.O., Stewart L.M., Kontos H.A., Hall J.A., Kishore P.R., Keenan R.L. & Marmarou A. Stable xenon versus radiolabelled microsphere cerebral blood flow measurements in baboons. Stroke 1989; 20:1716-1723

56 Shih T.T.F. & Huang K-M. Acute stroke: Detection of changes in cerebral perfusion with dynamic CT scanning. Radiology 1988; 169:469-474

57 Mullani N. & Gould K.L. First-pass measurements of regional blood flow with external detectors. Journal of Nuclear Medicine 1983; 24:577-581

58 Peters A.M., Gunasekera R., Henderson B.L., Brown J., Lavender J.P., De Souza M., Ash J.M. & Gilday D.L. Non-invasive measurements of blood flow and extraction fraction. Nuclear Medicine Communications 1987; 8:823-837

59 Peters A.M., Brown J., Hartnell G.G., Myers M.J., Haskell C. & Lavender J.P. Non-invasive measurment of renal blood flow with Tc^{99m} DTPA: A comparison with microspheres. Cardiovascular Research 1987; 21:830-834

60 Sarper R., Fajman W.A., Rypins E.B., Henderson J.M., Tarcan Y.A., Galambos J.T. & Warren W.D. A noninvasive method for measuring portal venous/total hepatic blood flow by hepatosplenic radionuclide angiography. Radiology 1981; 141:179-184

61 Fleming J.S., Ackery D.M., Walmsley B.H. & Karren S.J. Scintigraphic estimate of arterial and portal blood supply to the liver. Journal of Nuclear Medicine 1983; 24:1108-1113

62 Parkin A., Robinson P.J., Baxter P., Leveson S.H., Wiggins P.A. & Giles G.R. Liver perfusion scintigraphy - method, normal range and laparotomy correlation in 100 patients. Nuclear Medicine Communications 1983; 4:395-402

63 McLaren M.I., Fleming J.S., Walmsley B.H., Ackery D.M., Taylor I. & Karran S.I. Dynamic liver scanning in cirrhosis. British Journal of Surgery 1985;72:394-396

64 Bolton R.P., Mairiang E.O., Parkin A, Ware F., Robinson P. & Losowsky M.S. Dynamic liver scanning in cirrhosis. Nuclear Medicine Communications 1988; 9:235-247

65 Wraight E.P. Radionuclide imaging in postoperative assessment. In "Liver Transplantation." 2nd edition. Ed. Calne R. (Grune & Stratton, London) 1987 pp293-300

66 Kety S.S. The theory and applications of the exchange of inert gas at the lung and tissues. Pharmacological Reviews 1951; 3:1-41

67 Thompson H.K., Starmer C.F., Whalen R.E. & McIntosh H.D. Indicator transit time considered as a gamma variate. Circulation Research 1964; 14:502-515

68 Blaufox M.D., Fromowitz A., Gruskin A., Meng C-H. & Elkin M. Validation of the use of xenon 133 to measure intra renal distribution of blood flow. American Journal of Physiology 1970; 219:440-444

69 Gruenewald S.N., Nimmon C.C., Nawaz M.K. & Britton K.E. A non-invasive gamma camera technique for the measurement of intra-renal flow distribution in man. Clinical Science 1981; 61:385-389

70 Wraight E.P., Barber R.W. & Ritson A. Relative hepatic arterial and portal flow in liver scintigraphy. Nuclear Medicine Communications 1982; 3:273-279

71 Greenway C.V. & Lautt W.W. Hepatic circulation. in "Handbook of Physiology" eds Shultz S.G., Wood J.D. & Rauner B.B. (American Physiological Society, Bethseda Maryland) 1989 Section 6, Vol 1, Part II; pp 1519-1564

72 Ternberg J.L. & Butcher H.R. Jr. Blood-flow relation between hepatic artery and portal vein. Science 1965; 150:1030-1031

73 Ferguson D.J. Haemodynamics in surgery for portal hypertension. Annals of Surgery 1963; 158:383-386

74 Mathie R.T. Hepatic blood flow measurement with inert gas clearance. Journal of Surgical Research 1986; 41:92-110

75 Shiomi S., Kuroki T., Ueda T., Ikeoka N., Kobayashi K., Monna T. & Ochi H. Measurement of hepatic blood flow by use of per-rectal portal scintigraphy with ^{133}Xe. Nuclear Medicine Communications 1991; 12:235-242

76 Kashiwagi T., Kimura K., Suematsu T., Schichiri M., Kamada T. & Abe H. Heterogenous intrahepatic distribution of blood flow in humans. European Journal of Nuclear Medicine 1981; 6:545-549

77 Cole J.W., Krohmer J., Bronte F.J. & Schatten W. An experimental study of intrahepatic distribution of portal blood. Surgery, Gynaecology & Obstetrics 1956; 102:543-544

78 Gates G.F. & Dore E.K. Streamline flow in the human portal vein. Journal of Nuclear Medicine 1973: 14:79

79 Kahn D., Van Hoorn-Hickman R. & Terblanche J. Liver blood flow after partial hepatectomy in the pig. Journal of Surgical Research 1984; 37:290-294

80 Itai Y., Moss A.A. & Goldberg H.I. Transient hepatic attenuation difference of lobar or segmental distribution detected by dynamic computed tomography. Radiology 1982; 144:835-839

81 Chan S.C.H., Chan F-L., Chau E.M.T. & Mok F.P.T. Portal thrombosis complicating appendicitis: ultrasound detection and hepatic computed tomography lobar attenuation alteration. Journal of Computer Tomography 1988; 122:208-210

82 Mathieu D., Vasile N., Dibie C. & Grenier P. Portal cavernoma: Dynamic CT features and transient differences in hepatic attenuation. Radiology 1985; 154:743-748

83 Mathieu D., Vasile N., Fagniez P-L., Segui S., Grably D. & Larde D. Dynamic CT features of hepatic abscesses. Radiology 1985; 154:749-752

84 Williams R., Condon R.E., Williams H.S., Blendis L.M. & Kreel L. Splenic blood flow in cirrhosis and portal hypertension. Clinical Science 1968; 34:441-452

85 Gitlin N., Grahame G.R., Kreel L. Williams H.S & Sherlock S. Splenic blood flow and resistance in patients with cirrhosis before and after portacaval anastomoses. Gastroenterology 1970; 59:208-213

86 Ueda H., Kitani K, Kameda H, Takeda T., Cjiba K., Nagatani M., Yamada H. & Lio M. Splenic blood flow in idiopathic portal hypertension in Japan measured by 85 Kr clearance method. Acta Hepato-splenology 1971; 18:28-40

87 Huchzermeyer H., Schmitz-Feuerhake I. & Reblin T. Determination of splenic blood flow by inhalation of radioactive rare gases. European Journal of Clinical Investigation 1977; 7:345-349

88 Takahasi Y., Akasaka K., Tanaka Y., Syriyone S. & Uyama C. Studies on splenic hemodynamics and blood cell destruction by simulation analysis of radiosplenogram. 1st World Congress of Nuclear Medicine 1974 pp 97-101

89 Groom A. Microcirculation of the spleen: new concepts, new challanges. Microvascular research 1987; 34:269-289

90 Ayers A.B., Henry K., Russel S.B. & Steiner R.E. The microvasculature of the spleen. Clinical Radiology 1976; 27:259-264

91 Kubo S., Yamamoto K. Magata Y., Iwasaki Y., Tamaki N., Yonekura Y. & Konishi J. Assessment of pancreatic blood flow with positron emission tomography and oxygen-15 water. Annals of Nuclear Medicine 1991; 5:133-138

92 Kvietys P.R., Granger D.N. & Harper S.L. Circulation of the pancreas and salivary glands. in "Handbook of physiology." Eds Shultz S.G. Wood J.D. & Rauner B.B. (American Physiological Society, Bethseda Maryland) 1989 Section 6, Vol. 1, Part II;pp 1565-1595

93 Weaver F.C. Blood flow in the atrophied pancreas. Experimental Pathology 1990; 38:119-127

94 Jansson L. & Swenne I. Age-dependent changes of pancreatic islet blood flow in the rat. International Journal of Pancreatology. 1989; 5:157-163

95 Youngleman D.F., Kahng K.U., Dresner L.S., Munshi I.A. & Wait R.B. Cyclosporine-induced alterations in renal, intrarenal and pancreatic blood flow. Transplantation Proceedings 1991; 23:718-720

96 Petrie R., Freeman D., Wallace C., McDonald J., Stiller C. & Keown P. Effect of cyclosporine on urinary prostanoid excretion, renal blood flow and glomerulotubular function. Transplantation 1988; 45:883-889

97 Parkin A., Robinson P.J., Martinez D., Wilkinson D. & Kester R.C. Radionuclide limb blood flow in peripheral vascular disease: a review of 1100 measurements. Nuclear Medicine Communications 1991; 12:835-851

98 Lipton M.J., Higgins C.B. & Boyd D.P. Computed tomography of the heart: evaluation of anatomy and function. Journal of the American College of Cardiology 1985; (1 Suppl):55S-69S

99 Britten A.J., Fleming J.S., Flowerdew A.D.S., Taylor I., Karran S.J. & Ackery D.M. Regional indices of relative hepatic arterial perfusion from dynamic liver scintigraphy: the variability of indices and the use of parametric imaging. Nuclear Medicine Communications 1990; 11:29-36

100 Robertson J., Leen E., Goldberg J.A., Angerson W.J., Sutherland G.R. & McArdle C.S. Flow measurement using duplex Doppler ultrasound: Haemodynamic changes in patients with colorectal liver metastases. Clinical physics and physiological measurements. 1992; 13:709-721

101 Leen E., Angerson W.J., Warren J.A., Goldberg J.A., Lieberman D.P., Cooke T.G. & McArdle C.S. Hepatic arterial haemodynamics changes following intra-arterial Angiotensin II infusion: Duplex/colour Doppler sonography. Clinical Radiology 1993 47:321-324

102 Axel L. Blood flow effects in magnetic resonance imaging. American Journal of Roentgenology 1984; 143:1157-1166

103 Dumoulin C.L. & Hart H.R. Magnetic resonance angiography. Radiology 1986; 161:717-720

104 Lundin B, Cooper T.G., Meyer R.A. & Potchen E.J. Measurement of total and unilateral renal blood flow by oblique-angle velocity-encoded 2D-cine magnetic resonance angiography. Magnetic Resonance Imaging 1993; 2:51-59

105 Tang C., Blatter D.D. & Partker D.L. Accuracy of phase-contrast flow measurements in the presence of partial-volume effects. Journal of Magnetic Resonance Imaging 1993; 3:377-385

106 Underwood S.R., Firmin D.N., Rees R.S. & Longmore D.B.Magnetic resonance velocity mapping. Clinical Physics and Physiological Measurement 1990 11 Suppl A:37-43

107 Le Bihan D., Breton E., Lallemand D., Grenier P., Cabinis E. & Lavel-Jeantet M. MR imaging of intravoxel incoherent motions: application to diffusion and perfusion in neurologic disorders. Radiology 1986; 161:401-407

108 Choyke P.L., Frank J.A., Girton M.E., Inscoe S.W., Carvlin M.J., Black J.L., Austin H.A. & Dwyer A.J. Dynamic Gd-DTPA-enhanced MR imaging of the kidney: Experimental results. Radiology 1989; 170:713-720

109 Bandettini P.A., Wong E.C., Hinks R.S. & Hyde J.S. Time course EPI of human brain function during task activation. Magnetic Resonance in Medicine 1992; 25:390-397

110 Belliveau J.W., Kennedy D.N. Jr, McKinstry R.C. & Buchbinder B.R. Functional mapping of the human visual cortex by magnetic resonance imaging. Science 1991; 254:716-719

111 Le Goff R., Gerlot-Chiron P. & Bizias Y. Experimental validation of a model for blood flow measurement from DSA images. Computer Assisted Radiology '91 Ed. Lemke H.U., Rhodes M.L., Jaffe C.C. & Felix R. (Springer-Verlag, Berlin) 1991 pp73-78

112 Hunter J.V. Parametric imaging applied to renal digital subtraction angiography: establishment of normal ranges. Urological Radiology 1986; 8:204-208

113 Blomley M.J.K., Coulden R.J., Bufkin C, Lipton M.J. & Dawson P. Contrast bolus dynamic computed tomography for the measurement of solid organ perfusion. Investigative Radiology 1993; 28: Suppl 5, S72-S77

113a Blomley M.J.K. Personal Communication.

114 Piepsz A., Ham H.R. & Dupont A.G. Renal blood flow in renal disease and hypertension. In "Evaluation of renal function and disease with radionuclides: The upper urinary tract" 2nd Edition, edited by Blaufox MD, (Karger, Basel) 1989 pp 150-184

115 Miles K.A. Measurement of tissue perfusion by dynamic computed tomography. British Journal of Radiology 1991; 64:409-412

116 Miles K.A., Hayball M.P. & Dixon A.K. Functional images of hepatic perfusion obtained with dynamic computed tomography Radiology 1993; 188:405-411

1991, *The British Journal of Radiology, 64*, 409–412

Measurement of tissue perfusion by dynamic computed tomography

By K. A. Miles, MB, BS, FRCR

Departments of Radiology and Nuclear Medicine, Addenbrooke's Hospital, Hills Road, Cambridge CB2 2QQ, UK

(*Received July 1990 and in revised form December 1990*)

Keywords: Dynamic, Computed tomography, Perfusion, Measurement

Abstract. A method for quantifying tissue perfusion by dynamic computed tomography (CT) is described. By applying a nuclear medicine data processing technique to time-density data from a single-location dynamic CT sequence, tissue perfusion can be determined from the maximum gradient of the tissue time–density curve divided by the peak enhancement of the aorta. Using this method, splenic perfusion was measured at 1.2 ml min^{-1} ml^{-1}, normal renal cortical perfusion at 2.5 ml min^{-1} ml^{-1} and normal renal medullary perfusion at 1.1 ml min^{-1} ml^{-1}. Changes in cortical and medullary perfusion in renal failure and hypertension were demonstrated. The ability of dynamic CT to provide quantitative functional information is not well recognized and is potentially of value when studying structures, such as the renal cortex and medulla, that cannot be anatomically resolved by standard functional imaging techniques.

Dynamic computed tomography (CT) describes a rapid sequence of images acquired after the injection of intravascular contrast medium. If the sequence of scans is performed at the same slice location it is possible to construct time–density curves (TDCs) by defining a region of interest (ROI) over a particular structure. The curve will display the change in X-ray attenuation, and hence the change in iodine concentration within that structure with time. In this way, it is possible to treat the contrast agent as a physiological indicator and gain information about function.

The aim of this study was to determine whether quantitative information about tissue perfusion could be obtained from dynamic CT by applying a nuclear medicine data processing technique to the time–density data.

Patients and methods

The nuclear medicine data processing technique used was developed by Peters et al (1987a) to allow measurement of blood flow from first-pass studies using radioisotopes not completely extracted by the organ studied. The method was subsequently validated in animals (Peters et al, 1987b) and is based on the determination of blood flow as a proportion of cardiac output using radiolabelled microspheres. A time–activity curve over an organ after the injection of microspheres into the left ventricle will rise and reach a maximum height H (cts s^{-1}).

$$\frac{\text{OBF}}{\text{CO}} = \frac{H \times a}{\text{Dose injected}} \qquad (1)$$

where OBF is organ blood flow and CO is cardiac output. (The dose injected will be measured in MBq and a is a correction factor relating cts s^{-1} to MBq determined by detector efficiency and photon attenuation). If one considers the integrated arterial time–activity curve corrected for recirculation using a gamma function fit, its shape will be the same as that obtained from the organ using microspheres but reaching the plateau at a value A (cts) and with a maximal slope g_{arterial} (cts s^{-1}). A is also the area under the arterial curve before integration and g_{arterial} will be its maximum height. The integrated arterial curve and the organ curve will be related as follows:

$$\frac{g_{\text{organ}}\ (\text{cts s}^{-2})}{g_{\text{arterial}}\ (\text{cts s}^{-1})} = \frac{H\ (\text{cts s}^{-1})}{A\ (\text{cts})} \qquad (2)$$

where g_{organ} is the maximal slope of the organ time–activity curve (cts s^{-2}). However, a tracer that is not completely extracted by the organ on its first pass, such as $^{99}Tc^{m}$-DTPA, will produce a time–activity curve that will not reach this plateau value, but its maximal slope, g_{organ} will be the same as that obtained using microspheres. Thus by using Equation (2) to substitute for H in Equation (1):

$$\frac{\text{OBF}}{\text{CO}} = \frac{A}{\text{Dose injected}} \times \frac{g_{\text{organ}}}{g_{\text{arterial}}} \times a. \qquad (3)$$

Intravascular contrast medium has pharmacokinetics very similar to those of DTPA and thus the technique can be applied to dynamic CT by constructing TDCs from the aorta and the tissue to be studied. The concentration of contrast medium within any ROI can be determined with an increase in attenuation of 25 HU indicating an iodine concentration of 1 mg ml^{-1} (Hindmarsh, 1975). The correction factor a is not required with CT as A is measured in HU s and the dose injected can be expressed in HU ml. (As an iodine concentration of 1 mg ml^{-1} is equivalent to 25 HU, 1 mg of iodine is equivalent to 25 HU ml.) As it is

concentration, *i.e.* the amount of iodine per ml of tissue, that is measured, rather than total organ iodine, it is blood flow per ml of tissue, or perfusion, that is determined. Thus for CT:

$$\frac{\text{organ blood flow/ml tissue}}{\text{cardiac output}} = \frac{A\ (\text{HU s})}{\text{Dose (HU ml)}} \times \frac{g_{\text{organ}}\ (\text{HU s}^{-1})}{g_{\text{arterial}}\ (\text{HU})} \quad (4)$$

Furthermore, as the cardiac output can be determined by dynamic CT from the injected dose of iodine and the area under the arterial TDC after correction for recirculation (A) (Axel et al, 1979) by:

$$\text{CO} = \frac{\text{Dose injected (HU ml)}}{A\ (\text{HU s})} \quad (5)$$

the tissue perfusion is thus given by:

$$\text{tissue perfusion (ml s}^{-1}\text{ ml}^{-1}\text{ tissue)} = \frac{g_{\text{organ}}\ (\text{HU s}^{-1})}{g_{\text{arterial}}\ (\text{HU})} \quad (6)$$

g_{organ} is derived from the maximum gradient of tissue TDC and g_{arterial} is given by the peak height of the arterial TDC (before integration and after subtraction of the pre-contrast medium attenuation value). A multiplication factor of 60 converts ml s^{-1} ml^{-1} to ml min^{-1} ml^{-1}. The advantages of applying this method to CT are its simplicity and the avoidance of the correction factors required when using radioisotopes.

The patients studied were those undergoing dynamic CT for staging of renal carcinoma, diagnosis of renal vein thrombosis in the nephrotic syndrome or diagnosis of renal artery stenosis. The CT machine used was an IGE 8800 and a single-location dynamic sequence was performed at the level of the renal veins with scans performed as rapidly as possible, *i.e.* every 6 seconds, during quiet breathing. Fifty millilitres of iopamidol (370 mg ml^{-1}) were injected intravenously by hand as rapidly as possible and TDCs were derived from ROIs constructed over the abdominal aorta and the organ to be studied. Regions of interest were made as large as possible to reduce the effects of photon noise whilst avoiding partial volume effects.

To validate the method, TDCs derived from 12 spleens were studied and the value for splenic perfusion determined was compared with values derived for humans using intra-arterial xenon (Williams et al, 1968). The kidneys studied were contralateral kidneys in patients with renal tumours (18 kidneys), apparently normal portions of kidneys containing renal tumours (nine kidneys), patients with known renal failure (four kidneys) and hypertensive patients treated with captopril (six kidneys) and without (two kidneys). TDCs were constructed from the renal cortex and medulla.

Results

The mean value of splenic perfusion determined by CT was 1.2 ml min^{-1} ml^{-1} with a standard deviation of 0.4 ml min^{-1} ml^{-1}. The mean values and standard deviations for the renal cortex and medulla in the groups of kidneys studied are displayed in Figs 1–4 and examples of time–density curves are given in Fig. 5.

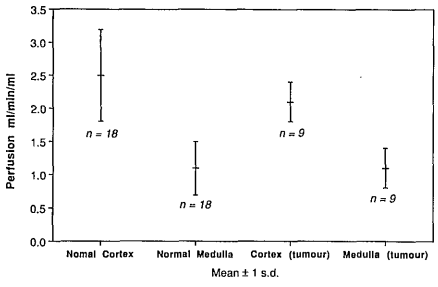

Figure 1. Mean values ± 1 standard deviation for cortical and medullary perfusion in normal kidneys and "normal" portions of tumorous kidneys.

There was no significant difference in cortical or medullary perfusion in the kidneys containing tumour when compared with normals, and perfusion appeared normal even in one case where the renal vein was occluded by tumour thrombus. Renal failure produced a significant decrease in medullary perfusion ($p < 0.01$, Wilcoxon rank-sum test) with reduced cortical perfusion also, but not reaching statistical significance ($p = 0.07$). Renal cortical perfusion was significantly reduced in hypertension without captopril treatment when compared with normals ($p < 0.05$, Wilcoxon rank-sum test), whereas in hypertensives treated with captopril, cortical perfusion was not significantly different from normal. Hypertension and captopril had no effect on medullary perfusion.

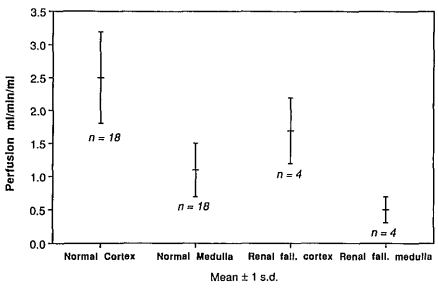

Figure 2. Mean values ± 1 standard deviation for cortical and medullary perfusion in normal kidneys and kidneys in patients with renal failure.

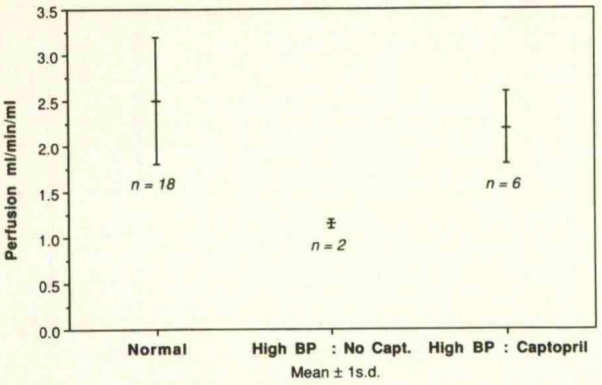

Figure 3. Mean values ± 1 standard deviation for cortical perfusion in normal kidneys and kidneys in patients with hypertension, with and without captopril.

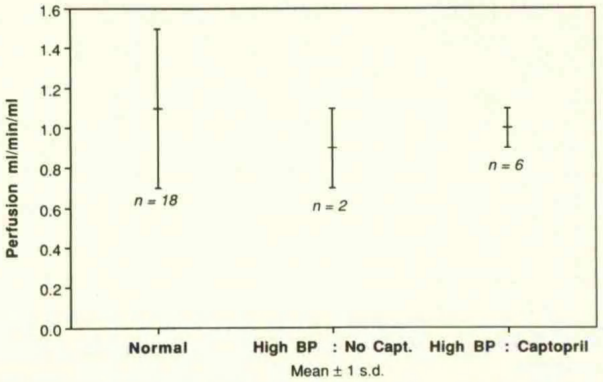

Figure 4. Mean values ± 1 standard deviation for medullary perfusion in normal kidneys and kidneys in patients with hypertension, with and without captopril.

Discussion

This study has shown that dynamic CT can provide quantitative functional information about tissue perfusion and that TDCs can be processed using nuclear medicine techniques. Quantitative functional information in the form of transit times has previously been derived from dynamic CT using deconvolution (Axel, 1983) and a semi-quantitative index of perfusion has also been described (Jansen et al, 1989), but absolute values for tissue perfusion from CT have not been previously reported. The technique is simple, requiring only the maximum slope of the tissue TDC and the peak enhancement in the aorta, and can be applied to most tissues. Changes with disease are seen indicating that the technique is potentially of value in diagnosis.

The value for splenic perfusion by CT of 1.2 ml min^{-1} ml^{-1} is close to the value of 0.96 ml min^{-1} g^{-1} obtained from intra-arterial xenon studies (Williams et al, 1968) and the standard deviation is similar. The higher value obtained from CT may reflect the vasodilatory effect of the contrast medium. Williams et al (1968) described an increase in splenic perfusion of 25% in one patient after intra-arterial contrast medium injection. Although non-ionic contrast

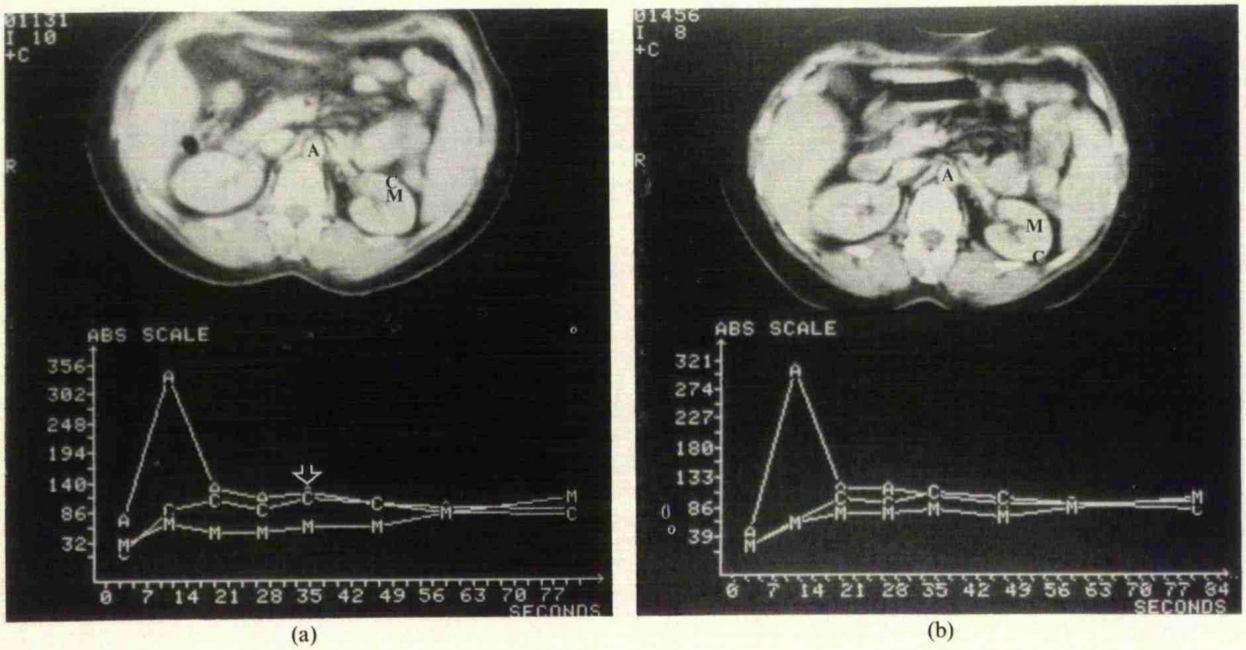

(a) (b)

Figure 5. Time–density curves from a hypertensive patient (a) with and (b) without captopril. (A = aorta, C = cortex, M = medulla. The arrow indicates the point of recirculation.) Note the increased slope of the cortical TDC after captopril.

medium, which is less vasodilatory, was used in these CT studies, this effect is likely to be of significance.

Other sources of error include the low sampling rate and the effects of photon noise. In these studies, the images were obtained every 6 seconds but newer machines have possible imaging rates of 1/second or less, which will reduce the problem but at the expense of greater radiation exposure. The main effect of low sampling rate will be underestimation of the height of the arterial curve and thus overestimation of the tissue perfusion. Photon noise was assessed for this machine by performing a dynamic scan sequence on a polythene phantom. An acceptable standard deviation of 3 HU during a seven-scan sequence was achieved with an ROI of 10 pixels. Thus, photon noise will not be significant for larger organs such as the spleen, but may become so for smaller ROIs. It is therefore important to keep ROIs as large as possible, whilst avoiding partial volume effects.

The mean value of 1.1 ml min^{-1} ml^{-1} for medullary perfusion in normal kidneys corresponds closely to the accepted value of 1 ml min^{-1} ml^{-1} derived from studies using intra-arterial xenon (Rosen, 1968) but the CT derived value of 2.5 ml min^{-1} ml^{-1} for cortical perfusion is significantly lower than the accepted value of 5 ml min^{-1} ml^{-1} (Rosen, 1968). Contrast agents are known to decrease renal blood flow (Russel & Sherwood, 1974) and this may account for the lower values obtained for the renal cortex. It should be remembered that the values obtained using xenon are derived using compartmental analysis, identifying a physiological rather than an anatomical compartment. To date, it has not been possible to study the renal cortex and medulla with separate anatomically defined regions and hence no true reference values are available.

The effect of contrast media on renal blood flow may be partially mediated by anti-diuretic hormone and the renin–angiotensin system (Trewhella et al, 1990). Renal cortical perfusion measured by dynamic CT was reduced in hypertension in keeping with the findings of Gruenewald (1980), but this reduction was reversed by captopril. It has been suggested that reduction in cortical blood flow may be the mechanism for contrast nephrotoxicity. This correction of cortical perfusion, as measured with contrast media and dynamic CT, is evidence that captopril is potentially of value in prevention of contrast medium nephrotoxicity—at least in patients where cortical perfusion is reduced, such as in hypertension, but also possibly in patients with renal failure, a high-risk group for contrast nephrotoxicity, where dynamic CT has demonstrated some reduction in cortical perfusion.

The ability of dynamic CT to provide quantitative functional information in addition to good anatomical detail is not well recognized. This method of determining tissue perfusion, applicable to most tissues, is of greatest potential benefit when the structures studied, such as the renal cortex and medulla, cannot be anatomically resolved by other functional imaging techniques.

Acknowledgment

The author would like to thank the staff of the Leicester Royal Infirmary CT scanner for their assistance in this work.

References

AXEL, L., 1983. Tissue mean transit time from dynamic computed tomography by a simple deconvolution technique. *Investigative Radiology, 18,* 94–99.

AXEL, L., HERFKENS, R. J. & LIPTON, M., 1979. Cardiac output determination by dynamic computerized tomography. *Investigative Radiology, 14,* 389.

GRUENEWALD, S., 1980. MSc Thesis in Nuclear Medicine, University of London. Also in *Clinical Nuclear Medicine 1983,* ed. by N. M. Maisey, K. E. Britton & D. L. Gilday (Chapman and Hall, London), pp. 108–109.

HINDMARSH, T., 1975. Elimination of water-soluble contrast media from the sub-arachnoid space. Investigation with computed tomography. *Acta Radiologica, 346,* 45–50.

JANSEN, O., GMELIN, E., BURMESTER, E., ROB, P. & WEISS, H. D., 1989. Analyse von dynamischen CT-kurven bei Neirentransplantaten mit Abstossungsreaktion und Cyclosporin-A-Intoxication. *ROFO, 151,* 473–476.

PETERS, A. M., GUNASEKERA, R. D., HENDERSON, B. L., BROWN, J., LAVENDER, J. P., DE SOUZA, M., ASH, J. M. & GILDAY, D. L., 1987a. Non-invasive measurements of blood flow and extraction fraction. *Nuclear Medicine Communications, 8,* 823–837.

PETERS, A. M., BROWN, J., HARTNELL, G. G., MYERS, M. J., HASKELL, C. & LAVENDER, J. P., 1987b. Non-invasive measurement of renal blood flow with ^{99m}Tc DTPA: a comparison with radiolabelled microspheres. *Cardiovascular Research, 21,* 830–834.

ROSEN, S. M., 1968. *Blood Flow Through Organs and Tissues,* ed. by W. H. Bain & A. M. Harper (E. and S. Livingstone, Edinburgh), pp. 458–465.

RUSSEL, S. B. & SHERWOOD, T., 1974. Monomer/dimer contrast media in the renal circulation: experimental angiography. *British Journal of Radiology, 47,* 268–271.

TREWHELLA, M., DAWSON, P., FORSLING, M., MCCARTHY, P. & O'DONNELL, C., 1990. Vasopressin release in response to intravenously injected contrast media. *British Journal of Radiology, 63,* 97–100.

WILLIAMS, R., CONDON, R. E., WILLIAMS, H. S., BLENDIS, L. M. & KREEL, L., 1968. Splenic blood flow in cirrhosis and portal hypertension. *Clinical Science, 34,* 441–452.

SHORT REPORTS

Efficacy of eyepad in corneal healing after corneal foreign body removal

MARK F. G. HULBERT

30 patients with corneal epithelial defect due to removal of corneal foreign bodies were randomly allocated to receive either chloramphenicol with continuous application of an eyepad or chloramphenicol without the eyepad. Almost all corneal defects were healed at 24 h, and all were healed by 48 h, with no statistically significant difference between the two groups. Discomfort at 24 h was greater in the eyepad group than in the control group. An eyepad seems to confer no benefit in healing and is uncomfortable.

Lancet 1991; **337**: 643.

The standard treatment of corneal epithelial loss is use of an eyepad with antibiotic drops or ointment. Indications for eyepad use vary substantially between centres. Such treatment is not entirely without risk; the eyepad removes binocular vision, with consequent reduction in visual field and depth perception, leading to delayed rehabilitation and risk of further injury. Many patients are more comfortable if the eye is left open.[1] Jackson[2] found that eyepads have no effect on healing rate of corneal abrasions. I decided to assess the effect of eyepad regimen on healing rate after corneal foreign body removal and on comfort during healing.

All patients attending the High Wycombe accident and emergency department, UK, between Oct 1, 1987, and Jan 1, 1988, with a corneal epithelial defect resulting from removal of a foreign body were included. Patients gave verbal consent to have details of their routine daily examination included in the study.

Patients were randomly allocated to "no eyepad" (control) and "eyepad" groups. After randomisation, patients in whom residual foreign body or stain remained after first attendance for removal were excluded to reduce the possibility of chemical or other interference with healing rate; 3 patients were excluded.

Size of epithelial defect was similar in the remaining patients (diameter range 1–2 mm, mean 1·6 mm and 1·8 mm in eyepad and control groups, respectively.) Eyepads consisted of gauze with enough bulk to exert slight pressure on the closed eye, secured by a bandage. The patient was instructed to keep the bandage on continuously. Two drops of 0·5% chloramphenicol were applied to the affected eye of all patients at each review. Patients were reviewed daily: staining with fluorescein (×4 magnification) was done to assess area of epithelial defect; to assess comfort, patients were asked to indicate "painful" or "painless". Patients were discharged from the study when there was no more visible corneal staining. The data were analysed by chi-square with Yates' correction for the small number of subjects.

30 patients (16 eyepad, 14 control) were included in the study. No patient defaulted from review. Almost all the corneal defects were healed at 24 h and all were healed by 48 h (table). The two groups were broadly similar with respect to healing rate. More patients in the eyepad than in the control group had discomfort at 24 h (75% *vs* 29%; risk ratio 7·5, 95% confidence interval 1·17–55·6).

The findings show that an eyepad seems to give no especial benefit in healing rate, and is associated with discomfort. Acheson et al[3] found that healing was faster with a soft contact lens than with eyepad and bandage; moreover, soft contact lenses were more comfortable and there was an earlier return to normal activities. Disadvantages include possible patient default from review with contact lens in situ, enhanced risk of infection of the damaged cornea, and increased cost (lessened by sterilisation and re-use of contact lenses). The treatment of a moderately benign and common condition such as corneal epithelial damage should be without risk of serious complication and low in cost. The findings reported here suggest that antibiotic treatment alone may be the best way to treat corneal epithelial loss after foreign body removal.

EFFECT OF EYEPAD ON HEALING AND COMFORT

—	Eyepad	Control
Healed		
1 day	14	14
2 days	2	0
*Comfort**		
Painless	4	10
Painful	12	4

*Eyepad *vs* control $\chi^2 = 4{\cdot}73$; $p = 0{\cdot}03$; comfort at 24 h.

I thank Mr J. S. Hillman, St James's University Hospital, for advice; Dr T. Malpass, Wycombe General Hospital, for allowing me to study patients under her care; and Mr T. DeDombal, University of Leeds, for statistical advice.

REFERENCES

1. Jackson H. Effect of eye-pads on healing of simple corneal abrasions. *Br Med J* 1960; **2**: 713.
2. Editorial. Traumatic corneal abrasion. *Lancet* 1987; ii: 1250.
3. Acheson JF, Joseph J, Spalton DJ. Use of soft contact lenses in an eye casualty department for the primary treatment of traumatic corneal abrasions. *Br J Ophthalmol* 1987; **71**: 285–89.

ADDRESS: **Department of Ophthalmology, St James's University Hospital, Leeds, UK** (Dr M. F. G. Hulbert, MB). Correspondence to Dr M. F. G. Hulbert, Lady Capel's Cottage, Hempstead Road, Watford, Hertfordshire WD1 3NL, UK.

Colour perfusion imaging: a new application of computed tomography

K. A. MILES M. HAYBALL A. K. DIXON

We describe a new application for imaging with computed tomography (CT) in which a quantifiable map of tissue perfusion is created and displayed by means of a colour scale. A rapid sequence of images is acquired without table movement immediately after a bolus intravenous injection of radiographic contrast medium. The rate of enhancement in each pixel within the chosen slice can then be used to determine perfusion. The technique provides a quantifiable display of regional perfusion combined with the high spatial resolution afforded by CT.

Lancet 1991; **337**: 643–45

Tissue perfusion can be measured by means of dynamic computed tomography (CT) by adaptation of a nuclear medicine data-processing technique.[1,2] A rapid sequence of

images is produced without table movement immediately after an intravenous injection of a bolus of iodinated contrast medium. The temporal changes in density within any organ in the chosen slice can be studied and displayed as a time-density curve (TDC). The iodine concentration within the organ can then be measured—25 HU (Hounsfield units) is equivalent to an iodine concentration of 1 mg/ml.[3]

The nuclear medicine technique[4,5] uses the following equation for measurement of blood flow in first pass studies with radiopharmaceuticals:

$$\frac{\text{Organ blood flow}}{\text{Cardiac output}} = \frac{g_k}{g_a} \times \frac{A}{D} \times a$$

where g_k = the maximum slope of the tissue time-activity curve, g_a = peak of arterial time-activity curve, A = the area under the gamma variate fit of the arterial curve, D = the dose injected, and a = a correction factor relating counts/s to MBq. Radiographic contrast media have similar pharmacokinetics to radiopharmaceuticals; this equation can be applied to TDCs derived from a single location dynamic CT study. The correction factor a is not required with CT since the dose is measured in HU and the area under the curve (A) in HU × units of time. Since iodine concentration rather than total organ iodine is measured, it is flow per unit volume of tissue, or perfusion, that is determined. Cardiac output can be calculated from dynamic CT[6] as D/A. By substitution into the first equation, it is found that:

$$\text{Perfusion } (\text{ml.min}^{-1}.\text{ml}^{-1}) = \frac{\text{Maximum slope of tissue TDC (HU/min)}}{\text{Peak of aortic TDC (HU)}}$$

Application of this analysis to a dynamic CT sequence pixel by pixel can create a perfusion map.

The CT machine used is a Siemens 'Somatom Plus'. A single location dynamic sequence of 1·0 s scans is done immediately after injection of 50 ml iopamidol ('Niopam', Merck) 300 mg/ml into an antecubital vein. Images are taken during quiet respiration at 0, 7 s, 10 s, 13 s, 16 s, 21 s, 26 s, 31 s, 37·5 s, and 44 s after the start of the injection. Images are subsequently compressed into a 256 × 256 matrix and transferred to a personal computer.

Software has been developed to derive a TDC for each pixel by use of the attenuation value from corresponding pixels in each image of the dynamic sequence. These TDCs are then analysed as above, yielding a value for perfusion for each pixel in the final image. To avoid artifacts due to slight movement of voxels with substantial amounts of air, fat, or bone creating rapid changes of attenuation within a pixel, any pixel in which the attenuation was ever above 400 HU or below − 30 HU is assigned a perfusion value of zero. On the map the perfusion in each pixel is represented by a colour from a 256 element colour scale.

The representative images shown (figure) are derived from a dynamic CT study of a patient with suspected liver disease. The high level of detail of the quantitative information in the images is shown by the relative perfusion of the renal cortex and medulla (figure, b). The absolute value of perfusion in $\text{ml.min}^{-1}.\text{ml}^{-1}$ can be read off from the colour bar.

This technique provides images of perfusion with greater spatial resolution than is available with single photon or positron emission tomography. It is more readily quantifiable than single photon emission tomographic studies, since no scatter or attenuation corrections are required. Magnetic resonance studies of intravoxel

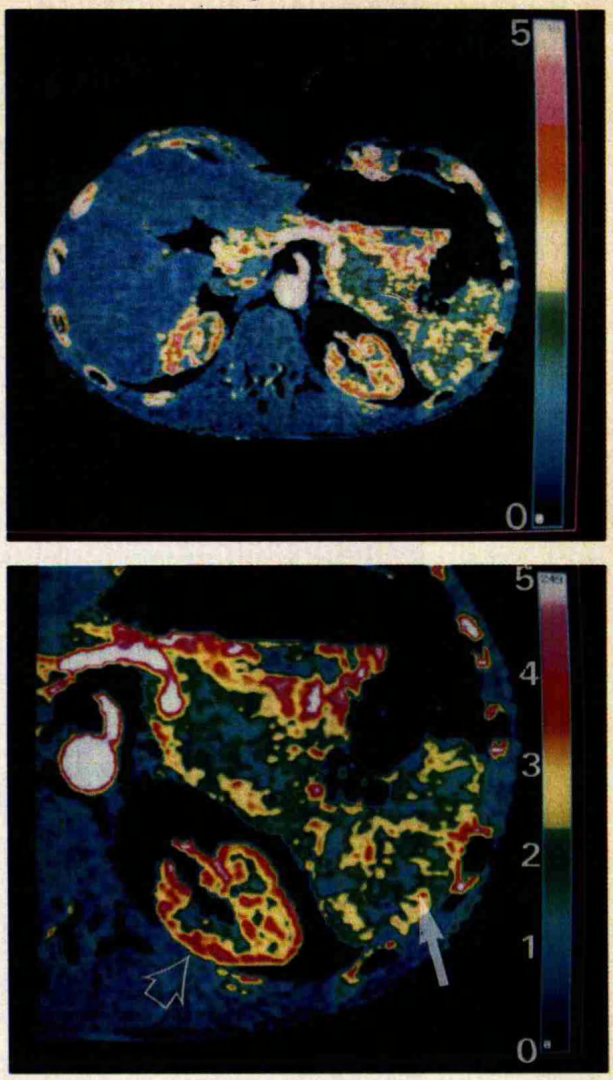

Perfusion images from patient with suspected liver disease.

A = axial slice in upper abdomen. Hepatic perfusion is reduced due to parenchymal liver disease.

B = enlarged portion of A, showing intrarenal perfusion (open arrow). Cortex (4 $\text{ml.min}^{-1}.\text{ml}^{-1}$, red/pink) is more greatly perfused than medulla (1·5 $\text{ml.min}^{-1}.\text{ml}^{-1}$, blue/green); cortico-medullary junction shows intermediate values (2·5 $\text{ml.min}^{-1}.\text{ml}^{-1}$, yellow/green). Note heterogeneous perfusion of spleen (arrow), a well-recognised normal phenomenon.

incoherent motions[7] will provide comparable images but these are difficult to carry out.

The technique depends on a CT system with low levels of photon noise. Large random fluctuations in the attenuation value within any pixel in the image sequence will create errors in the pixel TDCs and invalidate perfusion calculations.

There are three main sources of error. The method of analysis is valid only if the contrast medium is completely retained in an organ for a short period. This requirement seems to be met for solid organs, but not for blood vessels which will have a falsely low value. However, values for blood vessels could be used for relative flow studies. Movement of the patient (eg, respiration) may affect the pixel TDCs owing to varying partial volume effect of neighbouring structures. The effects of contrast media on blood flow must also be considered. The effect is usually

vasodilatory but they may cause a transient reduction in renal blood flow.[8]

The main benefit of the technique is that quantifiable information about perfusion is combined with good anatomical detail in one image. The technique is limited by the fact that only one slice location can be studied at any one time and by the radiation burden to the patient. Its potential applications are widespread but include studies of intrarenal blood flow, regional perfusion in tumours, and studies of cerebral perfusion. The technique is potentially applicable to many CT systems already installed and it may be useful in both clinical diagnosis and research.

REFERENCES

1. Miles KA. Measurement of renal cortical and medullary perfusion by dynamic computed tomography. *Br J Radiol* 1990; **63:** 991 (abstr).
2. Miles KA. Measurement of tissue perfusion by dynamic computed tomography. *Br J Radiol* (in press).
3. Hindmarsh T. Elimination of water-soluble contrast media from the sub-arachnoid space. Investigation with computed tomography. *Acta Radiol* 1975; **346:** 45–50.
4. Peters AM, Gunasekera RD, Henderson BL, et al. Non-invasive measurements of blood flow and extraction fraction. *Nuclear Med Commun* 1987; **8:** 823–37.
5. Peters AM, Brown J, Hartnell GG, Myers MJ, Haskell C, Lavender JP. Non-invasive measurement of renal blood flow with ^{99m}Tc DTPA: a comparison with radiolabelled microspheres. *Cardiovasc Res* 1987; **21:** 830–34.
6. Axel L, Herfkens RJ, Lipton M, Cardiac output determination by dynamic computerized tomography. *Invest Radiol* 1979; **14:** 389.
7. Le Bihan D, Breton E, Lallemand D, Grenier P, Cabanis E, Lavel-Jeantet M. MR imaging of intravoxel incoherent motions: application to diffusion and perfusion in neurologic disorders. *Radiology* 1986; **161:** 401–07.
8. Russel SB, Sherwood T. Monomer/dimer contrast media in the renal circulation: experimental angiography. *Br J Radiol* 1974; **47:** 268–71.

ADDRESSES: **Departments of Radiology, Nuclear Medicine, and Medical Physics, Addenbrooke's Hospital, Cambridge, UK** (K. A. Miles, FRCR, M. Hayball, BA, A. K. Dixon, FRCR). Correspondence to Dr K. A Miles, Departments of Radiology and Nuclear Medicine, Addenbrooke's Hospital, Hills Road, Cambridge CB2 2QQ, UK.

Stimulation of lymphocyte natural cytotoxicity by L-arginine

K. G. M. PARK P. D. HAYES P. J. GARLICK
H. SEWELL O. EREMIN

In vitro L-arginine enhanced natural-killer (NK) and lymphokine-activated-killer (LAK) cell activity; this cytotoxicity was mediated by CD56+ cells. In vivo arginine supplements (30 g/day for 3 days) increased the number of circulating CD56+ cells by a median of 32% in eight volunteers ($p<0.01$); this increase was associated with a mean rise of 91% in NK cell activity ($p=0.003$) and of 58% in LAK cell activity ($p=0.001$) in thirteen volunteers. These findings have potentially important implications for the modulation of natural cytotoxicity in a wide range of disease states.

Lancet 1991; **337:** 645–46.

Although the basic aminoacid L-arginine is regarded as being essential only during active growth, supplementary arginine has an immunostimulatory effect in adult animals which can reduce the growth and spread of several experimentally induced tumours.[1,2] In man arginine enhances lymphocyte transformations to polyclonal mitogens,[3] but little is known about the effects of arginine on other human immunological mechanisms. Natural-killer (NK) cells and their activated counterparts (lymphokine-activated-killer [LAK] cells) have an important role in human antitumour defences.[4] However, these cells may be inhibited by the malignant process itself.[4,5] We have examined the role of L-arginine as a possible biological modifier of human NK/LAK cells.

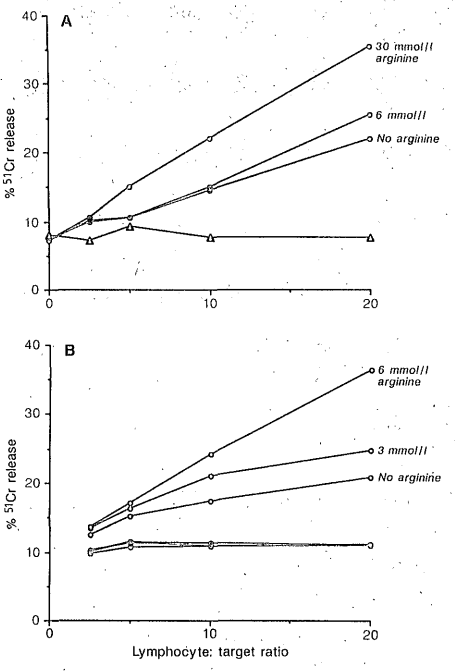

Effect of arginine on peripheral blood NK (A) and LAK (B) cell activity in vitro.

● = peripheral blood lymphocytes incubated in tissue culture medium plus arginine concentration shown for 24 h before assay.
○ = LAK cells generated by incubation with interleukin-2 (1000 u/ml) for 72 h plus arginine concentration shown.
△ = Viable cells, depleted of CD56+ lymphocytes.
Each assay was done in quadruplicate and reproducibility was >95%.

Peripheral blood lymphocytes from healthy male volunteers, aged 21–34 years, were used both for in-vitro and in-vivo studies. Cytotoxicity assays were carried out with lymphocytes obtained before and after arginine treatment (L-arginine base in gelatin capsules) by standard chromium-51 release assays; the results were expressed as lytic units (LU).[5,6] Phenotypic characterisation of peripheral blood lymphocytes used an indirect labelling technique, with appropriate monoclonal antibodies analysed by means of an EPICS C (Coulter) flow cytometer. The phenotypic data were analysed by Wilcoxon signed rank tests and the results of cytotoxicity assays by paired *t* tests on log-transformed data.

Pretreatment peripheral blood lymphocytes incubated with 30 mmol/l arginine showed greater NK activity than

CHANGE IN PHENOTYPIC EXPRESSION ON PERIPHERAL BLOOD LYMPHOCYTES WITH ARGININE TREATMENT

Subject	No of cells expressing antigen × 10^9/l before/after arginine *(% change)*			
	CD8	CD16	CD56	CD57
1	8·5/7·2 *(−12%)*	1·0/1·9 *(83%)*	2·0/2·4 *(18%)*	2·6/2·7 *(4%)*
2	6·6/6·4 *(−3%)*	3·2/2·6 *(−19%)*	3·0/4·4 *(32%)*	2·8/2·4 *(−14%)*
3	5·4/7·0 *(30%)*	1·0/1·4 *(40%)*	1·4/1·5 *(7%)*	2·1/2·1 *(0%)*
4	7·6/6·2 *(−18%)*	3·0/2·3 *(−25%)*	1·6/2·8 *(73%)*	2·7/2·6 *(−4%)*
5	6·2/5·0 *(−20%)*	2·2/2·1 *(−2%)*	1·3/3·4 *(171%)*	2·5/2·2 *(−14%)*
6	7·2/7·5 *(3%)*	3·5/2·8 *(−19%)*	4·8/6·3 *(32%)*	2·8/2·7 *(−4%)*
7	5·6/5·8 *(14%)*	1·5/1·7 *(11%)*	2·2/2·6 *(18%)*	3·0/2·4 *(−20%)*
8	6·1/7·4 *(21%)*	2·4/1·4 *(−42%)*	1·3/2·9 *(123%)*	2·3/1·2 *(−48%)*

those incubated with 6 mmol/l arginine or without arginine (figure, A). These cells were not cytotoxic to NK-resistant, LAK-sensitive, Daudi cells (figure, B). LAK cell activity also increased with arginine concentration (figure, B). Lymphocytes depleted of CD56+ cells, by means of monoclonal antibody coated magnetised beads, showed no NK or LAK cell activity (figure, A).

In thirteen volunteers oral arginine (30 g/day, in divided doses for 3 days) increased the NK cell cytotoxicity (mean [SD] 80·4 [45·2] LU to 130 [45·2] LU).* The mean individual increase after arginine over the pretreatment cytotoxicity was 91% ($p = 0·003$) with the greatest increase in four volunteers who had the lowest baseline activities (mean increase 195%). In vitro LAK cell generation was also enhanced by arginine treatment (mean increase 58% [SD 32%]; $p = 0·001$).

Phenotypic characterisation of peripheral blood lymphocytes was done before and after arginine treatment for eight of the volunteers (table). There was no significant change in the differential white cell count or absolute number of lymphocytes, but all subjects showed an increase in the number of CD56+ cells ($p < 0·001$). Six volunteers showed a reduction in the number of CD57+ cells ($p < 0·05$). Although this antigen is expressed on cells with similar morphology to NK cells, there is little correlation between CD57+ cells and cytotoxicity.[4] Dual fluorescence studies showed an increase in the population of the highly cytotoxic CD8+/CD56+ subset of NK cells (median [range] 63 [45–113] × 10^6/l to 105 [72–176] × 10^6/l) after arginine ingestion. There was also an increase in the number of CD8+ cells co-expressing the CD11b antigen (cytotoxic CD8 cells[7]) (96 to 206 × 10^6/l; 101 to 208 × 10^6/l; 108 to 324 × 10^6/l; 120 to 411 × 10^6/l).

Arginine (10 g/day for 3 days) was given to six volunteers who had responded to 30 g/day. NK cell activity increased by a mean of 52% over pretreatment but the rise was not consistent ($p = 0·035$). However, LAK generation was enhanced by a similar extent to the higher dose (mean increase 78%, $p = 0·005$). Phenotypic results were also similar.

We postulate that L-arginine has a direct effect on NK cells, as shown by the increased in-vitro cytotoxicity. In vivo the arginine-induced increase in the number of cells with the NK phenotype is probably due to release of these cells from the bone marrow—the number of B cells in blood is also higher after arginine ingestion.

The mechanism underlying these changes is not clear. Our in-vitro studies (unpublished) do not suggest that arginine enhances interleukin-2 production. Arginine is a potent endocrine secretagogue[1] but we found no evidence for a significant increase of insulin. Production of nitric oxide from arginine-treated macrophages and endothelial cells as a possible mediator of intracellular communications (changing the cyclic AMP/cyclic GMP ratios within target cells) has been proposed as a possible explanation of some of the previously observed effects of arginine.[8] A reduction of the cAMP/cGMP ratio would favour the production of interleukin-1,[9] which is known to activate NK cells and may directly enhance NK cell cytoxicity.[10]

The substantial enhancement of human NK and LAK cell activity by large doses of arginine could be useful in many immunosuppressed states, including malignant disease, AIDS, and HIV infection, in which depressed NK cell activity is an important component of the disease process.

K.G.M.P. was supported by the Jean V. Baxter and the Clinical Metabolism and Nutritional Support Group fellowships awarded by the Scottish Hospitals Endowments Research Trust and the Nutrition Society, respectively.

REFERENCES

1. Barbul A. Arginine: biochemistry, physiology, and therapeutic implications. *J Parenteral Enteral Nutr* 1986; **10:** 227–38.
2. Reynolds JV, Daly KM, Shou J, Sigal R, Naji A. Immunologic effects of arginine supplementation in tumour bearing and non-tumour-bearing hosts. *Ann Surg* 1990; **211:** 202–10.
3. Barbul A, Sisto DA, Wasserkrug HL, Efron G. Arginine stimulates lymphocyte immune response in healthy human beings. *Surgery* 1981; **90:** 244–51.
4. Trinchieri G. Biology of nartural killer cells. *Adv Immunol* 1989; **47:** 187–376.
5. Eremin O, Coombs RR, Ashby J. Lymphocytes infiltrating human breast cancers lack K cell activity and show low levels of NK cell activity. *Br J Cancer* 1981; **44:** 166–76.
6. Pross HF, Maroun JA. The standardization of NK cell assays for use in studies of biological response modifiers. *J Immunol Methods* 1984; **68:** 235–49.
7. Dianzani U, Zarcone D, Pistoia V, et al. CD8+ CD11b+ peripheral blood lymphocytes contain lymphokine-activated killer cell precursors. *Eur J Immunol* 1989; **19:** 1037–44.
8. Moncada S, Palmer RMJ, Higgs EA. Biosynthesis of nitric oxide from L-arginine: a pathway for the regulation of cell function and communication. *Biochem Pharmacol* 1989; **38:** 1709–15.
9. Knudsen PJ, Dinarello CA, Strom TB. Prostaglandins post-transcriptionally inhibit monocyte expression of interleukin-1 activity by increasing intracellular cyclic adenosine monophosphate. *J Immunol* 1986; **137:** 3189–94.
10. Roder JC, Klein M. Target-effector interactions in the natural killer cell system. IV. Modulation by cyclic nucleotides. *J Immunol* 1979; **123:** 2785–90.

*A fuller description of the methods used and a table giving NK and LAK cell activity in volunteers are available from *The Lancet*.

ADDRESSES: **Departments of Surgery** (K. G. M. Park, FRCSE, P. D. Hayes, BSc, Prof O. Eremin, FRCSE), **and Pathology** (Prof H. Sewell,* MRCPath), **University of Aberdeen, and Rowett Research Institute, Aberdeen, UK** (K. G. M. Park, P. J. Garlick, PhD). *Present address: Department of Immunology, University Hospital, Queen's Medical Centre, Nottingham. Correspondence to: Mr K. G. M. Park, Department of Surgery, University of Aberdeen, Polworth Building, Foresterhill, Aberdeen AB9 2ZD, UK.